University of Southampton

Faculty of Engineering and Physical Sciences

National Centre for Advanced Tribology

Protection, Remineralisation and Tubule Occlusion of Dentine by Desensitising Toothpastes

By

Behrad Mahmoodi

Academic Supervisory Team

Dr Richard B Cook

Prof Robert JK Wood

Thesis for the degree of Doctor of Philosophy

January 2020

University of Southampton

ABSTRACT

FACULTY OF ENGINEERING AND PHYSICAL SCIENCES
SCHOOL OF ENGINEERING

Thesis for the degree of Doctor of Philosophy

Protection, Remineralisation and Tubule Occlusion of Dentine by Desensitising Toothpastes

Behrad Mahmoodi

Enamel is one of the strongest and highly mineralised tissues in the human body and it protects the underlying dentine. The high mineral content of the enamel makes it susceptible to erosive wear via dissolution of the ions in low pH. Loss of the minerals also softens the enamel, making it vulnerable to further damage by mechanical and chemical challenges in the oral environment. The loss of enamel or gum recession along the gum lines exposes the dentine, causing dentine hypersensitivity (DH).

Active ingredients such as bioactive glasses, arginine and calcium silicate have been used in toothpastes to treat DH by depositing a layer over the dentine and occluding exposed tubules. As well as providing relief against sensitivity, these layers could protect the dentine against chemical and mechanical challenges.

The first aim of this study was to investigate the ability of 5 different layers formed on dentine to protect the tissue against these challenges. The layers were formed following brushing with 5 commercially available toothpastes containing chloro calcium phosphosilicate, fluoro calcium phosphosilicate, calcium sodium phosphosilicate, arginine with calcium carbonate, and calcium silicate with sodium phosphate.

60 bovine dentine discs were divided into 6 groups and were manually brushed twice a day for two minutes over 7 days with one of the toothpastes or artificial saliva as a control. In vitro techniques such as nanoindentation, nano scratch, scanning electron microscopy, nuclear magnetic resonance, X-ray-diffraction, Fourier-transform infrared spectroscopy, energy-dispersive x-ray, and Raman spectroscopy were used to characterise the layers. Acid resistivity of the layers was also investigated by immersion in 1 wt% citric acid (pH 3.1) for two minutes.

Results showed that all 5 active ingredients formed a protective layer onto the dentine surface, these layers were chemically and structurally similar to hydroxyapatite with higher hardness and Young's modulus compared to the control dentine. Calcium silicate with sodium phosphate formed the hardest layer with a hardness of 0.88 GPa compared to control dentine (0.55 GPa), however, it did not perform well under acid challenge. Arginine with calcium carbonate formed the second hardest layer with superior resistance to acid challenge, highest hardness/modulus ratio, elastic recovery, and lowest scratch penetration depth. This layer also had the highest average crystal size and crystallinity index. Therefore it would offer the best protection to the dental tissue.

Tubule occlusion is one of the most widely accepted methods in treating DH. Current techniques such as focused ion beam, scanning electron microscopy or hydraulic conductance that are used to determine tubule occlusion in vitro do not provide the depth of occlusion, are limited in terms of the volume of dentine tested or extremely time consuming and expensive. The second aim of this study was to use a unique serial block-face scanning electron microscopy (SBF-SEM) to overcome these limitations and to determine the level of tubule occlusion and mineralisation by Sensodyne® Repair and Protect and Rapid Relief toothpastes containing calcium sodium phosphosilicate (CSPS) and stannous fluoride (SnF_2) respectively.

Bovine dentine discs (n=6) were randomly divided into two treatment groups, one for each toothpaste (n=3). Discs were halved with one half treated with toothpaste and one as a control. 600 slices with a thickness of 60 nm were cut by a diamond knife in a microtome and the surface was imaged by a backscattered electron detector after each slice.

CSPS occluded 100% of the tubules at the surface compared to 83% for SnF_2. No tubules were occluded in the control group. CSPS also significantly reduced the diameter of the tubule opening, while no significant change was seen in the SnF_2 group. Both materials resulted in a greyscale value increase around the tubules with CSPS significantly higher than SnF_2. Therefore CSPS may provide better relief against DH and help with mineralisation due to a superior occlusion percentage and increased dentine mineralisation.

Table of Content

List of Figures

List of Tables

Academic Thesis: Declaration of Authorship

Name: **Behrad Mahmoodi**

Title of thesis: **Protection, Remineralisation and Tubule Occlusion of Dentine by Desensitising Toothpastes**

I declare that this thesis and the work presented in it is my own and has been generated by me as the result of my own original research.

I confirm that:

1. This work was done wholly or mainly while in candidature for a research degree at this University;

2. Where any part of this thesis has previously been submitted for a degree or any other qualification at this University or any other institution, this has been clearly stated;

3. Where I have consulted the published work of others, this is always clearly attributed;

4. Where I have quoted from the work of others, the source is always given. With the exception of such quotations, this thesis is entirely my own work;

5. I have acknowledged all main sources of help;

6. Where the thesis is based on work done by myself jointly with others, I have made clear exactly what was done by others and what I have contributed myself;

7. Parts of this work have been published as:

- B. Mahmoodi, R.J.K. Wood, R.B. Cook, Nanomechanical properties of hydroxyapatite like coatings formed by bioactive glasses, arginine and calcium silicate for dentine protection, J. Mech. Behav. Biomed. Mater. 105 (2020). doi:10.1016/j.jmbbm.2020.103702.

Signature: Date

Acknowledgement

I would like to take this opportunity to express my profound gratitude to my supervisors, Dr Richard Cook and Professor Robert Wood for their encouragement, valuable guidance, and support throughout my PhD. I would also like to show my sincere appreciation to all the staff in the department of chemistry and biomedical imaging unit at Southampton university hospital for giving me access to scanning electron microscopes, Ms Patricia Goggin for her help and constant support with the Serial Block Face experiments and Dr David Chatelet for helping me with image processing. Furthermore, I would like to thank the graduate school at the University of Southampton and GlaxoSmithKline for providing financial support to make this project happen.

I want to take the opportunity to thank my family and friends for their continuous and unparalleled love, help and support. I am grateful to my girlfriend Chiamaka Chiedozie for always being there for me during the ups and downs of this journey. It would not have been possible if not for them.

Finally, I would like to dedicate this thesis to my late father Behrouz Mahmoodi who I sadly lost in the first year of my PhD. I want to thank him for always believing in me and encouraging me to do better.

.

Glossary of Abbreviations

ADA	American Dental Association
AG	Arginine
AS	Artificial Saliva
BAG	Bioactive glass
BO	Bridging Oxygen
BSE	Backscattered electron
Ca^{2+}	Calcium Ions
$CaCl_2$	Calcium chloride
CCPS	Chloro Calcium Phosphosilicate
Cl^-	Chloride Ions
CMC	Carboxymethylcellulose
CSPS	Calcium Sodium Phosphosilicate
DEJ	Dentine Enamel Junction
DH	Dental Hypersensitivity
DI	Deionised
DSI	Depth Sensing Indentation
EDX	Energy Dispersive X ray microscopy
F^-	Fluoride ions
FCPS	Fluoro Calcium Phosphosilicate

GPa	Gigapascal
GSK	GlaxoSmithKline
GS	Grey Scale
GTFs	Glucosyltransferase
H^+	Hydrogen Ions
HA	Hydroxyapatite
K^+	Potassium Ions
KCl	Potassium Chloride
KO_2	Potassium Oxide
Mg^{2+}	Magnesium Ions
MgO	Magnesium Oxide
Na^+	Sodium Ions
$Na_2HPO_4.12H_2O$	Sodium Dihydrogen Phosphate Dodecahydrate
NaCl	Sodium Chloride
Na_2O	Sodium Oxide
NI	Nanoindentation
NBO	Non Bridging Oxygen
NC	Network Connectivity
OH^-	Hydroxyl Group
P_2O_5	Phosphorus Pentoxide
RDA	Relative Dentine Abrasivity

REA	Relative Enamel Abrasivity
S Mutants	Streptococci Mutans
SBF	Simulated Body Fluid
SEM	Scanning Electron Microscopy
SiO_2	Sodium Oxide
SnF_2	Stannous Fluoride
VMH	Vickers Microhardness

Chapter 1 Introduction

1.1 Background

Dentine hypersensitivity (DH) is described as a sharp pain that can last from a few seconds to a few minutes in response to external stimuli, commonly thermal, chemical or mechanical. The stimuli alter the fluid flow within the tubules, stimulating the nerve receptors within the pulp, triggering a painful response [1].

DH is one of the most common oral conditions affecting about 30% of the population at some time during their lifetime, peaking between the ages of 20 to 40. However, the quantification of DH has proven difficult as the determination of the number of people affected by DH can be subjective to the methods associated with determining DH. It arises when the tubules within dentine become exposed as a result of gum recessions or wear/damage to the protective enamel layer. At early stages it is possible to manage or treat the sensitivity symptoms by using toothpastes designed to occlude these tubules, limiting the movement of the fluid and therefore reducing sensitivity [2].

Bioactive glasses, an advanced calcium, and phosphate based material are the most common active ingredients used in toothpastes to occlude the dentine tubules and treat DH [3]. The first bioactive glass known as calcium sodium phosphosilicate, commonly referred to as “45S5” bioglass, was developed by Larry Hench to treat damaged bone. In 1997 Litkowski et al [3] proposed using the 45S5 bioglass in oral care products for sensitivity treatment.

When a bioactive glass comes in contact with saliva it releases calcium and phosphate ions. The initial steps of the reaction involve a rapid ionic exchange between the sodium and hydrogen ions from the saliva. This ionic exchange increases the local pH which promotes the formation of hydroxyapatite. Bioactive glass particles bind to the collagen of exposed dentine and once deposited these particles continue to react forming a calcium phosphate layer. These particles act as a calcium and phosphate reservoir which allows the crystallisation of this layer into a hydroxyapatite like layer. This layer is formed over dentine and within dentine tubules [4,5].

This layer reduces the permeability of the dentine by decreasing the fluid flow within the tubules and thereby reducing the activity of nerve endings. This provides relief from the pain of dentine hypersensitivity.

The 45S5 has been used as a base to develop other bioactive glasses such as Chloro calcium phosphosilicate (CCPS) and Fluoro calcium phosphosilicate (FCPS) with sodium substituted for fluoride and chloride ions respectively which have also been used in toothpastes to treat DH [6–9]. Other materials such as arginine (AG) coupled with calcium carbonated [10–12] and calcium silicate (CS) with sodium phosphate are also used for physical occlusion of tubules and remineralisation of the dental tissues [13–15]. Techniques such as scanning electron microscopy, focused ion beam and hydraulic conductance have been used to quantify the level of tubules occlusion by these materials. However, these methods are either limited in resolution, limited by the significant time required to prepare samples [16] or fail to provide the depth of occlusion. Therefore an alternative methodology needs to be considered to overcome these limitations.

Patients who suffer from dentine hypersensitivity are at higher risk of developing other dental related diseases such as tooth decay, cavity and pulp inflammation. This is because dentine is softer than the enamel and is susceptible to further damage within the harsh oral environment. Tooth cavity or pulp inflammation causes severe pain and discomfort to the individual. They also have a huge financial impact on the patient and the NHS as more substantial treatments such as fillings and root canals would be required.

With ever increasing life expectancy, keeping our natural teeth dentition is becoming more important. Consumption of soft drinks and processed food which are highly acidic and contain a large amount of sugar are on the rise. Therefore protecting the dental tissue is vital, not only to minimise the risk of developing a more serious dental condition but to also prevent healthy teeth from chemical and mechanical challenges.

As mentioned previously the above materials form a layer on the tooth surface and thus have the potential to act as a protective barrier against acid erosion and tribological wear. There is a gap in the literature regarding the level of protection these layers offer. Previous studies have used microhardness measurements to characterise these layers, and consequently, the interaction volumes of the indent would have included the dentine substrate and influenced the results [17–21].

These layers are inherently a thin coating of few microns and should be treated as such during testing. In addition, previous tests were carried out in a dry environment which is not representative of the oral environment and would affect the measured mechanics (hardness and modulus) as dentine tissue consists of 22% water (Vol%) in vivo [22].

1.2 Aims

To fill the gap in the literature, the research presented in this thesis initially aimed to compare the nanomechanical properties, acid resistivity, composition and structure of the layers formed by 5 desensitising toothpastes containing CCPS, FCPS, CSPS, AG and, CS to evaluate whether these layers can protect the dentine and what parameters influence the level of protection.

Stannous fluoride (SnF_2) is also a common active ingredient used in desensitising toothpastes for DH treatment. Therefore the project also aimed to measure and compare the level of tubules occlusion and mineralisation of SnF_2 compared to CSPS.

1.3 Objectives of Current Research

The primary objective of this thesis was to develop an understanding of dentine protection by novel mechanical and characterisation methodologies and testing. The combination of a wide range of testing and use of 5 different active ingredients will help to determine the most favourable material and the variable which alters the protection capability. This will make a significant contribution to the field of dental material and will help with the development of new toothpaste formulations for better and longer protection to dental tissue. To achieve this the mechanical properties of all 5 layers were characterised. This was followed by a detailed chemical and structural analysis to establish the parameter(s) influencing the mechanics.

The second objective of this thesis was to develop a novel imagining methodology to measure the depth of tubule occlusion by SnF_2 and CSPS with minimal sample preparation over a short period while testing a larger volume of dentine. Both by determining the number of occluded tubules per unit volume and the depth of penetration of the active ingredients down the tubules using a Serial block face scanning electron microscopy (SBF SEM).

SBF SEM combines an ultra-microtome with the high resolution imaging capability of an SEM to generate high resolution 3D images of samples. The use of backscattered images from the SBF SEM enables the evaluation of mineralisation potential of the two ingredients by using the greyscale values from the images. This methodology will be significantly useful in the development and research of new dental materials for dental hypersensitivity treatment as well as detecting remineralisation of the dental tissue. It would also be beneficial for the research of bone-like biomaterials with clinical applications.

The sub-objectives of the thesis are given below:

- To characterise the mechanical properties of the different layers formed by AG, CCPS, CS, CSPS and FCPS on a nano-scale to avoid any dentine substrate influence which has not been done before
- Use a unique liquid cell set up to keep the samples hydrated, mimicking the oral environment.
- To investigate the acid resistivity of the layers
- To investigate the elemental and structural differences between these layers
- To investigate what variables influence the protection capability of the layer
- To investigate the suitability of SBF SEM in cutting a hard material such as dentine
- To determine the level of tubule occlusions by two toothpastes containing CSPS and SnF_2 using SBF SEM
- To investigate the mineralisation of dentine using the backscatter electron imaging within SBF SEM to compare the mineral density of the dentine after treatment with CSPS and SnF_2

1.4 Analytical Methods Used To Fulfil the Objectives

Figure 1.1 below represents the flow chart of the experimental techniques used throughout this thesis to meet the aims and objectives of the project.

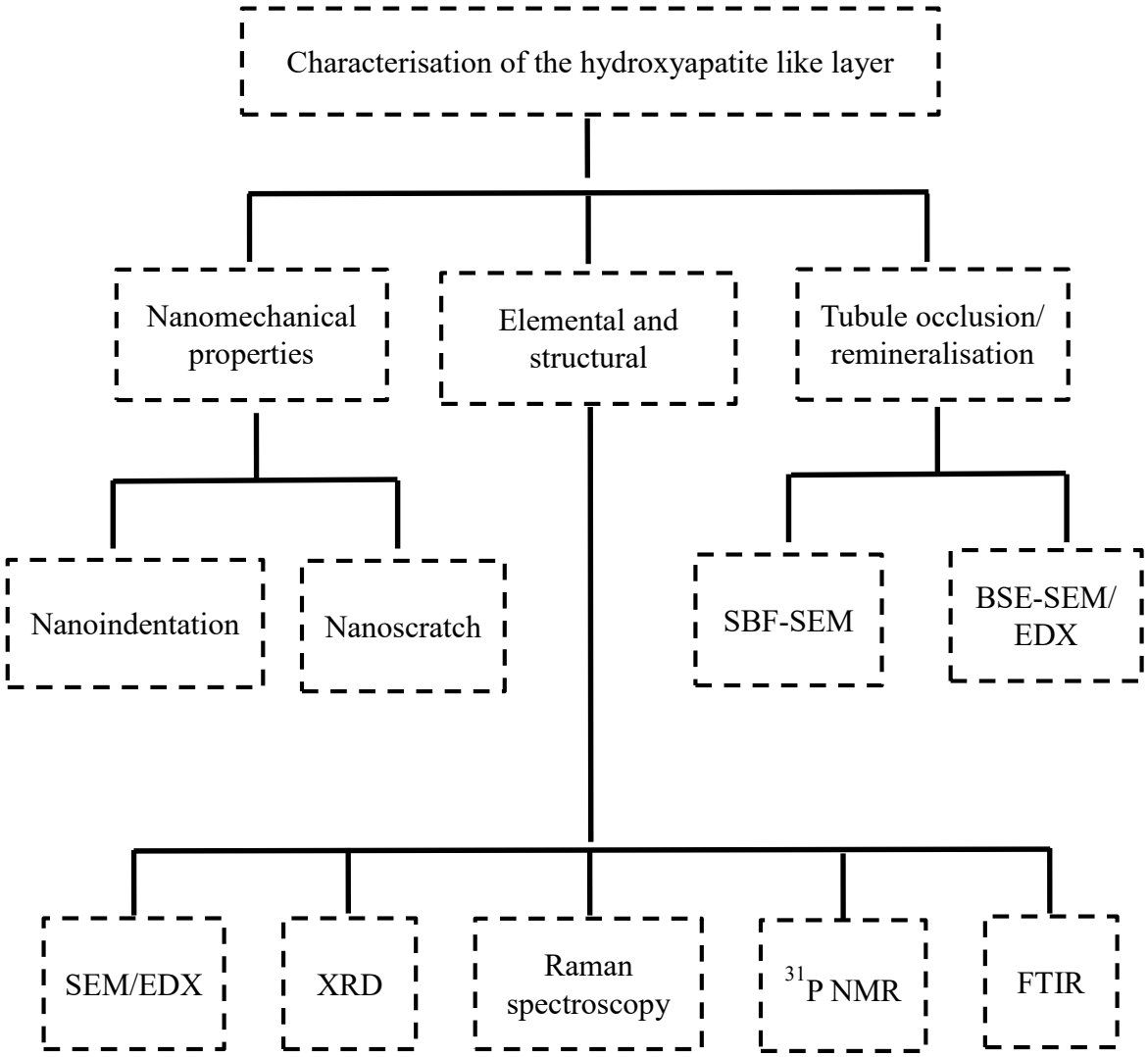

Figure 1. 1: Experimental techniques within this thesis

1.5 Thesis Outline

This thesis focused on improving the understanding of the nanomechanical properties and elemental composition of the different layers formed by different active ingredients and to identify the key parameter which influences these properties. This will aid the development of a new toothpaste formulated to provide better protection to exposed dentine. It also explored the use of SBF SEM as an alternative method to determine tubule occlusion and dentine mineralisation. The thesis starts with a literature review covering the basic mechanics of dental tissue, demineralisation/remineralisation process, causes of DH and possible treatments. The common active ingredients are then discussed with the main focus on the conventional 45S5 bioglass, its structure and the reaction mechanisms. Different elemental and structural techniques which were used throughout this thesis is also covered in this section. This chapter is concluded by covering the use of bioactive glasses (CSPS, CCPS, and FCPS) as well as other materials such as AG and CS for DH treatment and different methods for determining tubule occlusion.

In chapter 3 the nanomechanical properties of the different layers formed by these materials are investigated, including an acid resistivity challenge. Chapter 4 concentrates on using different analytical techniques to understand the link between the composition, structure and the mechanics of dental tissue. A comparison study was conducted in Chapter 5 where a unique SBF SEM was used to quantify tubule occlusion and depth of penetration as well as mineralisation of dentine by CSPS and SnF_2. Overall findings of the thesis and the future work are subsequently discussed and concluded in chapter 6.

Chapter 2 Literature Review

2.1 Introduction

Damage to the protective enamel layer and recession of the gum can leave dentine exposed. This would lead to dentine hypersensitivity (DH) and further damage to the dental tissue through mechanical and chemical challenges in the oral environment. Occlusion of the dentine tubules is widely regarded as one of the most acceptable courses of treatment for DH. Desensitising toothpastes use active ingredients such as bioactive glasses, arginine and calcium silicate to achieve occlusion via formation of a layer over exposed tubules.

In this chapter, the mechanical properties of the dental tissues, causes, and treatments of dentine hypersensitivity including an overview of the use of bioactive glasses, arginine and calcium silicate in dentistry are reviewed. This is followed by a more detailed description of remineralisation and demineralisation mechanisms of the tooth structure, hydroxyapatite like layer (HA) formation within the oral cavity and characterisation techniques such as scanning electron microscopy, Energy-dispersive X-ray analysis, X-ray-diffraction pattern, Fourier-transform infrared spectroscopy and Raman spectroscopy.

The chapter concludes by covering different methods used in the assessment of tubule occlusions and a summary of the literature findings highlighting the gap in the knowledge which lead to the aims and objectives of this thesis.

2.2 Tooth Structure

A tooth consists of a soft inner layer to provide the nutrient and a hard outer layer that provides protection. It is composed of four different tissues as shown in figure 2.1; Enamel, dentine, cementum and dental pulp. [23].

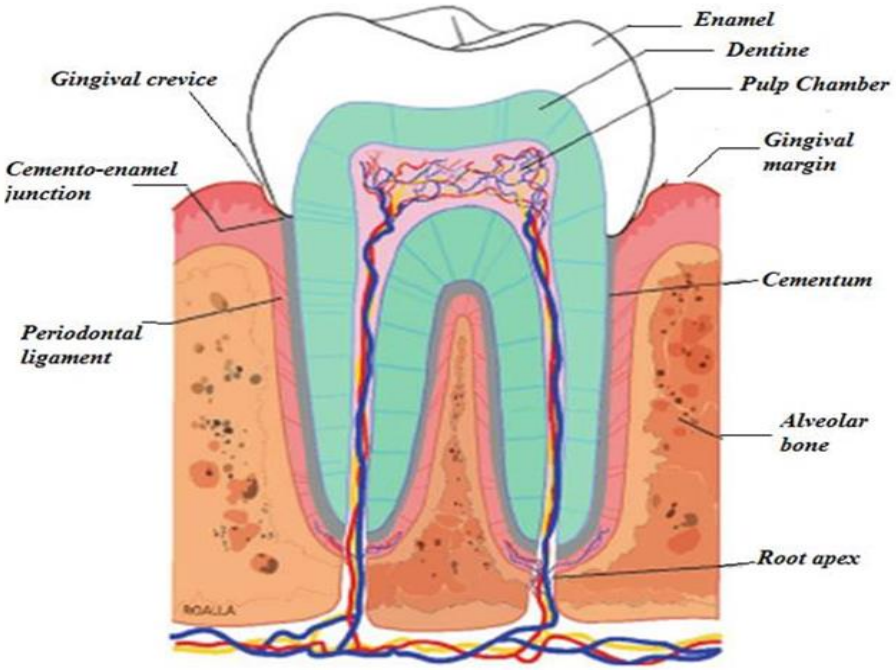

Figure 2. 1: Structure of human tooth [24]

Enamel is the outer layer of the tooth whose purpose is to protect the dentine and the pulp as well as providing the hard surface for mastication. Underneath the enamel is dentine, which makes up the majority of the tooth and provides support to the tooth structure. The pulp runs through the centre of the tooth to the root which is embedded in the jawbone. It consists of living odontoblast cells, blood vessels, and connective tissues. Forming dentine and supplying nutrients to the mineralised tissues is the main function of the pulp, it also plays a big role in protecting the surrounding tissues by forming secondary dentine [23]. Cementum covers the dentine and it facilitates the attachment of the tooth to the alveolar bone [25].

Teeth are surrounded by soft tissues called Gingivae, commonly known as the gum. These soft connective tissues are responsible for providing protection and support to the tooth and the underlying bone. Due to the tight sealing, Gingivae acts as a protective barrier for the periodontal ligament (PDL) which is a specialised connective tissue fibre that attaches the tooth to the alveolar bone. It also acts as a shock absorber, protecting the tooth from large forces during mastication [26]. Enamel and dentine, however, are the two major components of the tooth and are discussed in more detail below.

2.2.1 Enamel

The enamel is the hardest tissue in the human body. The highly mineralised structure consists of 95% hydroxyapatite (HA) crystals, 2 % protein in the form of type I collagen and 3% water. Enamel has a hierarchical structure that ranges from the nano (collagen/HA crystal composite) to micro-scale (rod and sheath) [27].

Hydroxyapatite is an inorganic mineral found extensively in the human body. Both enamel and dentine can be considered as a composite that is made up of HA crystals and collagen fibres that are tightly bonded via hydrogen bonding through the hydroxyl groups (OH^-) on the HA. Enamel is formed by epithelial cells called *ameloblasts* which lose their function once the crown is formed, therefore enamel lacks the ability to self-repair. Figure 2.2 is a schematic diagram of human premolar tooth cross-section, it demonstrates the microstructure of enamel consisting of rods. These rods have a diameter of ~5 µm and are perpendicular to the dentine enamel junction (DEJ). They are comprised of hydroxyapatite crystals with a length of 68 nm, 26 nm diameter and thickness of 2 nm [28].

The hydroxyapatite crystals are aligned parallel to the long axis of the rods at the centre and meet the axis at 45º at the margins of the rod resulting in a *keyhole-like* structure know as *rod sheath* (figure 2.2). The rod sheath has the most protein content thus is hypo-mineralised leading to the anisotropic properties of enamel [29].

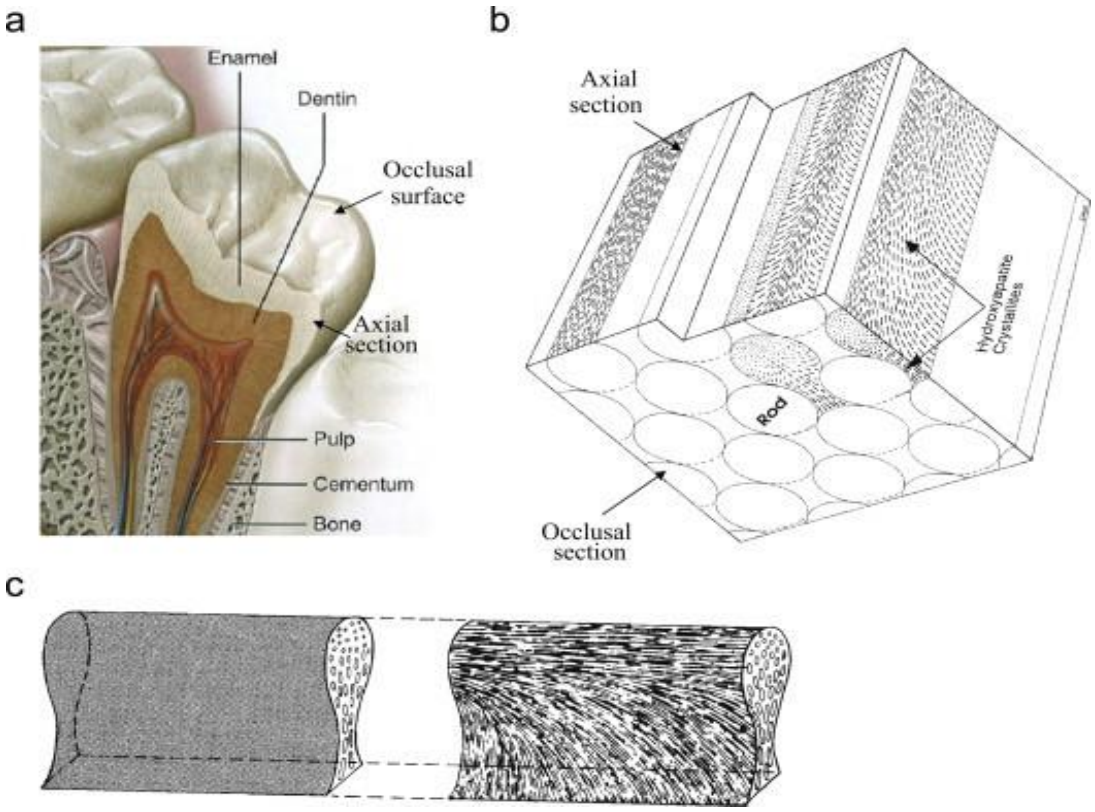

Figure 2. 2: Cross section (a), enamel sheath (b), enamel rode (c) [30]

2.2.2 Dentine

Dentine in other hand is classified as "living" and is continuously being formed by *Odontoblasts* cells throughout the life of the pulp. It is much softer than enamel and it is made up of 70% inorganic hydroxyapatite, 20% type I collagen and 10% water. The crystals within dentine are more randomly orientated and are approximately 20-100 nm in length and 20 nm wide [31].

Dentine structure consists of three morphologically different tissues [32]:

- Primary dentine
    - Is formed rapidly at a rate of approximately 4 μm per day before the eruption of the tooth
- Secondary dentine
    - Continuous formation of primary dentine after the tooth has erupted at a slower rate of 0.4 μm per day throughout the life of the tooth
- Tertiary dentine
    - Once dentine is damaged through decay, trauma or restorative procedures, odontoblast cells produce tertiary dentine as a healing mechanism. It has a fewer number of tubules and it is more mineralised compared to primary and secondary dentine, making it harder and less permeable to protect the pulp from any irritation.

Primary dentine is further split into [33];

- Intertubular dentine
    - It is made up of 30% collagen, 25% water and 45% minerals (carbonated apatite crystals) by volume
    - The largest portion of dentin and provides structural support to the enamel
- Peritubular dentine
    - More mineralised than intertubular dentine contains 95% (vol %) carbonated apatite crystals with the other 5% being water and collagen

Dentine consists of thousands of hollow tubules running down the entire structure (several millimetres), making dentine a permeable structure. These tubules are filled with fluid which transports nutrient to the tooth. Their density ranges between 15000 to 65000 tubules per mm^2, with a diameter of 0.9 µm at the dentine- enamel junction (DEJ) to 2.5 µm near the pulp [34].

2.3 Mechanical Properties of Dentine

Understanding the mechanical properties of the dental tissue lays a perfect foundation for dental material research. These properties include hardness (H) and elastic modulus (E). H is a commonly used parameter for evaluating and comparing materials and it is a measure of how hard or soft a material is. E also known as Young's modulus is a measure of the rigidity of a material and is defined as the ratio of stress and strain. It is indicative of the ability of a material to withstand plastic deformation.

With the advancement of characterisation techniques, the measurements of tooth properties have been shifting from macroscopic to microscopic and more recently to the nanoscale level. The most common methodology for calculating the hardness of a dental tissue include the Vickers hardness (VMH) and Knoop hardness. Vickers hardness uses a diamond indenter in the shape of a pyramid with opposite angles of 136º. The hardness is calculated by measuring the diagonal length of indentation and using the following formula [22]:

$$H_V = \frac{1.854P}{D^2} \quad (2.\ 1)$$

Where D is the average length of the two indent diagonal and P is the applied load. Vickers hardness uses applied loads in the range of 10–1200N with indentation depth of 1-100µm. Knoop hardness work on a similar principle with the difference of the diamond indenter having two unequal opposite angles. It uses lower loads of 2-40N with indention depth of 0.30-30µm. The Knoop hardness (KNH) is calculated using by [35]:

$$KNH = \frac{P}{A_p} = 14.22\frac{p}{l^2} \quad (2.\ 2)$$

Where P is the applied load (in kg) and l is the length (in mm) across the long axis of the impression.

Although microindention measurement is a more established technique in the field of dentistry, nanoindentation (NI) is gaining popularity amongst researchers to investigate the mechanical properties of dental tissues, dental lesions and remineralisation [36–38]. Dentine is a mineralised tissue comprised of water, inorganic and organic content. It also has a complex structure that is densely packed with dentinal tubules, therefore the mechanical properties of dentine are influenced by the structural, composition, location of the area tested and external environment, ie dry or wet.

Several studies [39,40] have reported that the elastic modulus decreases by 35% and the hardness decreases by 30% in a hydrated environment, therefore, it is important to consider the environment for research in this field. In terms of the location of testing, dentine has higher hardness and modulus close to DEJ which gradually decreases towards the pulp as it was demonstrated by Wang et al. [41]. This is due to variation in the mineral content at different locations as higher the mineral the higher the mechanics [42].

Nanomechanical properties of dentine reported by 8 different authors are given in table 2.1. It shows that the dentine near the pulp had the lowest H and E ranging from 0.18 to 0.52 GPa and 3.49 to 11.59 GPa respectively. There also was a difference between intertubular and peritubular dentine. Peritubular dentine is more mineralised in comparison to intertubular dentine with reported E of between 40 and 42 GPa, where intertubular dentine has an E of 17 GPa [38]. The H of peritubular dentine was independent of the location and ranged between 2.23 GPa at the pulp to 2.34 GPa at the DEJ. In contract, the H of intertubular dentine varied with location, and the values ranged from 0.12 GPa to 0.18 GPa near the pulp to and 0.49-0.52 GPa at DEJ. Kinney et al [43] also demonstrate that the H and E of dentine decrease with distance from DEJ by using nanoindentation set up.

Table 2.1: Summary of mechanical properties of dentine measured by nanoindentation

Author	Indenter	Condition	Site/ source	Load/mN	Hardness /GPa	Elastic modulus/ GPa
W Franzel et al [22]	Berkovich	Dry	Molar		0.78 ±0.10	22.40 ±2.60
Yi Chen et al [44]	Berkovich	Dry	Middle	3	0.51±0.20	16.25±3.57
Xingguo et al [45]	Berkovich	Dry	Dentine near DEJ Dentine in the middle Dentine of pulp wall	6	0.67 ±0.22 0.66 ±0.23 0.53 ±0.25	19.20±4.3 19.10 ±3.70 16.20 ±2.70
D Ziskind et al [46]	Berkovich	Dry	Intertubular Peritubular	0.3	0.60 ±0.20 1.34 ±0.50	17.40 ±3.50 29.30 ±6.70
Yl Chan et al [47]	Berkovich	Hydrated	DEJ	2	1.00 ±0.10	19.00 ±2.0
Marshall [48]	Berkovich	Hydrated	Intertubular (near DEJ) Intertubular (near Pulp)	50nm depth	0.49±0.02 0.18±0.06	21.70 17.70
Murray et al [49]	Berkovich	Dry	Dentine near DEJ Dentine near Pulp wall	30	0.88±0.032 0.217±0.004	17.9±0.5 3.49±0.07
Joves et al [50]	Berkovich	Dry	Dentine near DEJ	5	0.62±0.05	Not measured

2.4 Demineralisation and Remineralisation Mechanism

The tooth is one of the most mineralised tissues in our body, with hydroxyapatite (HA), $Ca_{10}(PO_4)_6(OH)_2$ as its main component of the inorganic phase. This mineral phase plays a crucial role in providing stability and hardness to the tooth. HA has a hexagonal crystal structure and it is primarily made up of calcium (Ca^{2+}) and phosphate (PO_4^{3-}) with a Ca:P ratio of 1.67 [51]. The HA crystals are highly adaptable with cations and anions readily substituted without distorting the lattice. For instance, Ca^{2+} can be replaced by other cations such as K^+, Na^+, Mg^{2+}, and Sr^{2+} while the hydroxide group can be substituted by F^- or Cl^- [52].

In the oral cavity, teeth are constantly undergoing demineralisation (loss of ions such as Ca^{2+} and PO_4^{3-}) and remineralisation (regaining these ions) processes due to fluctuations of the pH. At natural pH, saliva is supersaturated with Ca^{2+} and PO_4^{3-} ions which is essential for protecting the tooth from continuous dietary acid and acids such as Lactic and Acetic acid produced by bacteria in the mouth from dietary sugar. These acids lower the pH level to 4.5-5.5 within the oral cavity causing the apatite crystals to dissolve until the oral pH returns to normal [53]. The main bacteria responsible for the process of converting sugar into acid is "*Streptococci mutans*" (S.mutants) which also facilitates the formation of dental biofilms. It produces lactic acid by metabolizing sucrose using "*Glucansucrase*" enzyme also known as *"Glucosyltransferase (GTFs)"*. The pH is lowered which consequently demineralises the calcium phosphate in tooth enamel, resulting in tooth decay [54].

More Ca^{2+} and PO_4^{3-} ions are required to reverse the dissolution and return the system to the saturated state. The HA has a "*critical pH*" around 5.5 where an ionic equilibrium exists between the ions in the saliva and tooth structure, hence no dissolution/ precipitation takes place. Demineralisation and remineralisation occur below and above this level respectively [55].

Figure 2.3 shows the correlation between HA precipitation and dissolution at different pH and Ca^{2+} concentration. It is evident that at pH above 8 no dissolution occurs and minimal Ca^{2+} is required for precipitation of hydroxyapatite. As the pH is reduced more Ca^{2+} is required for precipitation and below a pH of around 4, HA dissolves with no remineralization [56].

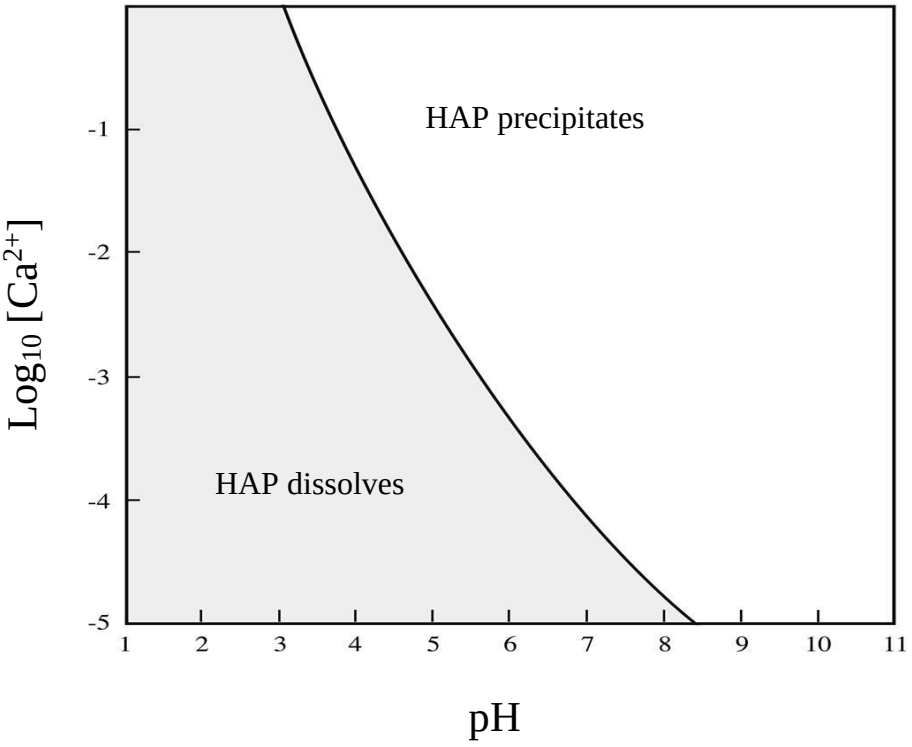

Figure 2. 3: Solubility of Hydroxyapatite at different pH [55]

When the pH drops below the critical level, PO_4^{3-} ions in the oral fluid bind with hydrogen ions (H^+) to form hydrogen phosphate molecules. This causes Phosphate ions from the enamel to moves outwards down the concentration gradient until a new equilibrium is reached, leading to enamel dissolution as represented in the following chemical reaction [57].

$$Ca_{10}(PO_4)_6(OH)_2 + 8H^+ \Rightarrow 10Ca^{2+} + 6HPO_4^{2-} + 2H_2O \qquad (2.3)$$

Demineralisation through acid erosion is of significant concern for the health of the tooth. Loss of Ca^{2+} and PO_4^{3-} ions weaken the structure of the tooth and lower the mechanics, making it more susceptible to dental decay, cavities, discoloration and dental sensitivity.

Nanoindentation has been used to detect remineralisation and demineralisation of dentine by measuring the change in the mechanical properties of the tissue. Chen et al. [44] investigated the ability of calcium phosphate solution to remineralise dentine. The specimens were initially demineralised via etching with 37% phosphoric acid followed by a remineralisation via immersing the discs in a remineralizing solution. EDX was used to monitor the mineral content before and post-treatment. Results showed that sound dentine had an H and E of 0.51 GPa and 16.25 GPa respectively. Demineralisation significantly reduced both properties to 0.03 GPa and 1.32GPa. The result taken after 7 days of remineralization procedure illustrated signs of recovery for both H and E to 0.22 GPa and 6.35 GPa respectively, with further improvement to 0.69 GPa and 15.99 GPa after 30 days. EDX results showed that Ca^{2+} (weight %) dropped from 33.2 to 4.09 after demineralization which later recovered to 28.4 and 36.2 after 7 and 30 days respectively. The same trend was seen for PO_4^{3-} ions (weight %) which dropped from 17.8 to 1.8 then recovered to 13.5 and 19.4 after remineralization.

Hairul Nizam et al. [58] investigated the effect of 30% hydrogen peroxide (HP) bleaching agent which is mainly used for tooth whitening on demineralisation of dentine. Human dentine discs were bleached with hydrogen peroxide for 24 hours and nanoindentation was used to measure the change in H. Results showed that HP lowered the H from 0.7 GPa to 0.4 GPa and E from 22 GPa to 18 GPa. This reduction was explained by the acidic nature of hydrogen peroxide which led to the dissolution of mineral within tooth structure [59].

Murray et al. [49] compared the H and E of sound and decayed dentine in the bovine tooth. Their results showed that the decay had lowered both properties where H was reduced from 0.9 GPa to 0.25 GPa and E decreased from 18 GPa to 4.6 GPa. Another study characterised the change in mechanics of carious dentine in by nanoindentation and a maximum load of 25 mN. The cavity had weakened the structure as was seen by a significant decrease in microhardness compared to the sound dentine with a progressive manner towards the cavity floor from pulp wall.

The H and E ranged between 0.1 GPa to 0.56 GPa and 0.15 GPa to 14.55 GPa, respectively, while those of sound dentine ranged from 0.52 GPa to 0.91 GPa and 11.59 GPa to 17.06 GPa, respectively [60].

To keep the teeth healthy and strong, the demineralisation process needs to be reversed by replacing the Ca^{2+} and PO_4^{3-} ions and remineralising the tissue. Saliva plays a key role in this by acting as a buffering agent and diluting erosive agents such as acid and protecting the tooth by forming a protective protein film called dental pellicle [61]. However, with the consumption of soft drinks that have a high concentration of phosphoric and citric acid or the processed food which are high in sugar and starch on the rise, the saliva alone cannot prevent or reverse the demineralisation process. Some patients also suffer from dry mouth or low salivary flow which makes it more difficult for a natural remineralisation process.

A number of materials such fluoride, amorphous calcium phosphate (ACP), calcium silicate, hydroxyapatite or bioactive glasses (BAG) have been used to help with the remineralisation process by providing an additional source of the ions necessary to return the tooth to a healthy state [62,63].

Remineralisation effect of 45S5 BAG on demineralised human dentine was assessed by Vollenweider et al. [64]. The study used a combination of different techniques such as Raman Spectroscopy, SEM and EDX to detect any apatite formation and mineral change after treatment with the BAG. They also compared nano-sized (30–50 nm) and micro (90–710μm) BAG particles. The existence of phosphate peak associated with apatite showed that regardless of the size BAG was capable of forming an apatite. However, as the nano BAG has a higher surface area it formed apatite at a much faster rate (after 24 hrs) and the release of Ca^{2+} and PO_4^{3-} ions was 20 times faster than the micro BAG when mixed in water.

Wang et al. [65] looked at the remineralisation effect of 45S5 on EDTA demineralised human dentine after 1, 3 and 7 days using FTIR, XRD and SEM and EDX. The peak associated with PO_4^{3-} ions increased with a number of treatment days. EDX showed that the mineral concentration increased from day 1 to day 7. XRD confirmed apatite formation with peaks similar to the ones seen in the dentine.

2.5 Dentine Hypersensitivity (DH)

Dentine hypersensitivity is a neurological response to external stimuli in the oral environment which lasts from few seconds to a couple of minutes caused by exposure of dentine tubules as the result of gum recession or damage to the protective enamel [1]. Stimuli such as pressure, temperature and osmotic, alters the fluid flow within the tubules, distorting the nerves in the pulp and initiating a neurological response. This is known as hydrodynamic theory described by Brannstromin 1963 [66].

Consumption of sugary, salty and acidic food that are considered high osmotic stimuli, can also change the fluid within the dentine tubules [67]. Alteration of the fluid flow causes an electrical excitation of the nerve ending within the pulp. Nerve cells within the inner membrane are negatively charged and are surrounded by passively charged ions such as Sodium (Na^+) and Potassium (K^+). Under rest conditions, the concentration of K^+ ions are higher within the cell and the concentration of Na^+ is higher outside of the cell. The stimuli alter the ionic balance that would otherwise exist under normal conditions, causing the diffusion of K^+ from the cells down the concentration gradient and influx of sodium ions through the cell membrane, irritating the nerve endings causing pain [68].

The Schematic diagram below (figure 2.4) summaries the mechanism of dental hypersensitivity.

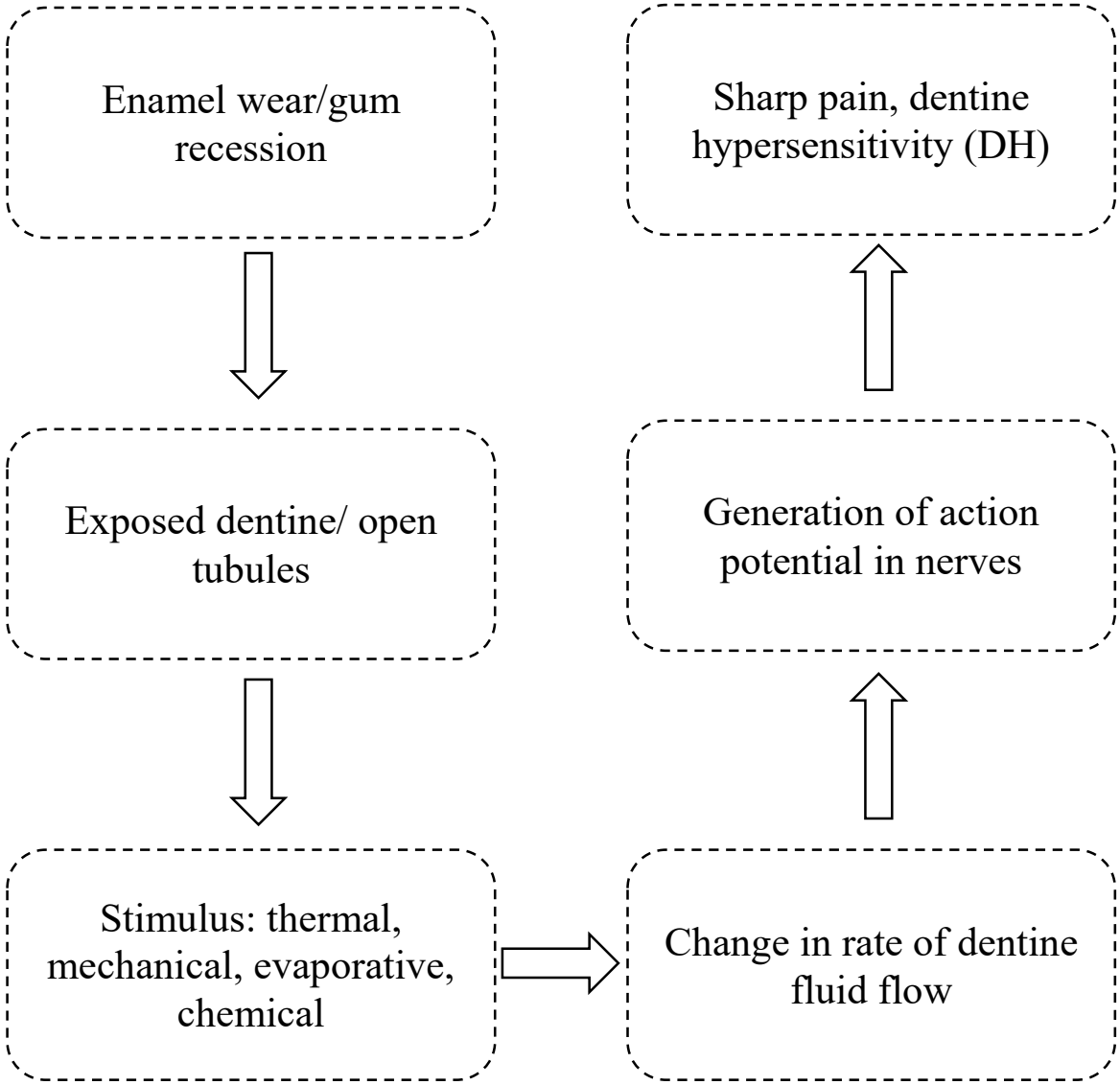

Figure 2. 4: Schematic diagram of DH mechanism

2.6 Causes of Dentine Hypersensitivity

Sensitivity occurs when dentine tubules become exposed. This occurs when the protective enamel layer is either lost due to tooth wear or gum recession which could be because of poor dental hygiene, excessive and aggressive brushing or acid erosion. Tubules are covered by a smear layer made up of a mixture of hydroxyapatite and collagen, acidic conditions in the oral environment can rapidly dissolve this smear layer and open up the tubules. This smear layer can be dissolved within 3 minutes under in vitro conditions Dental dentifrice can also remove this smear layer via the abrasive particles incorporated in them for removing plaque and stains [69].

2.6.1 Enamel Wear

Enamel wear is associated with the non carious loss of enamel surface as a result of erosion, abrasion, attrition, and abfraction. Figure 2.5 represents these 4 types of enamel wear; a) loss of tooth tissue along the gingival margin as a result of abfraction, b) acid erosion, c) exposed facial root surface due to abrasion, d) enamel loss due to attrition

Figure 2. 5: Enamel wear through abfraction (a), acid erosion (b), abrasion (c) and attrition (d) [70,71]

2.6.1.1 Erosion

Acidic dissolution of the enamel mineral results in the erosive wear of the tissue. Erosive wear is the most common cause of enamel loss due to an increase in consumption acid and sugary food and drinks [72]. Several factors contribute to the level of wear through acid erosion: the pH, contact time with the tooth and availability of saliva. Enamel loss through acid erosion can be described as recoverable and non-recoverable. Enamel softens when it comes in contact with acid due to loss of the minerals, saliva is known to act as a buffering agent and increase the pH, replacing some of the lost calcium and phosphate ions [73]. However, as it was discussed in section 2.4 if the amount of demineralisation exceeds the remineralisation the enamel loss becomes unrecoverable.

2.6.1.2 Abrasion

Foreign particles in dietary and dentifrice products cause abrasive wear via a mechanical process known as three-body wear when they repeatedly come in contact with the tooth [72]. As well as removing bacteria and breaking up dental plaque, toothpaste is used to improve the appearance of the tooth and remove stains. To do this, historically toothpaste contained insoluble abrasive particles such as silica, calcium carbonate, calcium phosphate and aluminium oxide. Particle hardness, size distribution and the shape are the most common factors influencing abrasive capability [74].

Kodaka et al. [75] investigated the effect of toothpaste containing silica as the abrasive particle used for sensitive teeth. Dentine discs were mounted on to an intra-oral appliance and exposed to the oral cavity and brushed for 1 minute per day. The degree of wear was measured using scanning laser microscopy. Results showed that 80 and 140 μm were removed from the dentine after 4 and 8 weeks respectively. This is a significant amount of wear as the average thickness of the human dentine is 3000μm [76] and to lose over 4% of the dentine under 2 months is concerning for the patient. Another study by Philpotts et al. [77] showed that toothpaste containing hydrated silica caused 7.13 μm wear to human dentine after 6 minutes of brushing.

It is essential to protect the dentine against abrasion wear or risk significant tooth loss which would lead to further complication and eventual loss of the tooth. Relative Dentine Abrasivity (RDA) or Relative Enamel Abrasivity (REA) are numeric scales used by the International Standard Organisation and are useful tools to compare between different toothpastes. Current American Dental Association (ADA) index recommended limit is 250 for RDA [78]. The limit is determined experimentally by calculation of a ratio relative to a reference abrasive.

To assess the reference abrasivity, dentine specimens are brushed in a so-called "*sandwich*" technique, i.e. they are first brushed with a slurry of the reference standard, then with a slurry made from the experimental product, and then again with a standard slurry. The common abrasive standards are calcium pyrophosphate and more recently silica [79]. The mass loss of the two brushing sequences with standard slurry is averaged and arbitrarily given the value 100. The data of the experimental product brushed in between is expressed as a percentage of the above standard value (Eq 2.4). For example, an experimental product with only half the abrasive power of the standard would have an RDA of 50. Range of RDA and their correspondence meaning in terms of abrasivity is given in table 2.2 [80,81].

$$\text{RDA} = \frac{\text{Mean abrasion of dentine by test dentifrice}}{\text{Mean abrasion of dentine by reference dentifrice}} \text{x}100 \qquad (2.4)$$

Table 2.2: RDA values set by the American Dental Association ADA

0-70	Low abrasivity
70-100	Medium abrasivity
100-250	High abrasivity

2.6.1.3 Attrition

Attrition is a two-body type of tooth wear caused by enamel to enamel contact through mechanisms such as bruxism (grinding) or clenching of the jaw where the surface of the opposing teeth come in contact with each other [78]. Attrition can further be described by adhesion and fatigue wear. When enamel sides over enamel in the attrition process, fragments of enamel can be transferred from one surface to another due to the presence of friction, leading to asperities on the surface. Fatigue wear can also result from the repeated compressive forces exerted on to the enamel surface when one surface slides over another. This would lead to Plastic deformation, cracks formation and propagation in the subsurface. These cracks eventually propagate to the surface of the enamel over time and enamel surrounded by the cracks is lost. This would produce rough and irregular enamel surface which would further potentiate attrition. The wear debris produced by adhesion and fatigue wear would change the two body wear into a three-body wear mechanism (abrasion) [82].

2.6.1.4 Abfraction

Finally, enamel can be lost due to cracks caused by a combination of compressive stress on the side which tooth bends and tensile stress on the other side from mastication. Micro-fractures are initiated in the enamel which propagates as a result of the load cycle on the tooth which eventually fail, this is called abfraction [83]. A clinical study conducted over 4 years used stereomicroscopy, impressions taken from patient's mouths and computer modelling to quantify the tooth wear and the results showed that on average a person loses 29 µm and 15µm from their molar and premolar teeth a year due to this type of wear [84].

2.6.2 Gingival Recession

Gingival recession is the process where the gum tissues surrounding the tooth is either detached or worn away exposing the root of the tooth. This creates gaps known as "pockets" between the tooth and the gum line. Food particles and bacteria build up in this pocket and if left untreated can cause severe damage to the bone attached to the tooth and eventually cause tooth loss. Gum recession occurs as a result of poor oral hygiene, aggressive tooth brushing and periodontal diseases. It is the most common cause of DH as cementum is eventually lost and dentine tubules exposed [85].

2.7 Treatment of Dentine Hypersensitivity

As was explained previously the sharp pain of sensitive tooth is associated with the fluid flow within tubules know as the hydrodynamic theory which stimulates the nerve ending. Therefore to treat dentine hypersensitivity (DH) symptoms the excitation of nerve ending needs to be prevented. This can be achieved by techniques and therapies ranging from dentists applied restorative treatments such as applying fluoride varnish and dental sealants to over the counter product such as gels, toothpastes, and mouthwash.

Over the counter product are easy to use, ideal for the treatment of mild DH and are divided into two categories [86]:

1) Products that interfere with the transmission of neural signals through the pulp.

2) Products that occlude tubules by either forming precipitation on the tooth surface or plugging the open tubules with occluding material.

Products belonging to group one consist of a potassium nitrate salt, K^+. This active ingredient is depolarising in nature and lowers the activity of sensory nerves by diffusing into the tubules and blocking the neurotransmission to the nerve endings [87].

Group 2 reduces sensitivity by occluding the tubules which block the fluid flow in the tubules. Poiseuille's law of fluid flow (Eq 2.5) describes the relationship between the size of the tubules, the number of exposed tubules and the pressure of fluid flow. This relationship shows that the rate of fluid flow is directly proportional to the radius (tubule opening) of the exposed tubule to the power of 4. Sensitive teeth have many more exposed tubules with bigger radius compared to non-sensitive teeth. Occluded tubules have a radius close to zero which would mean the Fluid flow, Q would also be zero regardless of other parameters [88].

$$Q = \frac{\pi r^4 P}{8VL} \tag{2. 5}$$

Where Q is the fluid flow, r is the radius of an exposed dentine tubule, P is the pressure,V is the dynamic viscosity and L is the length.

There are a number of active ingredients such as strontium, fluorides, stannous fluoride, calcium silicate, bioactive glasses and arginine currently used in dentifrices to occlude exposed tubules by either depositing an HA like layer on the surface or plugging materials down the tubules. Several in vitro studies [13,16,89–92] demonstrated that these materials were highly effective in occluding tubules and the layers were rich in calcium and phosphorus which can promote tooth remineralisation. Table 2.3 summarises the methodology and findings of these studies.

The suitability of these materials for treating DH is judged on their ability to resist the harsh oral environment such as constant fluctuation of pH, react in short space of time to provide rapid relief and the depth of penetration down the tubules. As well as treating DH the layers formed by these materials need to be mechanically robust to provide a protective barrier to the dental tissue minimising further wear and damage.

Table 2. 3: In vitro studies demonstrating the effectiveness of CSPS, arginine and calcium silicate in occluding tubules

Author	Aims and objectives	Techniques used	Findings	Limitations
Gillam et al [89]	To assess the suitability of 45S5 bioactive glass for tubule occlusion in toothpaste at various concentrations (0.00%, 2.5% and 7.5%)	• Scanning electron microscope (SEM)	• Inclusion of bioactive in the toothpaste formulation resulted in greater tubule occlusion compared to the control • The toothpaste with a higher concentration of bioactive glass occluded a significantly higher number of tubules compared to 2.5%	• Only SEM was used, further elemental characterisation missing
Earl et al [16]	To characterise the tubule occlusion of NovaMin to treat dentin hypersensitivity	• SEM • Focused ion beam (FIB) • Energy dispersive x-ray spectroscopy (EDS)	• A layer was formed on the treated dentin samples occluding tubules. • Chemical and structural analysis showed that it was hydroxyapatite-like	• FIB was time-consuming • Volume was limited • Depth of occlusion not known
Mahale et al [90]	To evaluate the effects of Novamin, Arginine and Strontium chloride on dentinal tubule occlusion	• SEM	• Arginine and Strontium chloride occluded the tubules • NovaMin resulted in partial occlusion.	• Characterization of apatite only by SEM
Wang et al [91]	To evaluate the tubule occlusion and acid resistivity of Novamin and Arginine	• Hydraulic conductance • SEM	• Both materials occluded tubules by forming a layer on dentine surface • tubules were still occluded after citric acid challenge • No significant difference was reported between both materials	• No structural characterisation was carried out
Litkowski et al [92]	To evaluate the effectiveness of NovaMin to treat HD in vivo	• Clinical • Sixty-six subjects with dentin hypersensitivity • The intensity of sensitivity was recorded on a visual analogue scale	• Reduction in sensitivity was recorded in the treated group compared to the control group	• Clinical data are subjective
Gandolfi et al [13]	To assess the effect of calcium silicate on dentine permeability	• Hydraulic conductance • SEM/EDX	• Dentine permeability was reduced after application of calcium silicate	• Depth of occlusion not studied • No acid challenge test

2.8 Bioactive Glass (BAG)

In 1969 Professor Larry Hench suggested that a silica based material containing the same minerals as hydroxyapatite, such as calcium and phosphate ions, would not be rejected by the body and could be used to repair damaged bone. Before this, it was common to use inert biomaterials, however, the formation of fibrous tissue resulted in a relatively high failure rate for these materials after implantation [93]. Using this theory he developed the first bioactive glass (BAG) called "45S5" or more commonly referred to as just bioglass®. It is made up of SiO_2, P_2O_5, CaO and Na_2O (the composition is shown in table 2.4). The most common manufacturing technique for bioglass is by melt derive where the oxides are mixed, heated to a high temperature of around 1400 C^o and annealed (slowly cooled) [8].

Table 2.4: Composition of "45S5" Bioactive glass

Glass	**SiO_2**	**Na_2O**	**CaO**	**P_2O_5**
wt. %	45	24.5	24.5	6
Mol %	46.13	24.35	26.91	2.6

2.8.1 Structure of Bioactive Glass

Bioactive glasses are amorphous materials with random structures whose atoms lack order and the degradation rate is largely dependent on the structure of the glass. Therefore when trying to explain the structure of the glass the conventional structure concepts such as unit cell and lattice vectors cannot be used. The silicon atom is the network former and has a tetrahedral structure with a coordination number of four where the silicon atom is at the centre of the structure surrounded by 4 oxygen atoms held together by strong covalent bonds [94].

The silicon is connected to other silicon atoms via oxygen atoms known as bridging oxygens (BO), although non-bridging oxygen atoms (NBO) are also present in the structure. The distribution of BOs in the tetrahedral unit is described by quantity denoted Q^n where Q is quaternary and n is the number of BO atoms. Q^n ranges from 0. (Single isolated unit with no BO atoms) to 4 (3D networks of tetrahedral silicon atoms.

- Q^4:4 BO, 0 NBO per silicon
- Q^3: 3 BO, 1 NBO per silicon
- Q^2: 2 BO, 2 NBO per silicon
- Q^1: 1 BO, 3 NBO per silicon
- Q^0: 0 BO, 4 NBO per silicon

A mixture of Q structure can be present within a glass structure. Addition of modifying oxides lower the Q^n by replacing the BO with NBO. Figure 2.6 demonstrates the Q^n for NBOs where black and blue represent bridging and non-bridging oxygen atoms respectively.

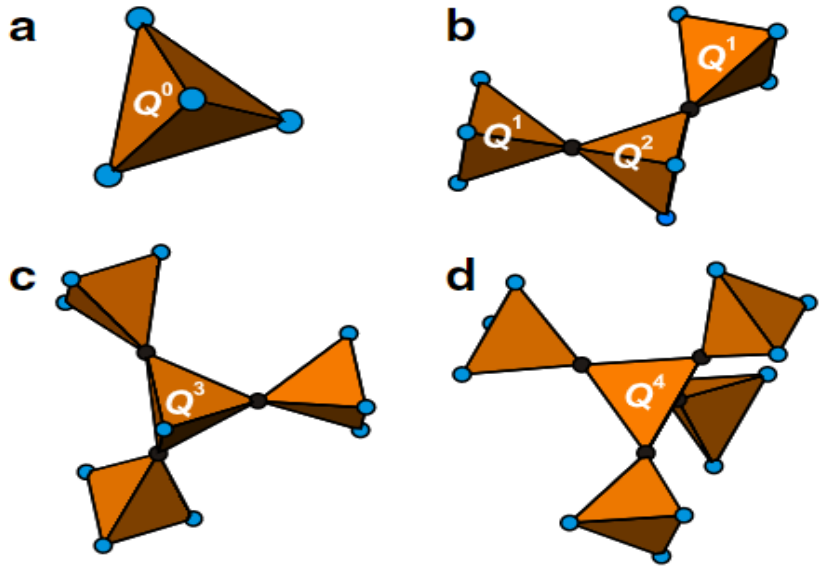

Figure 2. 6: Illustration of the Q^n, (a) Q^0 "Isolated" tetrahedron, (b) Q^2 unit bonded to two Q^1 terminal tetrahedra. (c) central Q^3 and Q4 (d) tetrahedron connected to Q1 units [95]

The role of each atom within the glass structure can be divided into 3 different categories known as network formers, network modifiers, and intermediates.

- Network former: Can form a glass network alone - Strong covalent bonding (Si^{4+}, B^{3+}, P^{5+})
- Network modifier: Break the linkages between network formers - More ionic bonding (Na^{+}, Ca^{2+})
- Intermediates: behaves like a network former but cannot form a network alone (TiO_2, Al_2O_3)

Figure 2.7 represents a schematic structure of glass with the addition of sodium (Na^{+}) and calcium (Ca^{2+}) ions which are the two most common network modifiers. The red oxygen atoms demonstrate the BOs. Structure (a) is a glass with three Si chains that are not linked covalently to the rest of the structure and therefore possess a high dissolution rate, compared the structure in (b) which has more silica in its structure that are covalently bonded through the addition of Si-O (blue).

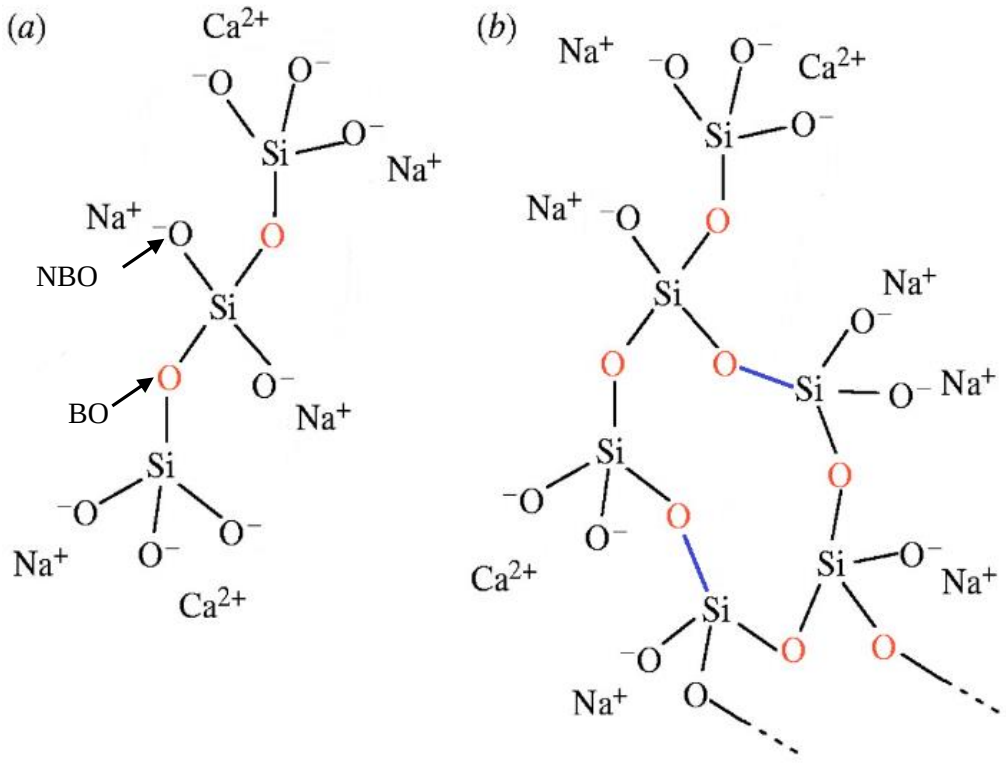

Figure 2. 7: Schematic diagram of the chemical structure of Bioglass [96]

2.8.2 Network Connectivity

The network connectivity (NC) is another way to characterise the glass structure. It measures the average number of BO on each tetrahedron and describes the level of cross-linking of the glass network. NC is a useful tool in predicting the bioactivity of bioactive glasses. NBO carry a negative charge and the glass network becomes more depolymerised with increasing the number of NBO. Network modifiers such as Na^+ or Ca^{2+} are positively charged ions and distort the structure by providing NBO atoms. An ionic bond is formed between these ions and NBO in the glass structure which is much weaker than the covalent bonds. This lowers the network connectivity and increases the dissolution of the silica network [97,98].

The rate at which bioactive glasses are dissolved in body fluid is governed by the NC of the silica, which is in turn dependent on the composition. The NC is dependent on the number of BO atoms per silicon atom as it measures the number of BO molecules for every SiO_4 and provides information on the degree of crosslinking of the structure [99]. NC is calculated by:

$$NC = 2 + \frac{BO - NBO}{G} \qquad (2.\ 6)$$

Where BO is the sum of bridging oxygen atoms, NBO is the sum of non-bridging oxygen atoms per network modifier and G is the sum of glass-forming components.

The NC for 45S5 Bioglass® can be calculated as follows [98]:

$$\mathrm{NC} = 2 + \frac{[(2\mathrm{xSiO_2}) + (2\mathrm{xP_2O_5})] - [(2\mathrm{xNa_2O}) + (2\mathrm{xCaO})]}{[\mathrm{SiO_2} + (2\mathrm{xP_2O_5})]} \qquad (2.\ 7)$$

Given the composition (in mol %) is made up of 46.13 SiO_2, 24.35 Na_2O, 26.91 CaO and 2.6 P_2O_5

$$NC = 2 + \frac{[(2 \text{ x } 46.13) + (2 \text{ x } 2.6)] - [(2 \text{ x } 24.35) + (2 \text{ x } 26.91)]}{[46.13 + (2 \text{ x } 2.6)]} = 1.9 \qquad (2.\ 8)$$

However in melt derived bioactive glasses phosphorus is believed to be only present as orthophosphate, PO_4^{3-} with no BO (Q^0) therefore is not part of the glass-forming component. Therefore the calculation needs to be modified:

$$NC' = 2 + \frac{[(2 \text{ x } SiO_2)] - [(2 \text{ x } Na_2O) + (2 \text{ x } CaO) + (2 \text{ x } P_2O_5 \text{ x } 3)]}{[SiO_2]} \qquad (2.\ 9)$$

$$NC' = 2 + \frac{[(2 \text{ x } 46.13)] - [(2 \text{ x } 24.35) + (2 \text{ x } 26.91) + (2 \text{ x } 2.6 \text{ x } 3)]}{[46.13]} \qquad (2.\ 10)$$

$$= 2.22$$

As NC increases there will be more Si-O-Si bonds to break, thus the network will depolymerise more slowly, significantly reducing the amount of HA formed. It has been suggested that the level of depolymerisation associated with an NC of approximately 2 is ideal for bioactivity [52].

Fujibayashi et al [100] investigated the relationship between in vivo bone growth and in vitro apatite formation of 5 different silica based P_2O_5 free Na_2O-Ca-OSi_2O bioactive glasses. The result showed as the SiO_2 content increased from 50% mol to 70% mol, both bone growth and apatite formation decreased significantly with no apatite formation for the glass with 70% mol SiO_2 due to the higher NC for the glass with higher silica content. Higher NC lowers the dissolution rate of the glass network, subsequently slowing down the release of calcium and phosphate ions.

Their data on network connectivity of bioactive glasses vs the number of days it took for apatite to form was plotted (figure 2.8) and based on their findings network connectivity of around 2 was recommended for optimum reactivity [101]. Hill [99] also suggested NC of 2 for bioactive glasses, while Eden [95] reported NC in a range of 2.0 and 2.6.

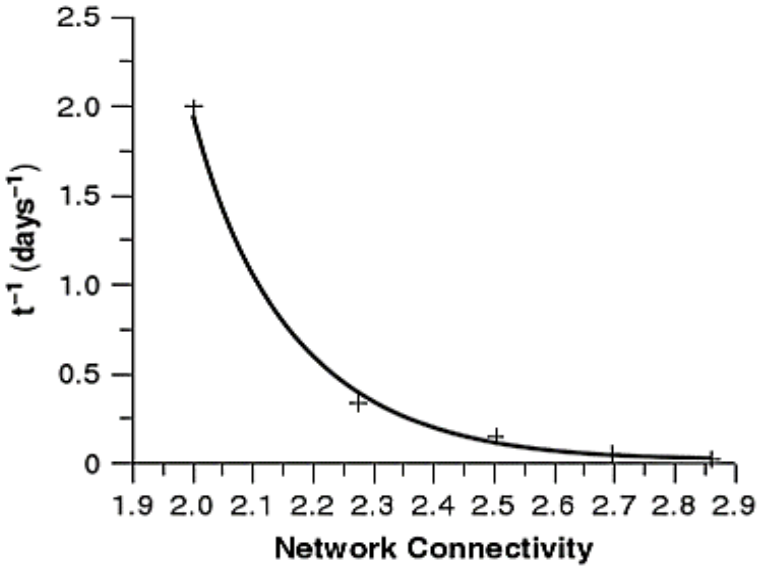

Figure 2. 8: Effect of NC on the rate of apatite formation in simulated body fluid [101]

2.8.3 Composition on Bioactivity

Approximately 65% of bone is made up of minerals in the form of hydroxyapatite (HA) and BAG provides the mineral necessary to form an HA-like layer on the damaged bone that can interact with the exposed collagen fibres [102]. To achieve a BAG that readily bonds to the bone and bone-like material such as dentine, the composition should contain (region A on figure 2.9) [103]:

- 35-60 mol% SiO_2,
- 10-50 mol% CaO
- 5-40 mol% Na_2O
- 4 to 11 wt% P_2O_5

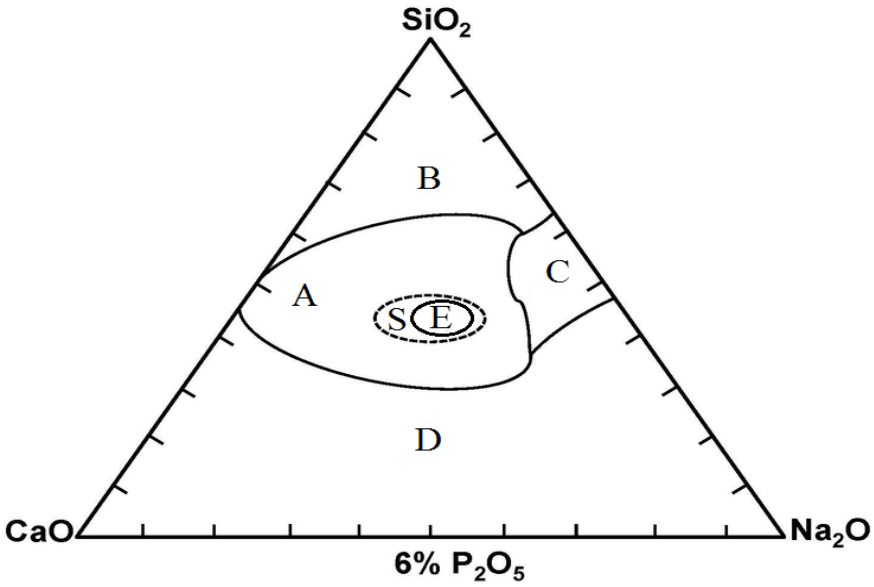

Figure 2. 9: Composition map of calcium sodium phosphosilicate glass [104]

A= Bone Bonding

B= Non-bonding, low reactivity

C= Non-bonding, high reactivity

D=Non-bonding, no glass formation

S= Soft tissue bonding

E= Bioglass® composition

In reference to figure 2.9, Glass with compositions that fall in region B are bio-inert and will not break down or generate HA as a result of high silica content. This is due to the silica network being highly dense and unreactive in the presence of physiological fluid. If the composition falls in region C, the increased sodium to silica ratio results in a distorted network by increasing the number of NBO, making it prone to dissolution in physiological environments, so the glass will resorb within 10 to 30 days. If the silica content drops below 35 wt% as in region D, a glass network can no longer be formed [103].

Addition of other elements will modify the network reducing the number of oxygen atoms connected to two silicon atoms. Therefore 1 or more oxygen atoms become non-bridging. This can explain why there is no glass formed in regions C and D of the glass phase diagram (figure 2.9) where due to a high quantity of sodium and calcium ions there is a large number of non-bridging oxygen atoms [52].

2.8.4 Hydroxyapatite Formation Mechanism

Degradation mechanism for BAG relies on an ionic exchange process. On exposure to body fluid, there is a rapid ionic exchange between the BAG and the fluid where Na^+ from the glass are swapped with hydrogen ions (H^+) from the fluid, this lead to a net negative charge on the surface and local increase in the pH. This ion swap facilitates the breakdown of the silica network, forming a silica-rich layer at the collagen interface which acts as the nucleation site for the reaction. Subsequently, Ca^{2+} and PO_4^{3-} ions are attracted to this silica-rich layer on which they precipitate, forming an amorphous layer of calcium phosphate ($CaO\text{-}P_2O_5$).

A further attraction of these ions from the surrounding solution allows the development of this layer. Within 3-6 hours this layer is crystallised into a hydroxyapatite layer by incorporation of OH^- ions, also from the surrounding solution. This layer is chemically and structurally similar to the mineral found in bone and it is described as the "*bonding layer"* [105]. The described reaction takes place within 12- 24 hours of the implant being inserted and the tissues start to attach to this layer therefore osteogenic cells do not recognise this as a foreign material.

This is a continuous mechanism over a long period which facilitates direct bonding between the material and bone which subsequently repair the damaged bone. In the oral cavity, BAG undergoes a similar mechanism (figure 2.10) which facilitates the formation of an HA like layer on the tooth surface [106].

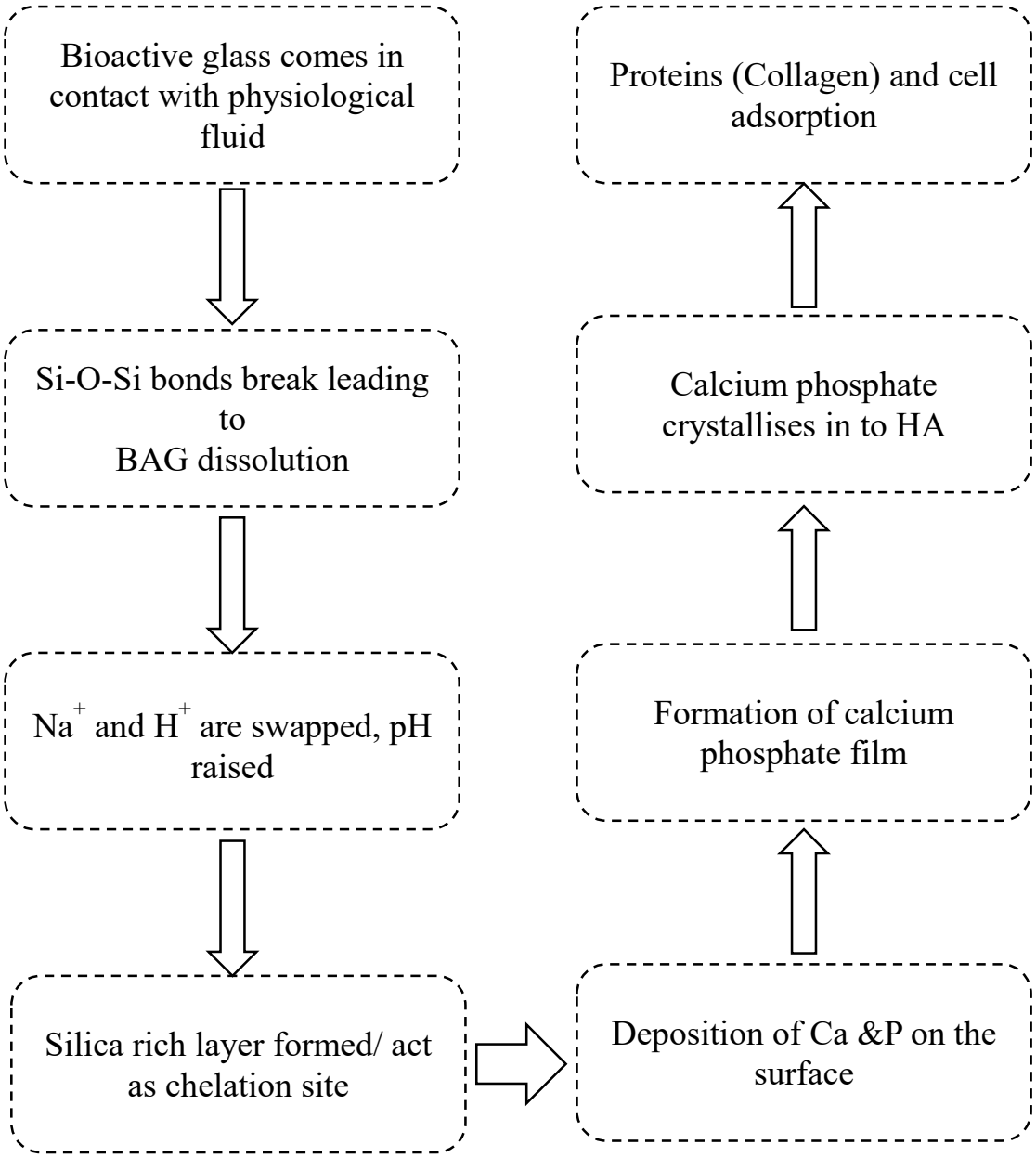

Figure 2. 10: Mechanism of bioactivity for bioactive glasses [105]

2.9 Characterisation Of the HA Layer

Different techniques have been used to examine the formation of apatite as well as morphological and elemental changes to the dental tissue after reaction with bioactive glasses. These include Scanning electron microscopy (SEM), Energy dispersive X-ray spectroscopy (EDX), X-ray diffraction (XRD), Raman spectroscopy, Fourier-transform infrared spectroscopy (FTIR) and Nuclear magnetic resonance (NMR).

2.9.1 SEM and EDX

SEM and EDX have been commonly used to assess the ability of BAG to form an HA like layer and monitor any elemental changes after the treatment. Forsback et al. [107] characterised the formation of hydroxyapatite on dentine after reaction with an S53P4 bioactive glass by SEM and they reported a layer formation after 14 days of treatment. A number of other studies [108–110] also used SEM and EDX to confirm tubule occlusion and apatite formation by BAG. Their results revealed more Ca^{2+} and PO_4^{3-} ions on the surface of dentine.

Wang et al. [65] evaluated the dentine remineralisation induced by BAG modified with soda lime particles. Dentine discs were initially demineralised by EDTA followed by application of BAG and immersion in artificial saliva for 1, 3 and 7 days. SEM images demonstrated complete coverage of the dentine tubules while EDX showed a gradual increase in phosphate peak at different time points up to day 7 on treated groups compared to the control. The mineral matrix ratio also showed that treated groups resulted in increasing mineral concentration from day 1 to day 7 relative to the control.

2.9.2 XRD

X-ray diffraction is a useful technique for determining the crystallographic structure and crystallite size. The system consists of an X-ray tube, a sample holder and a detector. X-ray is generated by heating a filament to produce electrons that are accelerated towards the sample by application of a current to give electrons sufficient energy. When X-ray interacts with the sample atoms or set of planes, it produces a diffracted ray, directions and intensities of reflect incident X-rays varies for each plane. The diffracted rays from a crystalline sample are separated by interplanar distance d and is calculate by Bragg equation [111]:

$$n\lambda=2d \sin \theta$$

Where n is the "order" of reflection, λ is the wavelength of the incident X-rays, d is the interplanar spacing of the crystal and θ is the angle of incidence. Multiple diffraction measurements are taken by rotating the beam and the detector at an angle of θ and 2θ respectively and the scattered incident X-ray beam at each of these angles will correspond to a different atomic spacing and crystal orientations.

XRD has been used to characterise the layer formed by BAG and to confirm whether the layer has been crystallised. Wang et al. [65] used XRD with scanning angles of 20° to 55° to confirm the formation of apatite on dentine disc by a BAG. Macon et al. [112] used this method to evaluate the effect of fluoride ions on the formation of apatite by calcium sodium phosphosilicate containing toothpaste. The diffraction was measured between 10º and 60º 2θ, with a 0.03ºstep size.

The results in these two studies showed crystalline sharp peaks at 26º and 32º as well as other peaks (47º, 50º, 53º) which match the standard for hydroxyapatite (ICSD 01-084-1998). Mneimne et al [9] also used the same testing conditions to determine the apatite formation of high phosphate fluoride-containing bioactive glasses. They also successfully used this technique to draw a comparison between the degrees of crystallinity of different glasses.

2.9.3 Raman Microscopy

Raman spectroscopy is a light scattering technique where an incident laser light interacts with a surface of a sample, exciting the molecules. Vibration motion of the molecules lead to a small amount of light losing energy and being scattered at longer wavelengths. The difference between the energy of the scattered and incident light (the molecular vibration energy (ΔE)) corresponds to a molecular vibration and lead to bands at specific characteristic frequency shift in the Raman spectrum. The intensity of the Raman peaks is proportional to the number of molecules within the volume of the scanned area [113].

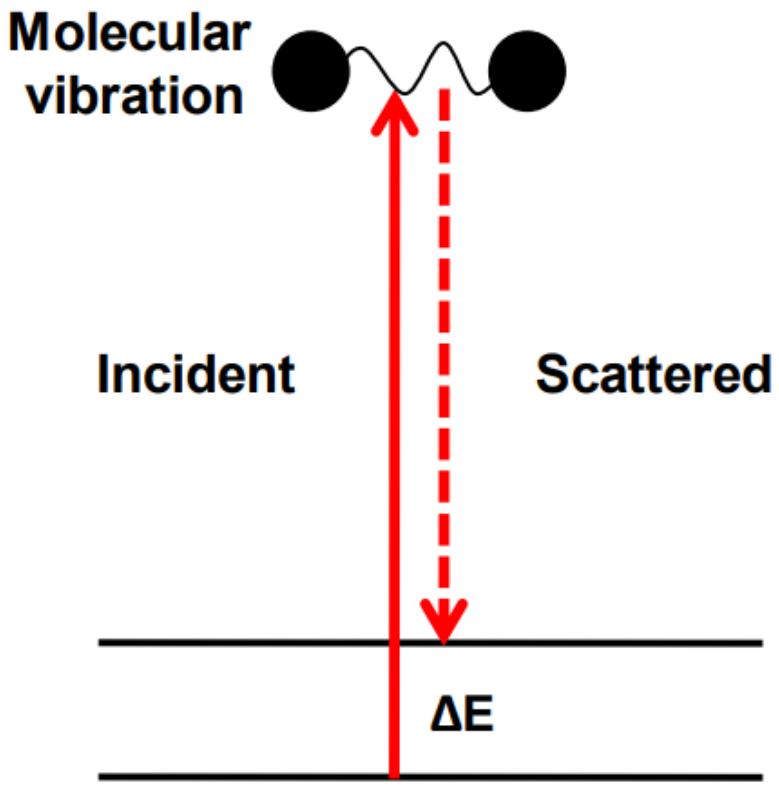

Figure 2. 11: Principle of Raman scattering [114]

The phosphate groups in hydroxyapatite would produce characteristic vibration bands at approximately 433 cm^{-1} (v_2, symmetric bending vibrational mode), 579 cm^{-1} (v_4, asymmetric bending vibrational mode), 960 cm^{-1} (v_1, symmetric stretching vibrational mode) and 1043 cm^{-1} (v_3, asymmetric stretching vibrational mode), with the most prominent peak at~960 cm^{-1} which is associated with the tetrahedral PO_4^{3-} [115,116].

2.9.4 ^{31}P NMR

Solid-state NMR is a useful characterisation technique used for probing the structure of the nuclei of the materials and is used to study biological structures at the atomic level. Hydroxyapatite mainly consists of calcium, phosphorus, oxygen, and hydrogen, each of which has an isotope that can be studied by NMR. In particular, ^{31}P NMR has been used to detect the formation of HA from bioactive glasses at different soaking intervals in SBF [117–119]. The HA features a broad signal around 3ppm which is associated with the calcium orthophosphate phase of the HA. A weak initial signal at around -6ppm was also reported as the result of P-O-Si bonds which diminished rapidly after 24 hrs of SBF reaction. These findings were in agreement with Hammami et al.[120] who tested synthetic HA with ^{31}P NMR, their spectra had a single peak at around 2.8 ppm relative to $H_3PO_4^{3-}$ similar to the phosphorus peak found in bone and teeth. A recent study by Kanwal et al.[121] investigated the ability of calcium sodium phosphosilicate BAG to form apatite in artificial saliva by ^{31}P NMR. The ^{31}P MAS NMR showed a broad peak with the position at 3.6 after 1 hour of immersion. The full width at half maximum (FWHM) of the peak started to reduce as the immersion time increased and subsequently giving a sharp peak at 2.9 ppm after 4 days, which is assigned to an appetite-like phase. They combined these results with XRD, FTIR, and measure of Ca and P concentration of the artificial saliva. The XRD patterns and FTIR absorption bands supported the apatite formation while a decrease in Ca and P concentration is indicative of precipitation of calcium phosphate. There was a hypothesis that fluroapatite (FAP) might be formed due to the presence of sodium monofluorophosphate. This would be preferential as FAP is more acid resistant and would protect the dental tissue against the constant fluctuation of pH in the oral environment [122]. This was further investigated by ^{19}F which showed partial formation of FAP with a peak at -104 ppm. These studies have demonstrated that NMR is a useful technique in investigating the formation and type of apatite.

2.9.5 FTIR

FTIR is a technique commonly used to identify compounds and their structures. The spectra consist of characteristic absorption bands at known IR wavelength which corresponds to functional groups of material. A beam of IR light containing various frequencies greater than 600 GHz is passed through a beam splitter which sends the light in two directions, to a stationary mirror and a moving mirror. The light is refracted back to the beam splitter from the mirrors, recombines and passes through the sample and reaches the detector [123].

Depending on the distance between the moving mirror and the beam splitter a different wavelength of light is reflected and is passed through the sample. This produces a wave pattern called interferogram which is the raw data of light absorption for each mirror position. If the IR at certain wavelength gets absorbed by the sample then the intensity of the interferogram for that particular wavelength will decrease and alters the interferogram that is detected by the detector. Fourier transform (FT) is then used to process the raw data into intensity against frequency [123].

FTIR is a useful tool in investigating the amount of HA present. It is can also be used to monitor the transition from amorphous HA into a crystallised HA. Like Raman spectra, the HA produces unique peaks at 1240, 1027, 603 and 500 cm^{-1} which are associated with the vibration of the covalent bonds within the PO_4^{3-} ions. The transition into a crystallised HA is accompanied by a gradual splitting of the 600 cm^{-1} phosphate band (ν4, in-plane bending). This splitting can be used to calculate the crystallinity in the form of an index, CI_{FTIR} which is described in more detail in section 4.2.8 [124].

It also has been used to assess the apatite formation by different bioactive glass compositions. Mneimne et al [9] investigated the rate of apatite formation by fluoride-containing bioactive glasses with different phosphate content. Si-O resulted in a peak at 920 cm^{-1} for unreacted bioactive glasses. After 7 days of immersion in the Tris buffer solution, this band disappeared and a new peak formed at 560 cm^{-1} that corresponds to P–O bonding vibrations in a PO_4^{3-} and indicates the presence of crystalline calcium phosphates. They also showed that higher phosphate content in the glass increased apatite formation.

FTIR can also be used to investigate the effect of caries on the mineral content of dentine and was successfully used by Liu et al [125] who took several 2 μm thick dentine films from sound and demineralised dentine discs by using a microtome. These slices were then placed on a 13mm diameter, 1mm-thick barium fluoride (BaF_2) disc. To ensure the flatness of the films, one additional BaF_2 disc was used to sandwich each film. The slices were then characterised over the infrared region of 2000–720 cm^{-1} and a spectral resolution of 16 cm^{-1} with 8 scans per pixel. The results showed peaks at ~1,035 cm^{-1} and ~872 cm^{-1} which corresponds to phosphate ν_3 vibration and carbonate ν_2 vibration respectively. The intensities of these peaks were lower for the demineralised samples. The infrared region used by Liu et al. [125] was not broad enough to capture the 603 and 500 cm^{-1} peaks.

2.10 Bioactive Glass (BAG) as an Active Ingredient in Toothpaste

In vitro studies had shown that bioactive glasses have a strong affinity towards the collagen content of the bone. As dentine is chemically similar to bone it was assumed that bioactive glasses would also appropriately interact with the surface of dentine. Efflandt et al [126] showed that a strong bond was formed between the dentine and bioactive glass and ions such as calcium and phosphate were deposited on the dentine surface. It was further hypothesised that this material is capable of forming a protective layer on to the dentine surface and provide relief against dentine hypersensitivity. Litkowski et al [3], first proposed using CSPS for oral care and their work showed significant tubule occlusion after the application of CSPS. This led to further investigation and development of oral care products containing BAG.

2.10.1 CSPS (Novamin®)

The work of Litkowski et al. [3] led to the establishment of Novamin® technology in 2003, the trade name for CSPS. Subsequently, it has been used as an active ingredient in oral care products to treat and prevent sensitivity, gum disease such as gingivitis, erosion, enhance appearances as a whitening agent and prevent or inhibit demineralization and boost long term remineralisation by slowly releasing ions [89,127,128]. This technology was bought by GlaxoSmithKline in 2011 which then launched Sensodyne® Repair and Protect toothpaste containing 5 % w/w NovaMin® to treat mild tooth sensitivity. As this material is highly reactive in the presence of water, a water-free base was used in the formulation of this toothpaste to protect the BAG particles from premature reactions [129].

CSPS treats DH by the formation of apatite over exposed tubules which would stop the stimuli from interfering with the fluid flow. It rapidly exchanges Na^+ ions with H^+ when it comes in contact with saliva or any aqueous media [130]. Si-O-Si bonds break, allowing silica to form Si-OH. Breakage of the silica network releases calcium and phosphate ions that precipitate into a calcium phosphate ($Ca\text{-}P_2O_5$) layer onto the tooth surface and binds to collagen fibres [131].

Silica plays a crucial role in the formation of the HA like layer, the silica atoms provide a nucleation site that attracts calcium and phosphate ions to the tooth surface [132]. Deposition and precipitation of these two ions continue and the Ca-P_2O_5 crystallises into an HA like layer on the tissue by incorporating OH^- from the saliva. Equation 2.11 illustrates the chemical reaction that takes place in the oral cavity after the use of bioglass [133,134].

$$5Ca^{2+} + 3PO_4^{3-} + OH^- \rightarrow Ca_5(PO4)_3(OH) \qquad (2.11)$$

Earls et al. [16] investigated the ability of CSPS containing toothpaste in forming a layer and they showed that the tubules were occluded to at least 1μm (depth of FIB slice). Another study by Earl et al [135] treated human dentine specimens with Sensodyne® repair and protect toothpaste containing 5% CSPS for 4 days twice daily and used Coca Cola® with pH of 2.5 or grapefruit juice with pH of 3 for to acid challenge the HA like layer for 5 minutes. The SEM data showed the HA layer was still intact after the acid challenge.

It is possible that fluroapatite (FAp) is formed rather than the expected HA due to the presence of fluoride salt in the toothpaste formulation, however in vivo conditions such as salivary flow and pH are not controlled and the concentration of fluoride might not be sufficient enough for the formation of FAp.

The study by Mneimne et al.[9] showed that incorporating fluoride into the glass structure would provide a slow release of F^- ions over time which would facilitate the formation of FAp with lower solubility compared to HA. They also showed that increasing phosphate content would increase the apatite formation. These changes resulted in the development of new BAG called fluoro calcium phosphosilicate which is coved in more detail in the next section.

As well as being acid resistant the HA layer also needs to withstand mechanical challenges within the oral cavity. This was also investigated by Earl et al. [135] by using optical profilometry to measure the surface thickness. Dentine discs were brushed with Sensodyne® Repair and Protect while the control dentine was brushed with deionised water. All samples were then mechanically challenged by 200 brush strokes. The mean step heights significantly increased from 0.1µm to 13.4µm after 5 days of treatment with CSPS the surface layer remained intact even after a challenge by mechanical brushing.

A comparison by Parkinson et al [21] investigated the effect of different toothpastes containing active ingredients such as Amine Fluoride, Arginine with Calcium carbonate and CSPS on mechanics of dentine after 2 and 4 days. Dentine discs were brushed twice per day and microhardness was measured by Knoop diamond indenter. Their results showed CSPS had a superior change in hardness for both days from baseline with a mean percentage change of almost 150% after 4 days. This increase in surface hardness following the treatment was explained with SEM and EDX data that showed the formation of the HA layer on the dentine surface and a higher concentration of calcium and phosphate ions. Formation of the hydroxyapatite layer on the surface after treatment with CSPS would have led to an increase in microhardness by covering the voids on the surface.

CSPS has also shown promising potential to remineralise the dental tissue. A number of authors (table 2.5) have used various techniques such as SEM, EDX, XRD, Raman spectroscopy, FIB, and some others to evaluate the remineralisation of dentine samples after treatment with CSPS glass. Mechanical testing has also been used to detect mineralisation via the hardening of the dentine. However, a combination of these techniques needs to be carried out to confirm apatite formation on the dentine surface and mineralisation of the tissue. This has been a limiting factor in some of these studies where only either SEM/EDX was used and the presence of apatite was not confirmed by structural analysis, or only the change in mechanics of the dentine was studied.

Table 2. 5: Number of dentine remineralisation studies

Author	Aims and objectives	Techniques used	Findings	Limitations
Wang et al [65]	To evaluate dentine remineralisation by 45S5 bioactive glass	• XRD • SEM/EDX • FTIR • AFM	• Significant tubule occlusion • Increase in calcium and phosphate • Apatite growth	• Mechanical properties of dentine were not investigated before or after treatment
Schmidlin et al [136]	To evaluate dentine remineralisation a bioactive glass	• Ultramicroindentation	• Demineralised dentine hardened after treatment with bioactive glass	• Apatite formation was not confirmed • Only change in mechanics of dentine was studied • Failed to mention the glass composition
Lynch et al [137]	Investigate the effect of incorporating fluoride in bioactive glass formulation	• XRD • SEM • Infrared emission spectroscopy	• Apatite formed within 6 h, • The glasses successfully occluded dentinal tubules by the formation of apatite crystals	• Apatite formation was not confirmed on dentine
Osorio et al [110]	To determine the remineralisation potential of bioactive glass containing cement	• SEM/EDX	• Higher calcium and phosphate concentration after treatment with the cement	• The apatite was not characterised further with appropriate techniques such as XRD FTIR and Raman spectroscopy
Curtis et al [109]	To evaluate the efficacy of a phosphate free, sol-gel nano bioactive glass to occlude tubules and form apatite on dentine	• SEM/EDX • FIB	• Apatite with a rod-like structure was formed inside of tubules • EDX showed higher concentrations of calcium and phosphate	• Only SEM was used to characterise apatite • FIB analysis was limited to a maximum of 10µm

Effectiveness of CSPS containing toothpaste in treating dentine hypersensitivity was also studied in clinical settings where it was compared to a conventional potassium nitrate toothpaste with promising results. Litkowski et al. [130] assessed the sensitivity symptoms of 66 patients who used toothpaste containing 0% (placebo group), 2.5% and 7.5% CSPS over 8 weeks. The patients that belonged to the 7.5% group reported a significant reduction in sensitivity symptoms compared to the placebo group. These results supported the finding reported by a number of other studies [89,138,139] where CSPS was successful in reducing dentine hypersensitivity by tubule occlusion.

2.10.2 BioMin® F and C

The composition of 45S5 bioglass has been used as a benchmark to develop other bioactive glasses with other metal oxides such as strontium, zinc, and fluoride substituting the network modifiers such as CaO or Na_2O. Fluoride has been used in toothpaste since 1891 to help fighting against cavities. Other benefits of adding fluoride to toothpastes include the potential formation of fluroapatite which is more acid resistant than the hydroxyapatite thus hindering the demineralisation process. While retaining the ability to treat DH by occluding dentine tubules. Fluoride has been incorporated into bioactive glasses by a number of authors [140–142]. This was achieved by replacing one of the network modifiers with CaF_2. It is important to consider that this would reduce the amount of NBO atoms present in the glass structure and increases the number of BO. This would lead to a higher cross-linked glass network which would have implications on the bioactivity of the glass.

Mneimne et al. [9] avoided this by keeping the ratio of pre-existing components the same. This ensured that the Q structure of the glass is not changed. When substituting ions within the glass structure the effect on bioactivity needs to be considered. Lusvardi et al. [143] replaced CaO in the 45S5 composition with calcium fluoride and the resultant bioactive glass had a reduced reactivity as the result of the addition of fluorides to 45S5. Hench et al [144]. also reported that replacing CaO with CaF_2 would reduce the reactivity because it will reduce the number of NBO in the glass network thus it becomes more crosslinked, preventing the glass from undergoing the condensation and repolymerisation reaction.

The effect of fluorine on the bioactivity of the bioactive glasses was also investigated by Brauer et al [145] who replaced Na_2O with CaF_2 and studied the effect of lowering phosphate and increasing the CaF_2 content on the reactivity of the glass. FTIR, MAS-NMR, and XRD analyses were used to evaluate apatite formation and it was suggested that the addition of CaF_2 led to the formation of FAp with sharper apatite XRD peaks compared to fluoride-free compositions. Mneimne et al [9] also confirmed this finding where small quantities of CaF_2 (5 mol%) favoured a FAp formation. Brauer et al [145] and Mneimne et al [9] showed that to see a positive result when incorporation fluoride in the glass composition, the ratio of other components and NC needs to remain constant. Hench et al [144] incorporated CaF_2 into the glass network by directly replacing CaO, subsequently removing NBO from the network which would increase the crosslinking and lower the apatite formation.

This led to the development of BioMinF toothpaste containing a fluoride-based BAG. This BAG is known as Fluoro Calcium Phosphosilicate (FCPS) where Na_2O has been replaced by CaF_2. Although the exact composition of this bioactive glass is confidential, it contains a higher amount of phosphate compared to CSPS. The same study [9] reported that higher phosphate content enhanced apatite formation which could be due to additional PO_4^{3-} ions within the formulation. FCPS also has a smaller particle size of around 6µm compared to 15-20 µm for CSPS.

The number of studies that have investigated this toothpaste is limited in the literature as this is a relatively new toothpaste. A recent in vitro study [146] which compared FCPS with CSPS and a standard fluoride toothpaste reported more dentine tubule occlusion achieved by FCPS compared to the other two groups by SEM analysis. Another in vitro study[147] looked at the remineralization potential of FCPS compared to standard fluoride toothpaste by measuring the microhardness of sound enamel discs, after demineralisation and microhardness recovery after identifies treatment. Distilled water was used as a control. Results showed FCPS achieved a significantly higher hardness recovery.

A clinical trial [148] compared two desensitizing toothpastes containing 5% FCPS and CSPS. 60 individuals over the age of 18 with at least two sensitive teeth were chosen and divided into 3 groups and each paste was randomly assigned to a group. Standard dentifrice containing fluoride was also used as a control. Sensitivity scores were measured at baseline, immediately after scaling and root planning, at 15, 30, and 60 days. Results showed all 3 groups significantly reduced DH. The finding of the control group was unexpected but was explained by the better brushing routine and oral hygiene as the subjects were participating in the study. FCSP had a significantly higher reduction in DH. Another clinical study by Patel et al. [149] compared the efficacy of FCPS, arginine with calcium carbonate and a placebo toothpaste to treat DH in 75 patients. They reported a better reduction in DH symptoms amongst the patients that were given FCPS but this was not statistically significant.

It is worth noting that data obtained from clinical trials are subjective as they are dependent on a participant rating a pain sensation experienced from different stimuli. As a result, conclusions taken from these studies evaluating DH should be treated cautiously.

BioMin® C, a fluoride-free version of BioMin® F toothpaste has also been developed. The bioactive glass in this toothpaste is chloro calcium phosphosilicate (CCPS) where chloride ions (Cl^-) have replaced the fluoride within the glass structure. This product is relatively new and currently, there appear to be limited in vitro or in vivo studies. Cruz et al. [150] demonstrated that chloride-containing bioactive glass was effective in occlusion of tubules by forming hydroxyapatite like layer on to the dentine surface, however, the fluoride-based bioactive glass resulted in greater tubule occlusion and was more acid resistant following an acid challenge.

2.11 Other Active Ingredients in Toothpastes

2.11.1 Arginine

Arginine (AG) is another active ingredient used in toothpastes in combination with calcium carbonate to treat dentine hypersensitivity. It attracts calcium and phosphate ions to the tooth surface and forms a calcium phosphate layer on to the dental tissue.

Initially, a product called ProClude® was released in the USA containing AG and calcium carbonate for dental sensitivity treatment. A clinical study showed that a single application of this paste after scaling and root planing procedure provided 28 days of sensitivity relief. Two further studies showed similar results [151–153]. This technology was later developed by Colgate with the addition of fluoride and was launched as Colgate's Pro-Relief toothpaste also known as Pro-Argin® technology. This toothpaste contains 8% arginine coupled with calcium carbonate with 1450 ppm fluoride.

Arginine is a naturally occurring, positively charged amino acid (AAs) that is also present in the saliva. AAs are the building blocks of proteins that play a crucial part in HA mineralization in bone and dentine. Once bound to the surface they create a supersaturation of Ca^{2+} and PO_4^{3-} ions which promote the formation of heterogeneous nucleation and crystallisation of HA.

AG (H_2Arg^+) contains several nitrogen atoms (figure 2.12) called α-amino groups that can carry positive charges which makes this amino acid positively charged. These positive cations have a high affinity towards the negatively charged dentine surface and once attracted to dentine acts as a crystallisation nuclei. The α- carboxyl group (COO^-) in the structure are active sites for the attraction of Ca^{2+} ions to the surface and play an important role in HA formation [151].

The amino group creates an ionic bond with the carboxyl group and can form a chelation ring with Ca^{2+}. The interaction of Ca^{2+} with these groups via electrostatic attraction form a $HArgCa^{2+}$ complex with a stability constant (log K) of 2.21[154]. PO_4^{3-} ions are attracted to the surface via the guanidyl side chain of AG and the complex that is formed has a stability constant of 1.9 [155]. The attraction of these ions to the surface results in HA crystal formation.

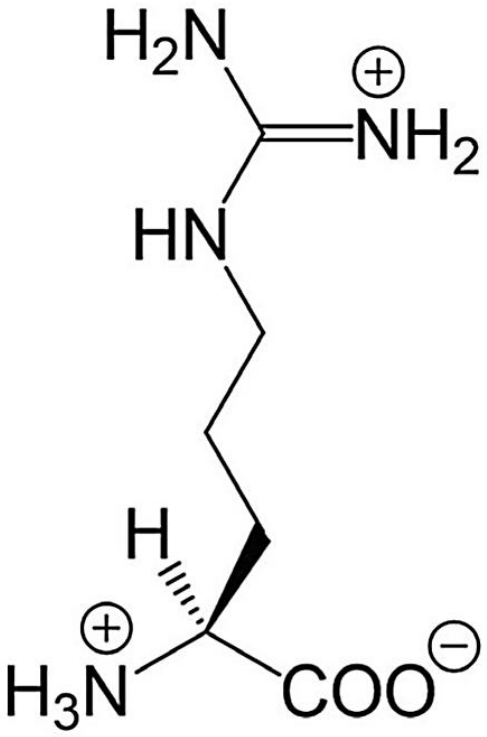

Figure 2. 12: Structure of arginine [156]

A number of in vitro studies [11,90,157] have demonstrated that arginine in combination with calcium carbonate is highly effective in occluding tubules. They also showed that the layers formed on to the dentine surface were rich in calcium and phosphorus which can promote tooth remineralisation (table 2.6).

Table 2.6: Number studies evaluating the efficacy of arginine for treating dentine hypersensitivity

Author	Aims and objectives	Techniques used	Findings	Limitations
Lavender et al [11]	To determine • level of tubule occlusion by AG • composition of occluding material	• CLSM • SEM • XPS	• AG was highly effective in occluding dentin tubules • Layer on the surface contained high levels of calcium, phosphorus, oxygen and carbonate. • AG was found incorporated into the dentin tubule • The layer was still intact after acid challenge	• No structural analysis to confirm hydroxyapatite formation • Mechanical properties were not investigated
Yuan et al [157]	To determine the level of occlusion by AG	• SEM • EDX	• Significant tubule occlusion after treatment • Higher calcium and phosphate concentration after treatment	• No acid challenge • No mechanical testing • No structural analysis
Mahale et al [90]	To Compare tubule occlusion capability of Arginine, Strontium chloride, and CSPS	• SEM	• Arginine had a significantly higher level of occlusion compared to the other two material	• No acid challenge • Only SEM was used • The layer was not characterised structurally or chemically
Davies et al [158]	To determine the acid resistivity of arginine, strontium, and fluoride containing toothpastes	• SEM • EDX	• Complete occlusion of tubules • 75% still after 2 minutes of citric acid challenge (pH of 3.2) • Higher calcium and phosphate concentration after treatment • Strontium based toothpaste was more acid resistant	• No mechanical testing • No structural analysis

2.11.2 Calcium Silicate

Calcium silicate is another active ingredient used in toothpaste as a calcium source to form a hydroxyapatite like layer over the tooth surface. When combined with the phosphate it forms a chemical bond with the dental tissue, occluding the dentine tubules and providing DH relief.

Tricalcium silicate has been studied for the purpose of occluding dentine tubules. Dong et al. [159] investigated the effectiveness of this material on dentine tubule occlusion and their results were positive. Tubules were successfully occluded after the treatment with Tricalcium silicate and artificial saliva. EDX and XRD were used to identify the composition and crystal phases of the layer on the dentine. The main components were oxygen, calcium, and phosphate with a Ca:P ratio of 1.6. Structurally the layer was similar to hydroxyapatite presence of some amorphous calcium phosphate phases leading to a Ca:P ratio of mineralized layers being slightly less than that of HA (1.67). After citric acid challenge (pH 4) the layer was removed and tubules had become patent.

Mechanism of HA formation by calcium silicate is similar to that of bioactive glasses, When it comes in contact with saliva, a rapid ionic exchange of Na^+ with H^+ the solution occurs. This forms a SiO_2-rich layer on the tooth surface which acts as a nucleation site for the attraction of Ca^{2+} and PO_4^{3-} from the solution, these react to form calcium phosphate which crystallises into hydroxyapatite like layer [160].

Unilever has developed dentifrices (Regenerate®), containing calcium silicate and sodium phosphate salts, also known as NR-5® technology. It is worth mentioning that this technology was mainly designed to replace the lost minerals within the enamel and protect it from acid erosion and not to treat DH. However, as it has the capability to form an HA like layer it has the potential to be used to protect dentine and provide relief against DH. This capability is investigated and discussed in this thesis.

2.12 Assessment to Tubule Occlusion

For effective treatment of DH, the tubules must be well occluded. Hydraulic conductance Study (HC) and SEM are the most common technique used to investigate the degree of occlusion (table 2.7)

The first studies where HC was used to measure the permeability of dentine by HC was in 1974 and was conducted by Outhwaite, et al.[161]. HC measures occlusion by measuring the rate of flow fluid across a defined surface area of dentine with a thickness of 1-2 mm (through the dentinal tubules) under a fixed pressure for a set amount of time. Tubule occlusion is quantified by measuring the rate of fluid flow on a dentine section followed by measuring the flow rate after a dentifrice treatment on the same area of dentine. If the tubules are occluded there will be a reduction in flow rate which is then expressed as a percentage reduction in flow rate and is calculated from the rate before and after treatment with the dentifrice. The fluid flow is calculated from [162];

$$\mathrm{Lp} = \frac{\mathrm{Jv}}{\mathrm{AtP}} \qquad (2.\ 12)$$

Where Lp is hydraulic conductance in $\mu L.cm^{-2}$. $Min.cm^{-1}.H_2O$, Jv is fluid flow in µL. min, A is the surface area of the dentine in cm^2, t is the time in seconds and P is hydrostatic pressure applied in cm of water. A large volume of dentine is required to assess tubule occlusion using these techniques. One major disadvantage of using HC and SEM for occlusion study is that the depth of occlusion can not be measured.

To overcome this focused ion beam (FIB) has been used to study the depth of tubule occlusion following treatment with desensitising toothpaste. Earl et al. [16] used FIB to investigate the depth of tubules occlusion after treatment with CSPS. The results showed that dentine tubules were occluded to at least the depth of the FIB cut which was approximately 1µm. FIB is an extremely time-consuming method as the material needs to be milled away, only a small volume of material can be tested and it is relatively expensive.

Table 2.7: Number of studies investigating the level of tubule occlusion by various toothpastes

Author	Aims and objectives	Techniques used	Findings	Limitations
Cruz et al [150]	• To compare tubule occlusion of CSPS,FCPS a chloride glass	• SEM	• 100% occlusion (CSPS) • 60% occluded,40% partial (FCPS) • 90% occluded, 8% partial, 2% open (chloride)	• Depth of tubule occlusion was not investigated
Gupta et al [163]	• To evaluate the dentinal tubule occlusion by CSPS	• SEM	• 91.5% of the dentinal tubules showed complete dentinal tubule occlusion, 6.61% showed partial occlusion and 1.89% remained unoccluded	• Depth of tubule occlusion was not investigated
Wang et al.[91]	• To evaluate the dentinal tubule occlusion by CSPS after brushing and immersion in artificial saliva and after citric acid challenge	• SEM • HC	• Permeability was reduced from 100% to 18.5% • After acid challenge (6 wt% citric acid, pH1.5, 1 min) permeability increased to 46.8%	• Percentage of tubules occluded was not investigated by using the SEM data • Depth of tubule occlusion was not investigated
Bakri et al [164]	• To compare occlusion potential of CSPS and arginine containing toothpaste	• SEM	• 75% occlusion (CSPS) • 68% occlusion (Arginine)	• Depth of tubule occlusion was not investigated
Earl et al [16]	• Characterise the HA like layer and tubule occlusion by CSPS	• SEM • FIB	• 100% tubule occlusion • Occlusion to at least depth of 1µm	• Time consuming • Depth limited to fib slice (1µm) • Percentage of tubules occluded was not investigated by using the SEM data

Serial block-face scanning electron microscopy (SBF SEM) is an alternative 3D imaging technique, which has been successfully used on soft materials and it allows collecting data over substantial volumes. It is equipped with a diamond knife in a microtome that cut nanometre-sized slices from the sample and backscattered images of freshly cut block face are collected sequentially. The process of cutting and acquisition of 3D ultrastructure is fully automated, lowering the operating time. The internal structure of the material can be reconstructed, providing 3D information with an imaging resolution typical for SEM [165].

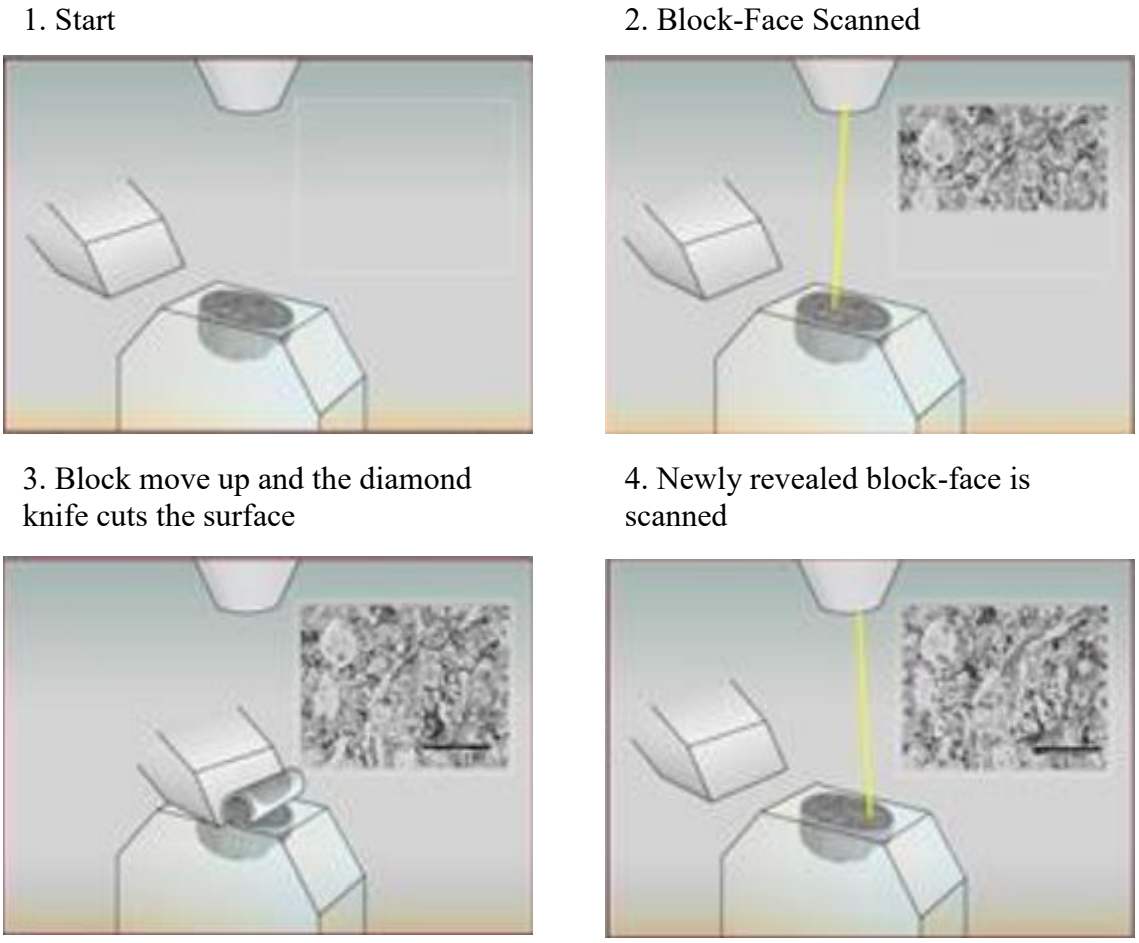

Figure 2. 13: Principle of SBF SEM (adopted from Gatan Inc) scale bar-10µm

This method has been used in material science to investigate polymeric materials [166,167]. The use of a low vacuum allows imaging nonconductive samples without the need for conductive materials. SBF SEM has been successful in sectioning and imaging biological samples and it has the potential to be used on dentine. It would be a unique technique that can be applied in dental research. Particularly it can be used to investigate tubule occlusion in terms of numbers and depth as well as detecting mineralisation by taking greyscale measurements from the backscattered images. Chapter 5 explores the use of SBF SEM for tubule occlusion and mineralisation further.

2.13 Summary

Gum recession or the wear, damage and chemical dissolution of tooth enamel, can leave dentine exposed to the oral environment, this leaves the dental tissue vulnerable to further damage and dentine hypersensitivity (DH). The tubules within the dentine are filled with a dentinal fluid whose flow can be altered by thermal, chemical, evaporative, mechanical or osmotic stimuli leading to a characteristic sharp pain [168]. Dentine is softer than enamel and once exposed it requires protection to minimise further loss of the tissue but also to prevent DH [169].

Bioactive glasses, arginine and calcium silicate have been used toothpastes for treating dental hypersensitivity and remineralisation of dental tissues. These active ingredients deposit calcium (Ca^{2+}) and phosphate (PO_4^{3-}) ions on to the tooth surface after reaction with saliva forming calcium phosphate, which crystallises into a hydroxyapatite (HA) like layer. These dentifrices can enhance remineralisation, minimise demineralization and reduce caries activity more effectively than current fluoride toothpastes and contribute to better oral health.

These layers also have the potential to provide protection to the dental tissue, an area that has not been explored. Previous studies [17–21] have used different testing machines such as Vickers hardness and Knoop hardness to characterise the dental tissues after treatment with these materials and reported increased hardness of 10 to 50 percent. However, they have failed to consider that these layers are thin coatings of only a few micrometres thickness. The high loads used in these studies would have produced indents too large to only characterise this HA like layer.

They have reported an increase in mechanical properties of dental tissue but the result would have been the combination of the layer mechanics and the dentine substrate. With this in mind, it is hard to conclude that these materials have hardened the tissue.

In terms of protection, the robustness of the HA like layer was evaluated comparatively by recording material loss, however, it failed to provide any other measure of tribological performance [135]. In addition, previous tests were carried out in a dry environment which is not representative of the oral environment and would affect the measured mechanics (hardness and modulus) as dentine tissue consists of ~22% water (Vol%) in vivo [22].

The remineralisation studies used EDX to examine the surface after treatment and though they showed an increase in mineral, this could be due to the deposition of calcium phosphate-rich layer on the surface which is giving the higher measurements [65,109,110].

In regards to assessing the level of tubule occlusion the previously used techniques such as SEM and HC are qualitative and limited to the percentage of tubules occluded and not the depth to which occlusion has occurred. FIB can be used to overcome this, however, it is limited to a small testing volume, it is extremely time-consuming and expensive. Serial block-face SEM can be used as an alternative to these methods which requires minimal sample preparation and a large volume of dental tissue can be examined over a much shorter time.

To be able to develop a dentifrice that offers the best protection and relief against DH, we need to understand the parameter which influences the protection capability of the HA like layers and develop a method to measure the depth of tubule occlusion with minimal sample preparation. Therefore the work presented in this thesis aimed to investigate the nanomechanical properties of the HA like layers formed by chloro calcium-phosphosilicate, calcium sodium phosphosilicate, fluoro calcium phosphosilicate, arginine coupled with calcium carbonated and calcium silicate with sodium phosphate and improve the understanding of the relationship between the mechanics, the minerals, crystal structure and density of these layers and their resistance to acid challenge.

This was achieved through utilising nanomechanical testing with a unique liquid cell set up to characterise the layers on a nanoscale level to avoid the substrate effect and to keep the dental tissue hydrated to provide a better mimic of in vivo conditions.

The project also aimed to assess the suitability of the serial block-face scanning electron microscope (SBF-SEM) in cutting a hard material such as dentine. If successful SBF-SEM combines an ultra-microtome with the high-resolution imaging capability of an SEM to generate high-resolution 3D images of samples and can be used to investigate the percentage and depth of tubule occlusion. SBF-SEM also uses a backscattered detector (BSE) and the images can be used to measure the mineral density of the dental tissue and detect any possible mineralisation. This methodology can result in a better understanding of the therapeutic materials used in dentine hypersensitivity research.

Chapter 3 Nanomechanics of the Protective Layer

The study presented in this chapter aimed to investigate the nanomechanical properties of the layers formed by 3 bioactive glasses: chloro calcium phosphosilicate (CCPS), calcium sodium phosphosilicate (CSPS) and fluoro calcium phosphosilicate (FCPS) as well as Arginine (AG) coupled with calcium carbonated and calcium silicate (CS) with sodium phosphate. The aim was fulfilled by utilising nanomechanical testing with a unique liquid cell set up to characterise the layers on a nanoscale level to avoid the substrate effect and to keep the dental tissue hydrated to provide a better mimic of in vivo conditions. Initially, SEM was used to confirm layer formation, the hardness, modulus elastic recovery parameter, and ratio between hardness and modulus of these layers were then measured by nanoindentation. The layers were then subjected to a citric acid challenge to investigate their acid resistivity. Finally, nanoscratch was used in a ramped load mode to measure the adhesion of the layers to the dentine by detecting the critical failure load (if one exists). The null hypothesis tested in this in vitro study was that the layers formed by these different active ingredients will have similar mechanical properties.

3.1 Introduction

Mechanical properties such as hardness and modulus are the key parameters for quantification and comparison of the protective nature of these layers. They will provide information about the mechanical and tribological properties of the layers.

Indentation techniques such as Vickers hardness and Knoop hardness are widely used in the field of dentistry to characterise the dental tissues such as enamel and dentine. Indentation is a simple characterisation technique that involves touching a material with unknown properties with a tip whose properties are known. In a conventional indentation, the desired properties are calculated from measuring the dimensions of the residual impression left on the sample surface by the indenter upon removal of the load.

Nanoindentation is an indentation test where the depth of the tip penetration is at the nanometre scale. This results in the size of the residuals being very small and in most cases impossible to or extremely difficult to measure.

To overcome this, nanoindentation systems rely on measuring the load vs depth of penetration of the tip into the material of interest. This combined with the known geometry of the tip allows the indirect calculation of the area of contact at full load, from which the hardness and modulus are calculated. Therefore it is also referred to as depth-sensing indentation (DSI).

The testing involves an initial elastic-plastic loading sequence followed by unloading. The forces involved are in millinewton range and depth of penetration is on the order of few microns. The conventional indentation cannot apply low enough load to give a penetration depth less than 10% of the layer thickness which is required to avoid the influence of the substrate on the mechanical measurement of the specimen.

Most modern NI systems are equipped with an automated *x-y* stage which enables the user to perform many individual mechanical tests on a surface of the material. This is a useful tool especially in biomaterial science, as most biological tissues are inhomogeneous and by mapping the surface the variation in mechanical properties can be investigated. Another advantage of NI is that a large number of indentations can be performed on a small area of the specimen, due to the testing being in nm to μm range.

Figure 3.1 represents the schematic diagram of the NanoTest Vantage System (Micro-materials Ltd, UK) that was used for the nanoindentation and nano scratch experiments presented within this thesis. The coil and the magnet located at the top of the pendulum apply the load to the surface of the sample when it comes in contact with the calibrated diamond tip. The frictionless pivot which has 4 springs supports the pendulum. A sensitive capacitive transducer records the displacement of the tip into the surface and is given as a function of load.

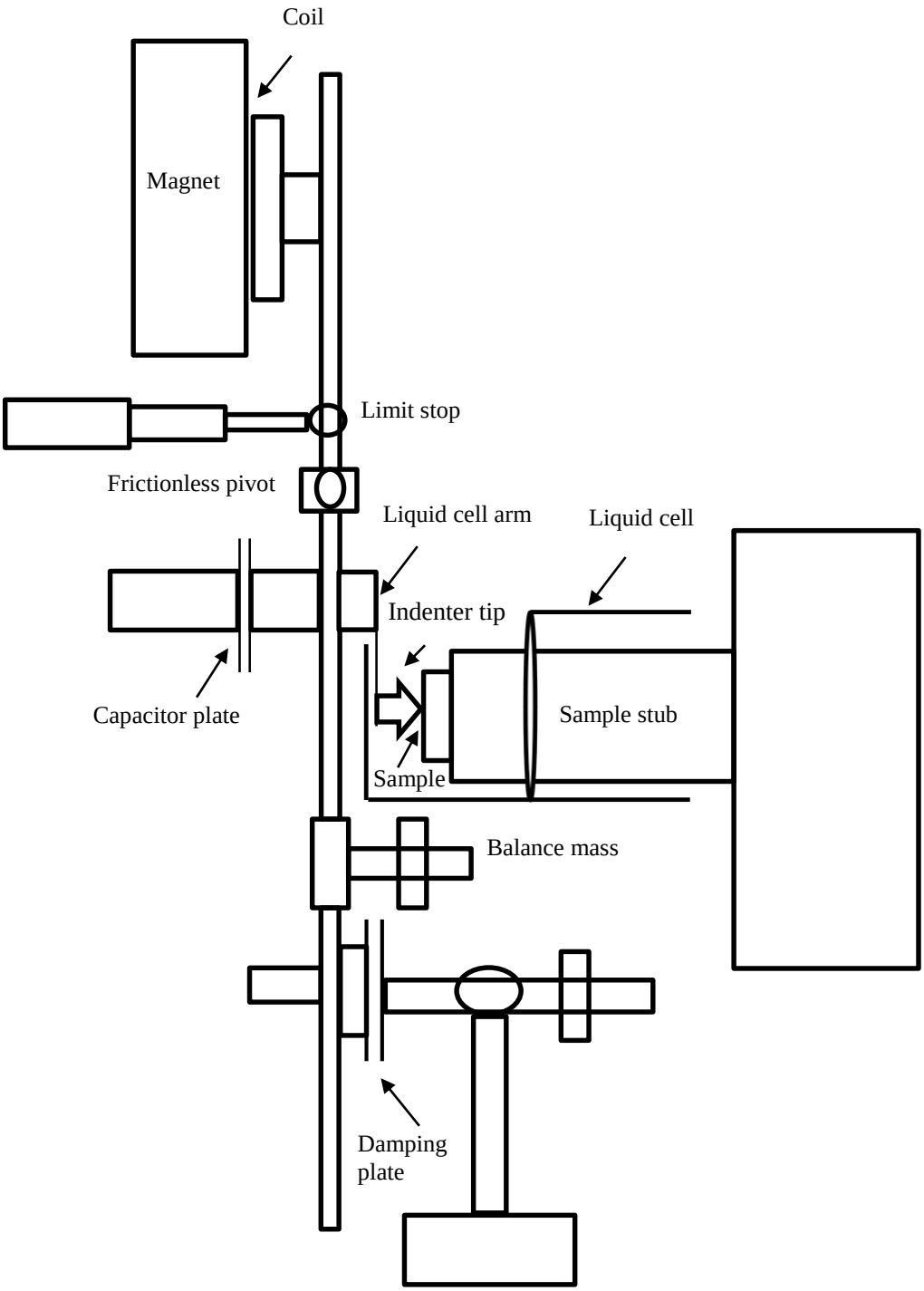

Figure 3. 1: Schematic of the features of the nanoindentation instrument

Nano scratch technique was also used as a means of simulating a single asperity contact between the diamond tip and the layers to determine the delamination load (if one exists) and to measure the ratio of plastic deformation to elastic recovery of the surface. A load ramped multi-pass test was used to characterise the adhesion of the HA-like layer to the dentine substrate. Usually, a multi-pass wear test with 3 scans is used to evaluate the wear behaviour of the sample however the number of passes can be modified to the desired number if the wear properties after multiple tests are of interest. 3 pass test involves scanning the surface which gives the initial topography, this is followed by moving the tip over the surface with a pre-set load producing a scratch on the sample. A perpendicular load is applied to the tip by the pendulum while the sample is moved positively in z direction while the length of scratch, topography load and scratch load are set by the user. Finally, the tip passes over the surface for the third time to record the topography after scratch.

3.2 Materials and Method

3.2.1 Bovine Dentin

The use of human teeth for in vitro studies would require ethical approval. It can be a difficult and lengthy process. Moreover, the supply in large quantities would be challenging without links to dental schools as was the case at the University of Southampton, therefore significantly more expensive.

Bovine teeth are readily available and can be easily handled for disc preparation due to their bigger size [170]. Moreover bovine dentine has a simillar surface microhadness [171] and tubule diameter [172] to the human dentine. As this was a comparative study focusing on the mechanical properties and tubule occlusion of dentine, it was deemed suitable to use bovine dentine as a substitute for human dentine because of these similarities and the other listed reasons.

60 dentine discs with a thickness of 1.0 ± 0.2 mm were manufactured from bovine incisors (n=60) and supplied by Modus Laboratories Ltd (Reading, UK). The discs were taken from the facial side of the tooth, polished down through the pulp cavity on the lingual face to produce a solid dentine specimen, and stored in a 0.2% thymol solution to avoid bacteria growth. Each disc was polished using 3 µm and 1µm diamond suspension to get

a smooth surface finish, etched with 1% citric acid for 30 seconds to remove the smear layer and washed with deionised water (DI) for 1 minute. This approach was chosen to minimise damage to the dentine collagen which was necessary for the formation of the layers.

3.2.2 Artificial Saliva Preparation

The natural saliva in humans consists of approximately 99.5% water while ions such as potassium, calcium and sodium, enzymes, white blood cells, mucins, antimicrobial agents, and nitrogenous products, such as urea and ammonia making up the remaining 0.5%. The complexity of natural saliva makes reproduction very challenging. Therefore artificial saliva (AS) with a variety of compositions has been used for in vitro dental research [173]. The AS composition used in this study was adapted from Fusayama – Meyer's artificial saliva to resemble natural saliva as closely as possible [174]. The AS ingredients were individually weighed and added together in the following order: 5g of Carboxymethylcellulose (CMC) was added to 50g of glycerol, 800ml of DI water was then added and the solution was mixed for 1.5 hours using a magnetic stirrer with the hot plate what was set to 37 ºC to help the mixing process. 0.58g of Sodium phosphate dibasic dodecahydrate ($Na_2HPO_4.12H_2O$) was then added to the solution followed by the addition of further 20ml of DI water, 1g of Urea, 0.4g Sodium Chloride (NaCl), 0.4g of Potassium chloride (KCl) and 0.6 g of Calcium chloride ($CaCl_2$). Finally, 180ml of DI water was added and the solution was stirred for 30 minutes. pH meter was used to measure the pH adjust to 6.5 using sodium hydroxide (NaOH) if it was necessary. The AS solution was kept refrigerated at around 5 °C and was used within 7 days after manufacture [174]. The concentrations of calcium (0.16g/L) and phosphate (0.15g/L) were slightly higher in the AS composition than the concentrations found in natural saliva (0.12g/L and 0.11 g/L respectively). This was chosen to facilitate the formation of the layers more rapidly for prompt testing.

3.2.3 Toothpaste Treatments

Five commercially available toothpastes containing 3 different bioactive glasses, arginine and calcium silicate as active ingredients were chosen for the current work. Table 3.1 summarises the different toothpastes, their active ingredient, and the company they are manufactured by. These toothpastes were chosen for this study as their active ingredients are capable of forming a layer on the dentine surface which were the focus of the study. Bovine dentine discs were divided into 6 sets (5 treatment and 1 control group) of 10 discs. Each toothpaste was randomly assigned to one of the treatment groups. 2.0 mg (± 0.1 mg) of respective toothpaste was weighed onto a medium manual toothbrush (Colgate) and brushed on to the dentine discs for two minutes, twice per day for 7 days. 0.50 ml of the AS was pipetted on to the toothbrush with toothpaste to stimulate the reaction of active ingredients in conditions that were more representative of the oral environment. Discs were then stored in 15ml of AS which was changed every 24 hrs. The presence of calcium and phosphate in AS meant that the solution was supersaturated with respect to these ions. This supersaturation coupled with the release of Ca^{2+} and PO_4^{3-} from the active ingredients create a thermodynamic driving force for the formation of hydroxyapatite. This adds further ions to an already supersaturated solution, creating a more favourable environment for the formation of apatite [175]. The 6^{th} group (negative control) were only brushed with AS.

Table 3. 1: Toothpastes and their active ingredient

Toothpaste	Active ingredient	Other ingredients	Company
Colgate Pro-Relief ®	Arginine (AG)	calcium carbonate, aqua, sorbitol, bicarbonate, sodium lauryl sulfate, sodium monofluorophosphate (1450 ppm), aroma, cellulose gum, sodium bicarbonate, tetrasodium pyrophosphate, titanium dioxide, benzyl alcohol, sodium saccharin, xanthan gum, limonene	Colgate-Palmolive
Regenerate®	Calcium silicate (CS)	glycerin, PEG-8, hydrated silica, trisodium phosphate, sodium phosphate, aqua, sodium lauryl sulfate, sodium monofluorophosphate, aroma flavour, synthetic fluorphlogopite, sodium saccharin, polyacrylic acid, tin oxide, limonene	Unilever
Sensodyne repair and protect®	Calcium Sodium Phosphosilicate (CSPS)	glycerin, PEG-8, hydrated silica, cocamidopropyl betaine, sodium methyl cocoyl taurate, aroma, titanium dioxide, carbomer, sodium saccharin, sodium fluoride (1450ppm)	GlaxoSmithKline
BioMinC®	Chloro calcium phosphosilicate (CCPS)	glycerin, silica, PEG, sodium lauryl sulphate, titanium dioxide, flavouring, carbopol, potassium acesulfame	BioMin
BioMinF®	Fluoro calcium phosphosilicate (FCPS)	glycerin, silica, PEG 400, sodium lauryl sulphate, titanium dioxide, aroma, carbomer, potassium acesulfame	BioMin

3.2.4 Citric Acid Preparation and Challenge

A further 30 bovine dentine discs were prepared using the method outlined in 3.2.1 for acid challenge experiments and were randomly split into 6 groups (n=5 per group). One of the toothpastes from table 3.1 was assigned to each group with artificial saliva was used as the control. The discs were subjected to the brushing treatment described in section 3.2.3. Dentine discs were immersed into 15 ml of 1 wt% citric acid (pH 3.1) for 2 minutes to evaluate the resistance of the hydroxyapatite like layers that had formed by each toothpaste to an acid challenge. The pH was chosen to be similar to that of fruit juices [35]. The citric acid solution was prepared by weighing 5g of citric acid salt (Sigma–Aldrich) and adding it to 495ml of DI water. The pH was measured using a pH meter and adjusted to 3.1 by 1M of NaOH solution that was prepared from NaOH pellets (Sigma-Aldrich). After the acid exposure, the discs were washed with DI water for 2 minutes and indented using NI to evaluate the change in hardness after acid exposure.

3.2.5 SEM

Random discs (n=3) were chosen from each treatment group, air-dried at room temperature (21–23 °C, 24hr), and gold-coated for SEM and EDX analysis (JEOL JSM 6500F, JEOL, Germany). The surface of the discs was imaged using the following parameters: accelerating voltage of 15 kV, the working distance of 9.5 mm, and 3000x magnification.

3.2.6 Nanoindentation (NI)

The dentine discs (n=10) from each group were indented 20 times each (200 indents per group) while fully immersed in DI (NanoTest Vantage system, Micro Materials Ltd) using a 5μm radius spherical diamond tip with a loading and unloading rate of 0.5 mN/s to a maximum load of 10 mN. The small 10 mN load was chosen to ensure the interaction volume of the indents did not include the dentine substrate. The maximum load was held for 60 seconds to allow for creep run out, with a 60 second hold at 10% load during unloading to determine the thermal drift. The indents were spaced 30μm apart to prevent overlapping of adjacent indent interaction volumes.

Table 3.2 summarises the experimental parameters used for the NI experiments. Figure 3.2 represents the nanoindentation set up where a dentine disc is being indented in a liquid cell.

Table 3. 2: Indentation experiment parameters

Experimental type	Depth vs load, fixed rate load and unload
Thermal drift correction	Post indentation,60 seconds
Method	Load controlled, 10 mN
Loading/ unloading rate/mN/s	0.50
Dwell period at maximum load/s	60

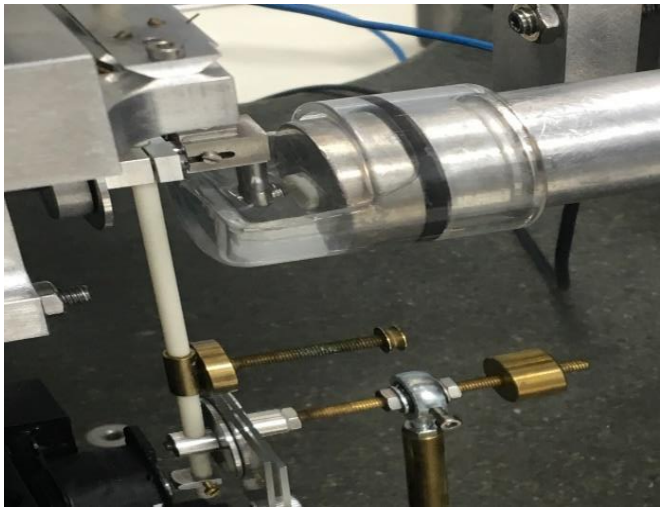

Figure 3. 2: Dentine disc being indented

3.2.7 Data Analysis

Load vs depth is outputted by the system which is then used to calculate the hardness and modulus of the layers. Figure 3.3 represents a schematic illustration of an indentation load-displacement curve.

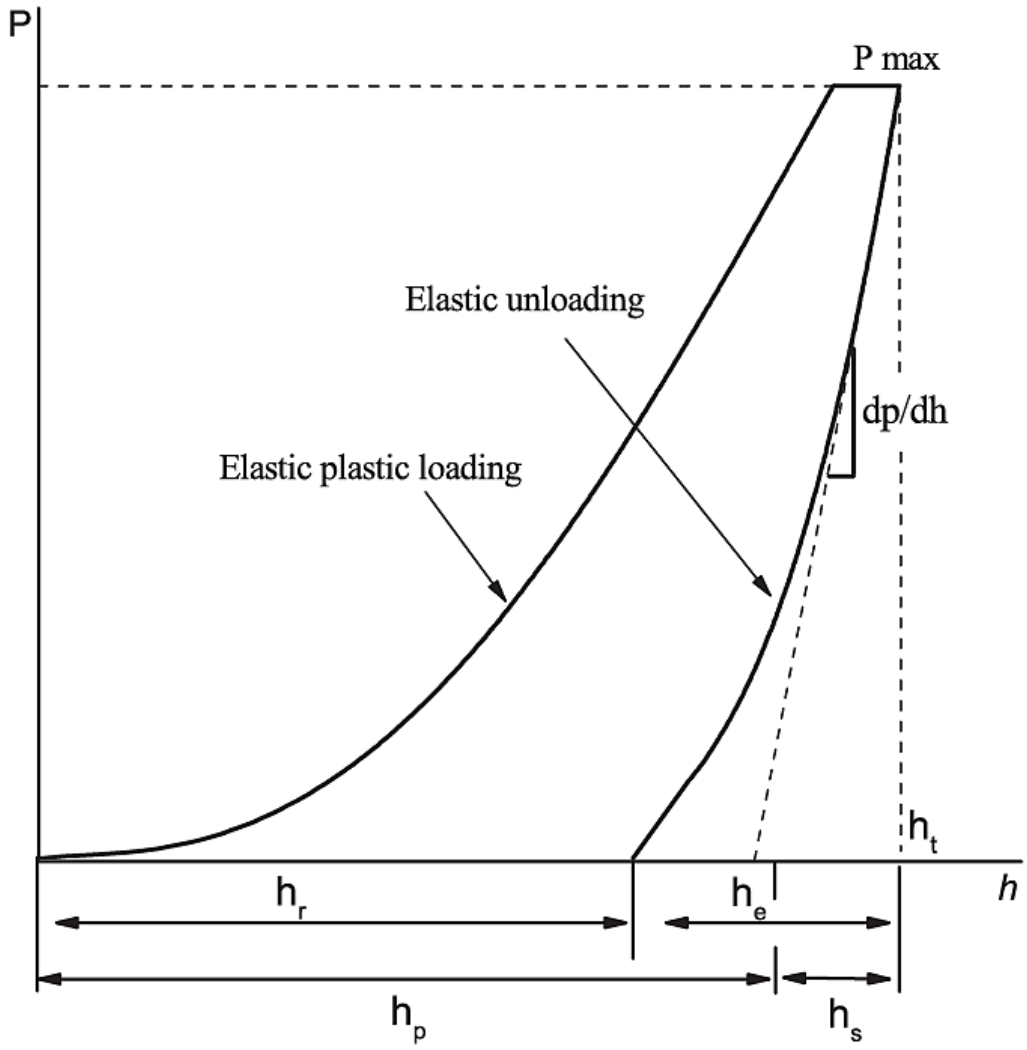

Figure 3. 3 Schematic illustration of an indentation load-displacement curve

- h_t – Total indentation depth at P_{max}
- h_r – Residual indentation after a load is removed
- h_e – Elastic displacement during unloading
- h_p – Contact depth or plastic depth
- dP/dh – Stiffness
- h_s– Distance between the edge of actual contact to the specimens surface at full load

Hardness (H) of the layers was calculated by Eq (3.1) using Eq (3.2) and Eq (3.3).

$$H = \frac{p_{max}}{A_c} \tag{3. 1}$$

$$h_c = h_t - 0.75\frac{P_{max}}{S} \tag{3. 2}$$

$$A_c = \pi(2Rh_c - h_c^2) \tag{3. 3}$$

The contact area from Eq (3.3) and contact stiffness S from the slope of the unloading curve at maximum load was used to calculate the reduced modulus (elastic deformation in both the specimen and the indenter tip), E_r. β is the correction factor for the shape of the indenter. In the case of the sphere, indenter β is equal to 1. Young's modulus (E) was then calculated using E_r and Eq (3.5)

$$E_r = \frac{\sqrt{\pi}}{2\beta}\frac{S}{\sqrt{A_c}} \tag{3. 4}$$

$$E = \frac{1 - v_s^2}{\left(\frac{1}{E_r}\right) - \left(\frac{(1 - v_i^2)}{E_i}\right)} \tag{3. 5}$$

Where v_s is the layers Poisson's ratio which was taken as 0.27 (synthetic HA), E_i (1141GPa), and v_i (0.07) are the E and Poisson's ratio of the indenter respectively.

Wear resistivity of the layers are also important in protecting the tissues. There is a linear relationship between the volume loss per sliding distance and applied load which is proportional to hardness, however, it is not necessarily the main requirement for wear resistance. Elastic modulus of a coating is an important factor in predicting abrasive wear. Therefore using the ratio between H and E ('elastic strain to failure') to rank the HA layers in terms of wear is more appropriate [176]. Higher the H/E ratio would suggest an enhanced wear resistance due to the deformation under contact being elastic.

The elastic recovery parameter (ERP) provides a measure of the elastic recovery of the sample after the indentation load is removed. It was calculated by;

$$\mathrm{ERP} = \frac{(h_t - h_r)}{h_t} \tag{3. 6}$$

Where h_r is the final depth after the load is removed.

3.2.8 Nano scratch

NanoTest Vantage system (Micro Materials Ltd) equipped with a liquid cell was also used for nanoscratch testing in a multi-pass wear mode. The surface of the dentine discs (n=3) from each group was initially scanned by a 5μm spherical indenter and a load of 0.2mN, followed by a ramped scratch test to 300mN at a loading rate of 14.85mN/s and scanning velocity of 100μm/s to simulate a single abrasive particle contact and to measure the ratio of plastic deformation to elastic recovery of the layers. The scratch test was ramped to determine the load at which any cracking or adhesive failure (delamination) of the coating occurred. The low load (0.2mN) pass was then repeated to provide the resultant post-scratch surface topography. Each specimen was scratched 5 times with a spacing of 400 μm and the elastic, plastic deformation measurements were taken by measuring the depth change between the scratch and final topography.

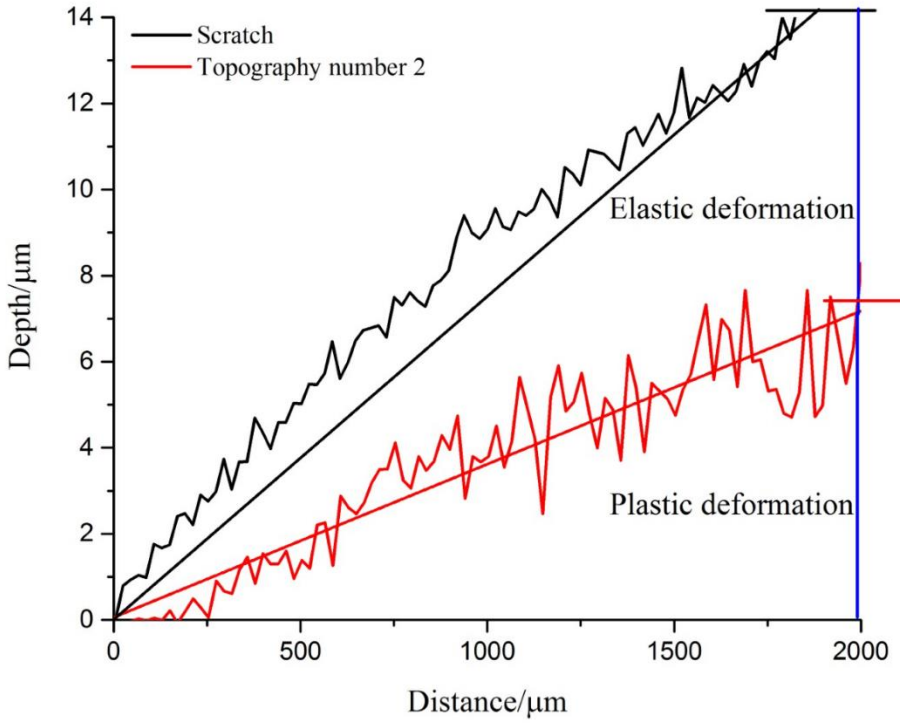

Figure 3. 4: Example of a scratch test curve

The initial topography was used to baseline the scratch measurements. This outputted two lines, the scratch and final topography taken after the scratch experiment. To measure the elastic, plastic deformation, and the maximum penetration depth, a line of best fit was drawn as represented in figure 3.4. The depth and the endpoint of the topography scan (red line) represent the plastic depth while elastic depth was calculated by subtracting this depth from the penetration depth at the endpoint of the scratch (black line). This also represented the maximum scratch penetration depth at a maximum load of 300 mN.

3.2.9 Statistics

The means of the 6 groups presented in this chapter were initially analysed using a one-way analysis of variance (ANOVA) to determine whether they were significant. This was followed with a *t*-test (assuming equal variance) to identify any significant differences between the means of the groups with post hoc Bonferroni correction, denoting a $P \leq 0.0083$ to be significant.

3.3 Results

3.3.1 SEM

Figure 3.5 shows the SEM micrographs of the control and treated dentine samples. The images show coverage and occlusion of the dentine tubules after treatment with their respective toothpastes and open tubules in the control group.

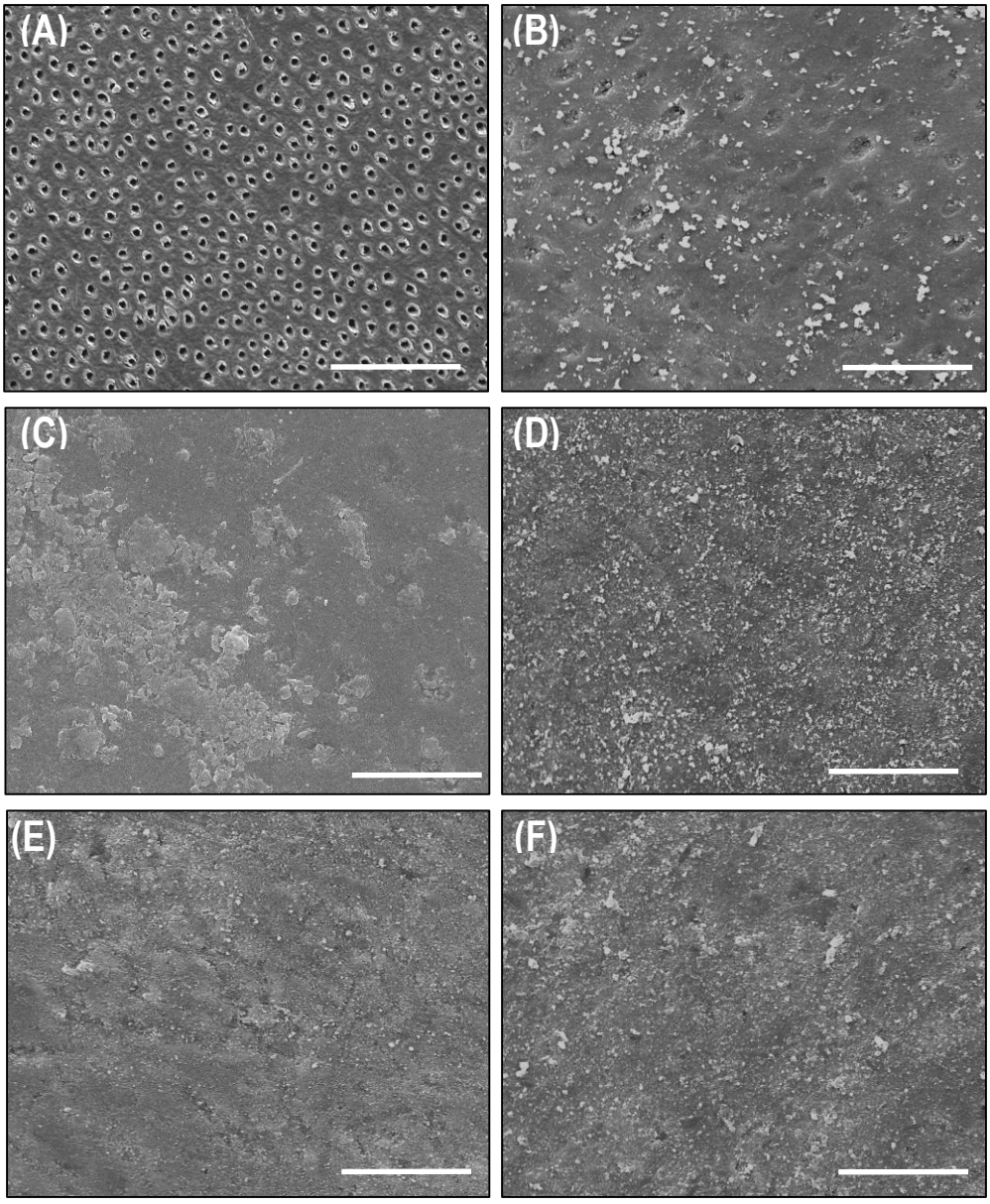

Figure 3. 5: Secondary electron SEM images are taken from the surface of the dentine discs following 7 days of treatment; artificial saliva (a), AG (b), CCPS (c), CS (d), CSPS (e), FCPS (f), 3000X magnification, scale bar represent 20µm

3.3.2 Nanoindentation

Figure 3.6 shows the average depth vs load for dentine at maximum load for all 6 groups. The indentation curves shifted to the left for all the 5 active ingredients in relation to the control group, suggesting the diamond tip did not penetrate as far into the layers at 10 mN load which is indicative of a harder layer. The control group had the highest penetration depth of 865.43±252.04 nm compared to CS with a lower penetration depth of 436.71 ±70.30 nm. Table 3.3 summarises the mean penetration depth for the layers and the control dentine.

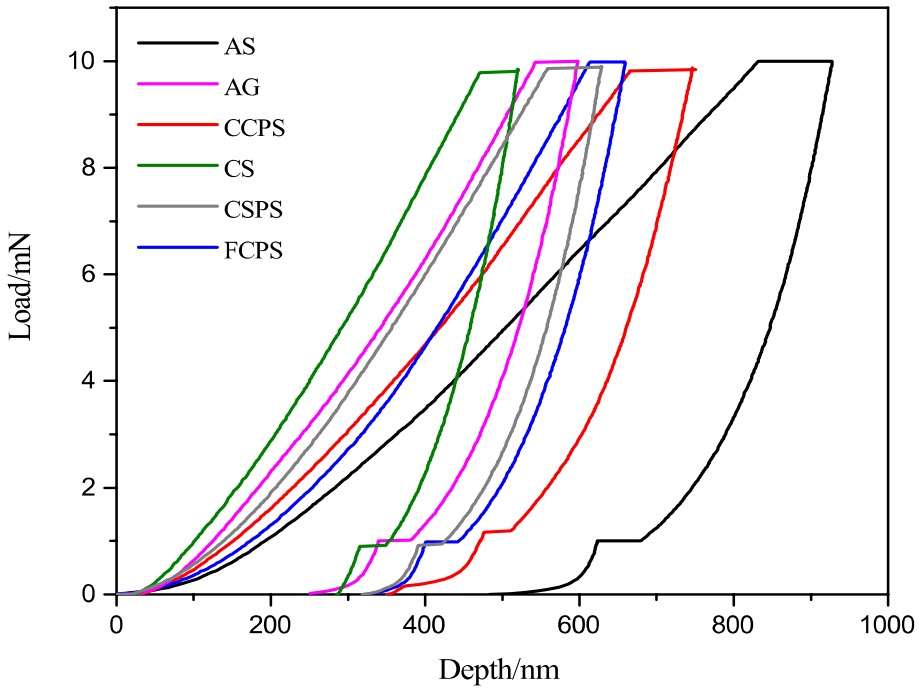

Figure 3. 6: Average load vs penetration depth data from NI experiments for the 6 groups

Table 3. 3: Mean ±standard deviation (SD) of penetration depth/nm

Group	Penetration depth/nm
AS	865.43 (±252.04)
AG	490.91 (±83.61)
CCPS	592.10 (±69.27)
CS	436.71(±70.30)
CSPS	529.43 (±92.93)
FCPS	541.13 (±69.08)

Hardness (H) and modulus (E) of the layers were significantly higher compared to the dentine surface in the control group ($P \leq 0.0083$) (figure 3.7). The Control dentine discs had an average hardness of 0.55±0.05 GPa and modulus of 14.43±1.40 GPa while CS formed the hardest layer with H value of 0.88 ±0.11GPa and stiffest layer with an E value of 23.61 ±2.37 GPa on the dentine surface. The second hardest layer was formed by AG which had an average hardness of 0.81±0.10 GPa, Young's modulus of 19.05±1.75 GPa. Tables 3.4 summarises demonstrates the average H and E values for all groups. There was a significant difference ($P \leq 0.0083$) between CS, AG, and the 3 bioactive glasses, however, no significant differences were seen between CCPS, CSPS and FCPS ($P \geq 0.0083$).

Table 3. 4: Mean hardness and Modulus of control dentine and the layers

Group	H/GPa	E/ GPa
AS	0.55 (±0.05)	14.43 (±1.40)
AG	0.81 (±0.10)	19.05 (±1.75)
CCPS	0.72 (±0.08)	17.92 (±2.10)
CS	0.88 (±0.11)	23.61 (±2.31)
CSPS	0.75 (±0.09)	18.04 (±1.61)
FCPS	0.74 (±0.07)	18.60 (±1.35)

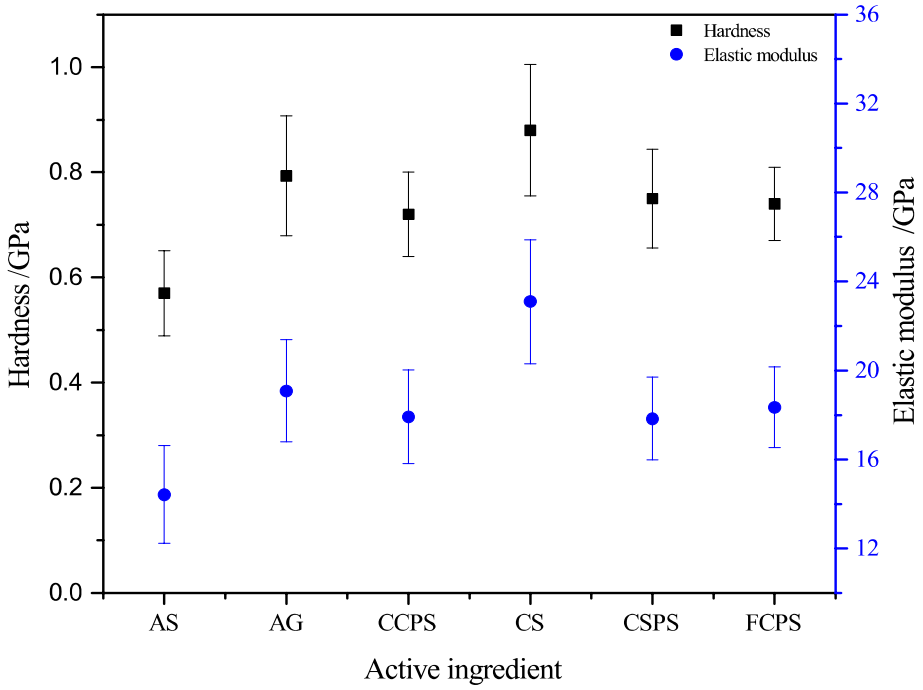

Figure 3. 7: H and E of control and treated dentine discs

H/E ratio and ERP of the layers and control dentine are given in Table 3.5. AG layer had a significantly higher H/E compared to AS and CS groups followed by CSPS, CCPS and FCPS ($P \leq 0.0083$). The layers from all 5 treatment groups had significantly higher ERP values compared to the control ($P \leq 0.0083$) with the AG layer having the highest ERP ($P \leq 0.0083$). The ERP for the 3 BAG and CS were not statistically significant ($P \geq 0.0083$).

Table 3. 5: Mean ±standard deviation (SD) of H/E and ERP values of all six groups

Group	H/E	ERP
AS	0.038 (±0.005)	0.13 (±0.033)
AG	0.043 (±0.003)	0.19 (±0.031)
CCPS	0.040 (±0.002)	0.17 (±0.034)
CS	0.037 (±0.003)	0.18 (±0.029)
CSPS	0.042 (±0.002)	0.18 (±0.027)
FCPS	0.040 (±0.003)	0.17 (±0.025)

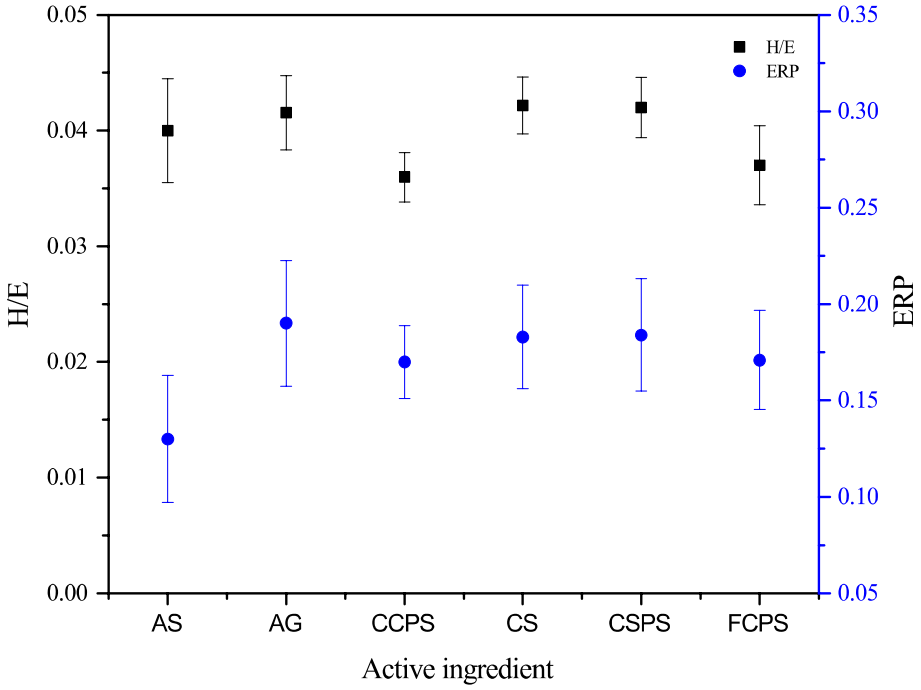

Figure 3. 8: H/E and ERP of control and treated dentine discs

3.3.3 Nano scratch

5 scratches were performed on each specimen (Figure 3.9a). No delamination of the layers was seen during the scratch test. For all of the layers, the tip cut and displaced the layer material to the sides of the scratch as demonstrated in figure 3.9b. Penetration depth at which the tip penetrated to at maximum scratch load (300 mN) is given in table 3.6. The AG layer had a significantly lower penetration depth compared to the other treatment groups (AG<CSPS<CS<FCPS<CCPS) ($P \leq 0.0083$).

The purpose of the scratch test was to compare the abrasion resistivity between the different HA like layers however the experiment was also performed on control specimen for comparison purposes. The penetration depth (figure 3.10) for the control was significantly lower than all treatment groups ($P \leq 0.0083$) except AG with whom no significant difference was seen ($P \geq 0.0083$). This is not surprising as there was no layer on the control specimen and dentine was being removed during the test. However, in the treated group the penetration depth would have been influenced by the presence of the layers on the dentine substrate. AG layer also had a significantly higher elastic recovery to the plastic deformation ratio compared to other treatment groups ($P \leq 0.0083$).

There was no significant difference between the ratios of the three BAG ($P \geq 0.0083$), although they were significantly higher than CS ($P \leq 0.0083$).

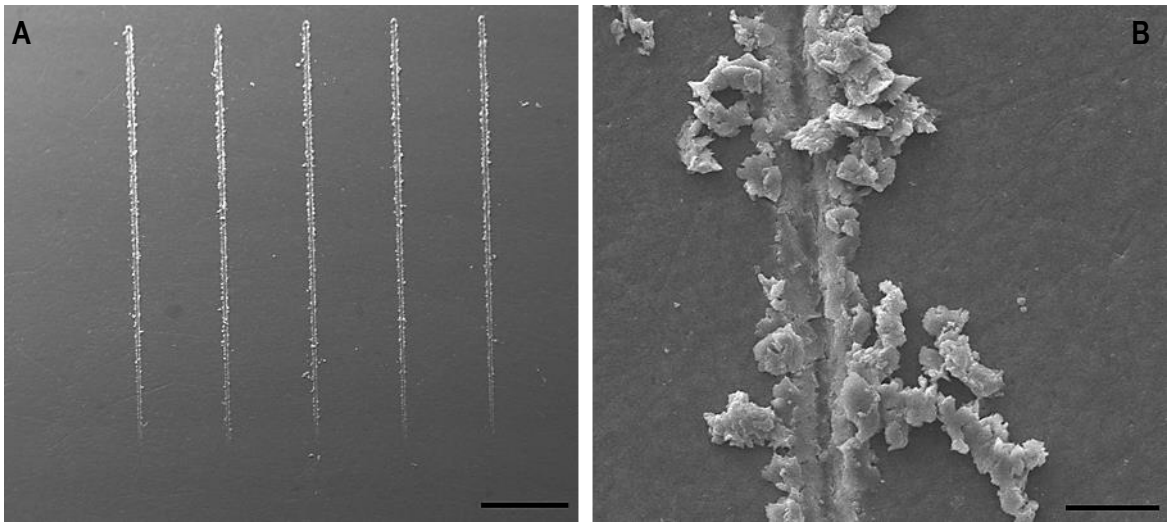

Figure 3. 9: Example of the scratch test taken from; overview of the surface after 5 scratches (A) and higher magnification of a scratch showing material being pushed aside (B), scale bar represents 400µm

Table 3. 6: Mean ±standard deviation (SD) of scratch penetration depth and elastic: plastic ratio values of all six groups

Group	Scratch penetration depth /µm	Elastic: Plastic ratio
AS	10.71 (±0.37)	1.18 (±0.09)
AG	10.44 (±0.98)	1.89 (±0.21)
CCPS	14.09 (±0.81)	1.31 (±0.23)
CS	12.9 (±0.35)	1.11 (±0.15)
CSPS	12.72 (±0.40)	1.47 (±0.17)
FCPS	13.46(±0.33)	1.36 (±0.29)

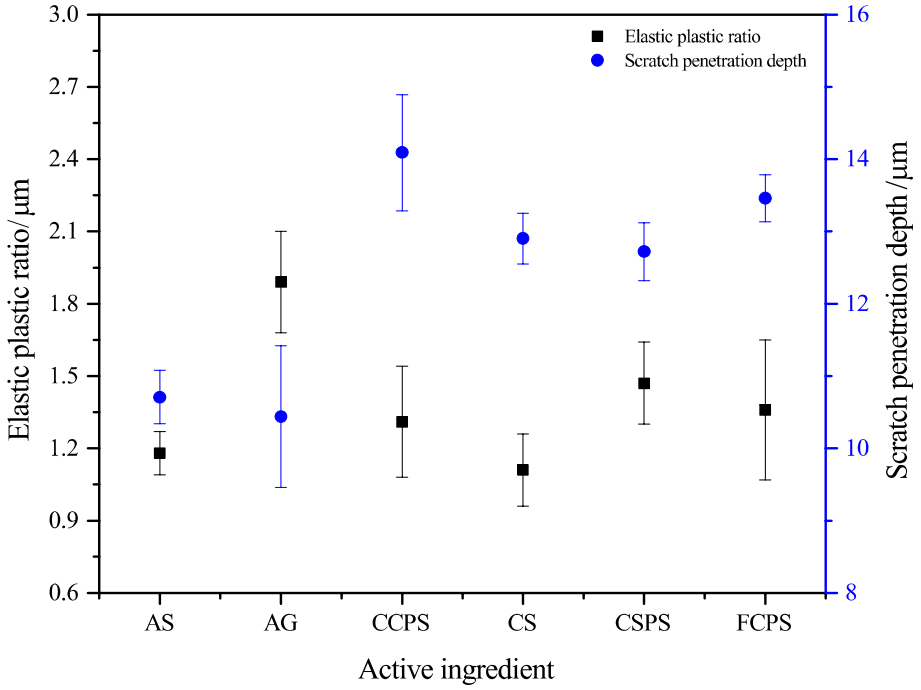

Figure 3. 10: Elastic-Plastic ratio and perpetration depth at maximum load

3.3.4 Acid Challenge

Citric acid removed the protective layer in CCPS, CS and FCPS while the layer in AG and CSPS groups had remained partially intact. There was still evidence of tubules occlusion in all but the CS group (Figure 3.11). The mean percentage of hardness change (Figure 3.12) demonstrated a reduction in all treatment groups. The layer formed by AG had a significantly smaller hardness reduction compared to other groups ($P \leq 0.0083$). AS and CS performed poorly under acid challenge with significant hardness loss ($P \leq 0.0083$). There was no significant difference between the 3 BAG groups ($P \geq 0.0083$), however, CCPS was not as acid resistant as CSPS and FCPS.

Table 3. 7: Mean ±standard deviation (SD) H of the layers before and after citric acid treatment

	AS	AG	CCPS	CS	CSPS	FCPS
After Brushing	0.54 (±0.013)	0.8 (±0.05)	0.72 (±0.08)	0.82 (±0.06)	0.76 (±0.03)	0.73 (±0.03)
After Acid challenge	0.36 (±0.016)	0.7 (±0.06)	0.58 (±0.04)	0.58 (±0.05)	0.65 (±0.02)	0.61 (±0.04)
Mean hardness % change	33.54 (±3.48)	12.52 (±2.81)	19.4 (±4.8)	29.27 (±5.78)	14.92 (±1.67)	16.45 (±1.52)

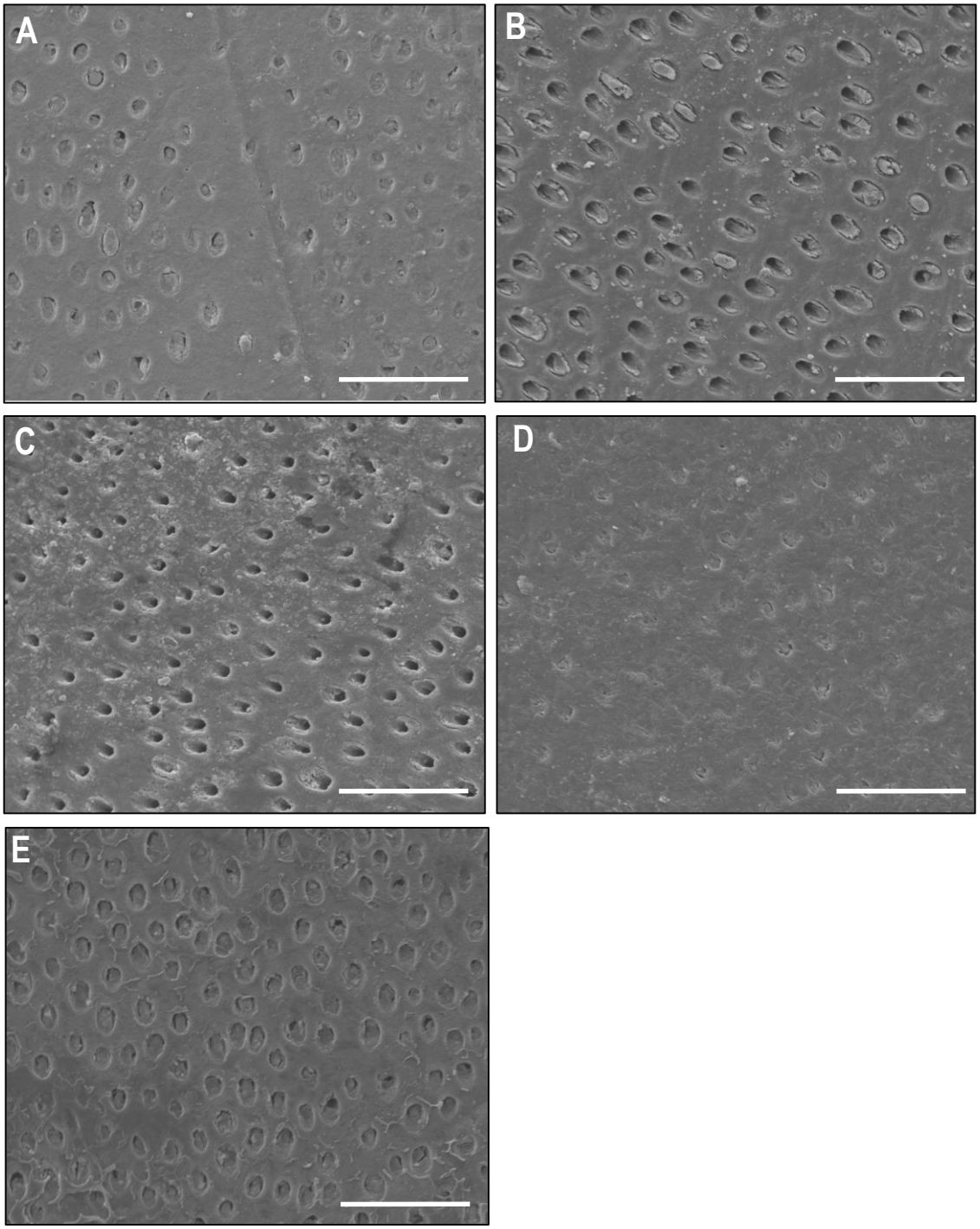

Figure 3. 11: SEM images taken after acid treatment; AG(A), CCPS(B), CS(C), CSPS(D), FCPS(E), 3000X magnification, scale bar represent 20µm

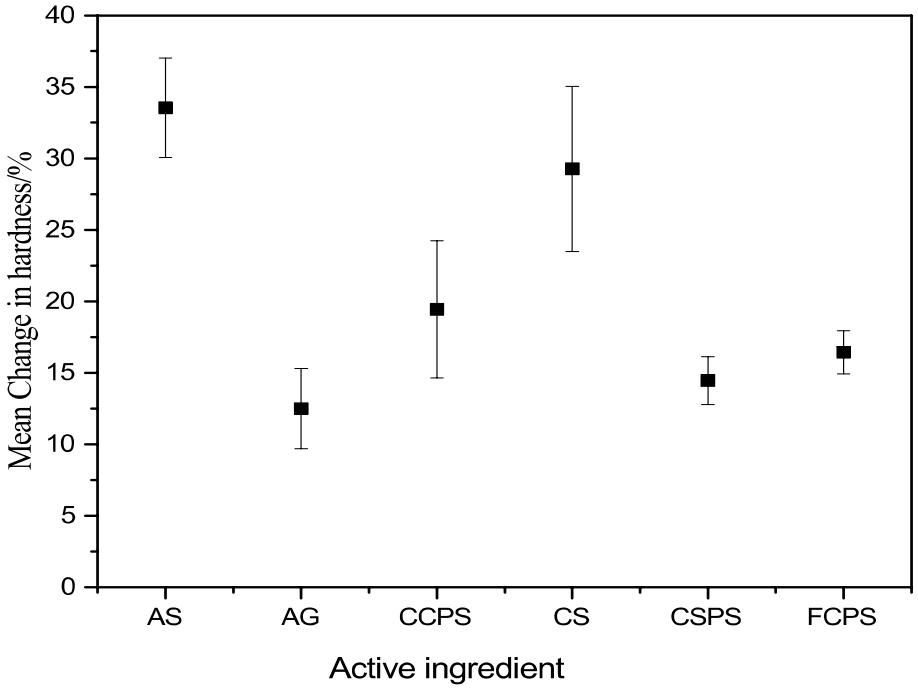

Figure 3. 12: Mean hardness change in percentage after citric acid challenge

3.4 Discussion

The key approach to treating dentine hypersensitivity and protecting the dental tissue from further damage is to form a protective layer over the open tubules. As well as shielding the tubules from stimuli these layers need to be acid and abrasion resistant to be able to protect the dentine in the harsh oral environment.

The SEM images demonstrated that chloro calcium Phosphosilicate (CCPS), calcium sodium phosphosilicate (CSPS), fluoro calcium phosphosilicate (FCPS), calcium silicate (CS) with sodium phosphate and arginine (AG) with calcium carbonate are capable of forming a layer on to the dentine surface after 7 days of brushing experiments. The findings are in agreement with the previous in vitro studies [16,90–92,133,177] which have demonstrated that these materials are effective in occluding tubules by forming a layer over the exposed tubules which is essential for treating DH.

AG (H_2Arg^+) is a positively charged amino acid that is attracted to the negatively charged dentine surface and acts as a crystallisation nuclei. AG consists of α- carboxyl and the α-amino groups which are active sites for the attraction of Ca^{2+} ions to the surface and play an important role in HA formation. The interaction of Ca^{2+} with these groups via electrostatic attraction form a $HArgCa^{2+}$ complex that has a stability constant (log K) of

2.21 [154]. PO_4^{3-} ions interact with the guanidyl side chain of AG to produce guanidinium/phosphate complex with a stability constant of 1.9 [155]. This amino group creates an ionic bond with the carboxyl group and can form a chelation ring with Ca^{2+} increasing the attraction of PO_4^{3-} ions, raising the local supersaturation which results in HA crystal formation. The calcium carbonate used in conjunction with AG act as a source of calcium and the interaction of the two promotes the deposition of phosphate ions from the saliva and the toothpaste.

Silica act as the crystallisation nuclei in CCPS, CSPS, FCPS, and CS. On contact with saliva, the silica network splits by hydrolysis of Si-O-Si bonds via OH^- ions forming a negatively charged silica rich gel on to the dentine surface attracting the Ca^{2+} and PO_4^{3-} ions. These ions then precipitate into a calcium phosphate ($CaO\text{-}P_2O_5$) rich layer. A further contribution of these ions from the surrounding solution facilitates the growth and crystallisation of $CaO\text{-}P_2O_5$ into an HA like layer [178].

Nanoindentation measurements showed that these layers were harder and stiffer than the control dentine. The H and E values for dentine (0.55±0.05 GPa and of 14.43±1.40 GPa respectively) were within the range for intertubular dentine [36,38,179]. However, some authors have reported higher H and E values for dentine.

For example, the nanoindentation data by Murry et al [49] revealed that dentine had a hardness of 0.89 GPa and modulus of 17.9 GPa. Poolthong et al [180] reported hardness of 0.9 GPa for intertubular dentine while another nanoindentation experiment on Human dentine from a third molar by Habelitz et al [181] showed that dentine had a modulus of 23.7 GPa, this finding was in agreement with the finding by Zheng et al [182] that revealed dry dentine had reduced modulus of 24 GPa. The control dentine discs were kept artificial saliva and were tested while fully immersed in deionised water. Therefore it was fully hydrated which can explain the lower mechanics compared to these studies.

Maris et al.[183] investigated the influence of hydration on the properties of compact Bovine bone. They found that the presence of water decreased the hardness and modulus by~40%. They explained that this was due to the water altering the interaction between minerals and surrounding collagen. In the presence of water hydrogen bonds are formed between the collagen and minerals which is weaker than the peptide bones that would form in the absence of water. The dentine has a strong similarity to the bone and it is

made up of type I collagen and hydroxyapatite, therefore, it is appropriate to assume the same mechanism is involved.

Within the treatment groups, CS formed the hardest and stiffest layer followed by AG, CSPS, FCPS and CCPS respectively. Aguiar et al.[19] investigated the hardness of dentine after treatment with toothpastes containing CSPS and AG by using microhardness measurements with a load of 0.5N. Their hardness value for control dentine was 0.54 GPa, which is in agreement with what has been reported in this thesis. The hardness increased to 0.64 GPa and 0.67 GPa after treatment with AG and CSPS respectively with weren't statistically significant. These values are lower than the values obtained from the nanoindentation experiment represented in section 3.3 which will be due to the high loads used and influence of the dentine substrate beneath the layers.

The H/E ratio (elastic strain to failure also referred to as 'plasticity index') for the layers was higher compared to the control dentine. Although hardness is a primary material property used to define wear resistance, the elastic modulus is also influential in defining the wear resistivity of a material, particularly in abrasion, impact and erosive wear. Therefore raking materials according to their H/E ratio can provide a better prediction of their wear resistivity [184]. The control dentine had an H/E ratio of 0.038 Which is within the range of 0.035 to 0.049 which is reported in the literature for dentine [22,45,49]. The layers had a higher H/E ratio than the control dentine, with an exception for the CS group. This would mean that the deformation of the surface under contact is more elastic.

Elastic recovery parameter (ERP) is another useful measurement obtained from NI, it provides a measure of the elastic recovery of the sample after the indentation load is removed, or in other words the ability of the surface to accumulate or store energy during indentation [185]. As for H/E results, the layers had higher ERP than the control dentine. AG group had the highest ERP compared to the other treatment groups. These results suggest that the layer which was formed by AG would be more resistant to wear as it responds more elastically to mechanical challenges.

Scratch testing is a commonly used technique for the characterisation of the adhesion of thin film coatings to their substrates and was used to detect the delamination load of the layer (if one exists) as well as the ratio of plastic deformation to elastic recovery of the surface. The ramped load scratch experiments detected no delamination load within the layers and the material was cut and displaced to the side by the tip. AG group had the lowest penetration depth and highest elastic/plastic ratio which supports the H/E and ERP findings in the sense that the layer behaves more elastically compared to the other layers. As a result of these differences between the properties, the initial null hypothesis on the mechanical properties of these layers was rejected.

As well as shielding the tubules from stimuli these layer needs to be acid and abrasion resistant to be able to protect the dentine in the harsh oral environment. Citric acid is one of the major acids found in fruits, fruit juices and soft drinks. Fruit juice pH levels range from 3.2 to 4.2, therefore, 1 % citric acid at pH 3.2 was chosen to test the resistance of the layers to acid challenge. The results showed that the control dentine had a significantly higher hardness loss compared to the treated samples with a layer on the surface. Although CS had the highest hardness and modulus, it did not perform well when it was subjected to citric acid treatment and subsequently its hardness was reduced by 29.27%. However, it was still harder than the control dentine. AG had a superior acid resistance compared to other groups followed by CSPS.

These findings were in agreement with Chen et al [186]. They compared the effectiveness of arginine and CSPS containing toothpastes in occluding tubules by SEM and challenged the dentine discs to a citric acid solution (pH 2). Their results showed that arginine containing toothpaste had a significantly higher level of occlusion with better acid resistivity compared to CSPS. Contrary to our acid challenge results Shaikh et al. [146] showed that FCPS was more acid resistant than CSPS by an SEM study, they compared the number of occluded tubules before and after citric acid challenge. However, this was done by manual counting and it is open to human error.

Currently, there is a lack of any published studies comparing these desensitizing dentifrices, making the comparison of the data presented in this chapter to the literature difficult. this demonstrates the novelty of this work. Data within this chapter demonstrated that the layers formed by all 5 materials have different mechanical properties and acid resistivity. The extensive comparison between the 5 different active

ingredients not only provided an insight into which material provides the best protection, but it also paved the way for further evaluation of what variable contributes to the formation of a more superior protective barrier.

It was hypothesised that there are structural and/ or compositional differences amongst the layers that influence these properties which were further investigated in the next chapter (chapter 4). The use of the unique liquid cell also provided a more representative testing condition to the oral environment while the nanoindentation and nano scratch set up ensured the data was not influenced by the dentine substrate.

3.5 Limitations

The creation and characterisation of the layers presented within this chapter were done under a very controlled environment. Therefore it needs to be acknowledged that the harsh conditions within the oral cavity could influence the formation of these layers. The environment in the mouth is not as stable as the in-lab conditions due to the constant fluctuation of pH and the presence of microbial species. The time it takes for the layers to form in vivo and their mechanical properties could be influenced as the result. Another limitation of this study was the lack of control over the brushing load which would have resulted in some variation in brushing strokes and load between brushings. However, the brushing process was done by a single operator. This approach is consistent with other studies [150,164,187]. It was anticipated that variation would have evened out over the course of the 14 brushing events and the large number of samples tested and ultimately wouldn’t have significantly affected the results.

3.6 Conclusions

The H and E measurements provide information about the mechanical properties of the layers and their ability to protect the dental tissue against mechanical and chemical (acid) challenge. SEM results within this chapter showed that all 5 materials have similar tubule occlusion capabilities by forming an HA like layer over exposed dentine. The layer with the highest H was formed by CS with sodium phosphate however it did not perform well under acid challenge. AG coupled with calcium carbonate formed the second hardest layer and it had a superior acid resistivity compared to other treatment groups. It also had an enhanced H/E ratio and ERP. The scratch penetration depth and elastic-plastic ratio data also suggest that this layer behaves more elastically under abrasion which would result in a more wear resistant HA. It can be concluded that even though all 5 materials can provide protective barriers to dentine, AG can form a layer with more superior properties and therefore it may provide better protection against the mechanical, chemical and abrasive challenges within the oral cavity.

CHAPTER 4 Characterisation of HA-Like Layers

4.1 Introduction

Data presented in chapter 3 demonstrated that the layers which were formed on the dentine surface by chloro calcium Phosphosilicate (CCPS), calcium sodium phosphosilicate (CSPS), fluoro calcium phosphosilicate (FCPS), calcium silicate (CS) with sodium phosphate and arginine (AG) with calcium carbonate had superior nanomechanical properties compared to the control dentine surface. These properties however varied between each treatment group. To be able to explain the differences between these layers, further characterisation techniques such as scanning electron microscopy (SEM) with backscattered electron detector (BSE), nuclear magnetic resonance (NMR), X-ray-diffraction (XRD), Fourier-transform infrared spectroscopy (FTIR), Energy-dispersive X-ray (EDX) and Raman-spectroscopy were used to determine the elemental and structural differences between the layers.

The backscattered imaging was used for quantifying the mineral density of the layers by using the greyscale values. This is based on the principle that a fraction of electrons which collide with the sample and then detected increases with the atomic number of the sample. This atomic number is proportional to the signal of BSE and the gray level of the image [188].

The elemental composition of the layers and crystallisation of the calcium phosphate into apatite was then investigated by EDX and XRD respectively. NMR and Raman spectroscopy was also used to provide information about the chemical structure of the layers at the molecular scale while the mineral crystallinity was determined by FTIR. Raman peak intensity is proportional to the number of molecules within the volume of the scanned area. HA produces a Raman phosphate peak at 959 cm^{-1} which characterises the tetrahedral PO_4 group (P–O bond) within HA [189].

The chemical shift produced by NMR Provide a method of determining the structure and composition of the HA like layers. The compactness of the structure can be predicted using this density data which can be compared to BSE imaging results [190].

Understanding the relationship between the mechanics, the minerals, crystal structure and density of these layers can aid the development of a new formulation for better and prolonged protection of dental tissue in a harsh oral environment.

4.2 Methodology

4.2.5 Backscattered Electron Imaging (BSE) and EDX

BSE images were taken in the same way as the SEM images (section 3.2.5). The greyscale values of each image were measured using the ImageJ software. The values were taken from 100 random points from each image and averaged to give a greyscale value for each group.

EDX was performed with a scan time of 120 seconds to identify the elemental makeup and ratios within the layers. To minimise the dentine substrate effect on the result and to ensure the interaction volume was small enough to characterise the content of the layers only, the accelerating voltage was reduced to 10 kV.

4.2.6 XRD

The layers were investigated using XRD (SmartLab, Rigaku, Japan) to detect the formation of crystalline apatite. XRD data were collected at room temperature with a 0.033º 2θ step size and a count rate of 99.6 s step^{-1}, from 2θ values of 10º to 60º. The average crystal size within the layers was then calculated from the XRD pattern using the Scherrer equation:

$$D = \frac{K\lambda}{\beta \cos\theta} \tag{4.1}$$

Where D is the Crystallite size

K is Scherrer constant = 0.9

λ is the wavelength of the X- ray= 0.15406 nm

β is full width at the half maximum (FWHM) (figure 4.1)

θ is the peak position

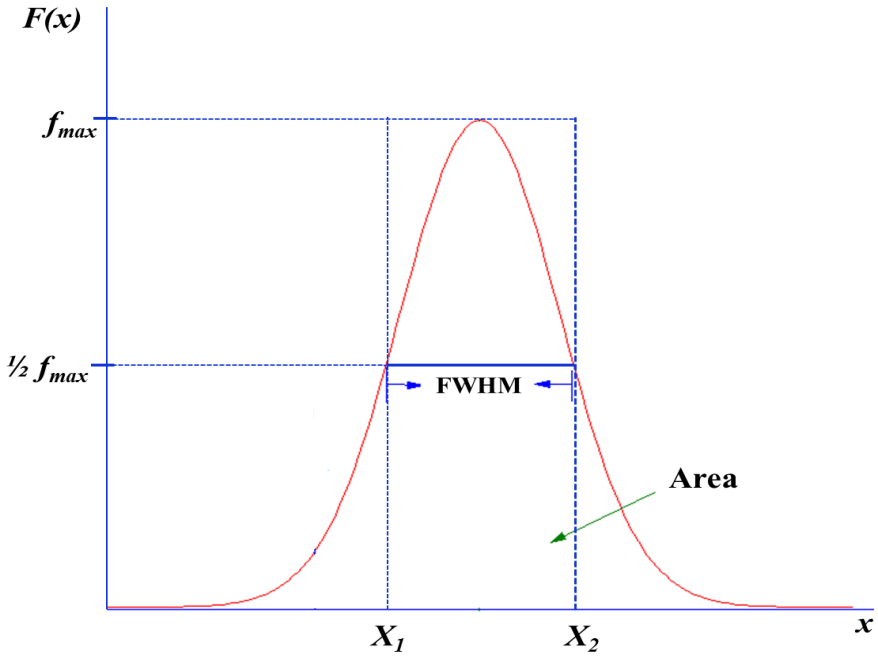

Figure 4. 1: Full Width at Half Maximum of a Peak

The Scherrer equation can either be applied to either a single peak or a combination of several peaks to calculate the crystallite size. Hanschin et al. [191] argued that the multiple peak approach could not provide an accurate measurement due to overlapping of the peaks within the regions of 30º to 25º 2θ that contain the (211), (112), (300), and (202) peaks. The (002) peak at 26º was identified as the best for calculating the crystallinity of human bone as it is not affected by any peak overlap. Several other authors [192–194] also have used the single peak (the (002) peak at 26º) method to estimate the crystal size of hydroxyapatite.

This approach was employed in this study to calculate the crystal size of the different hydroxyapatite like layers. The position and FWHM for (002) peak were measured by using the peak analyser function in the origin software then entered into equation 4.1 to calculate the crystal size for each layer.

4.2.7 NMR

Random discs from each group (n=2) were chosen to be further examined by ^{31}P MAS NMR Experiments using a Bruker 200 MHz Spectrometer under spinning conditions of 2.5 kHz in a 6 mm rotor. Spectra were collected with a 250 second delay time with 32 scans. To calibrate the ^{31}P chemical shift H_3PO_4 solution was used as a reference. The smaller number of samples for these experiments was due to a lack of access to the equipment. The ^{31}P isotops were choses over ^{19}F and ^{29}Si as phosphate were thought to be the common ion present in all 5 layers as well as the hydroxyapatite for control dentine. CCSP lack fluoride in its formulation while AG lacks silica therefore using the respective isotops would not have been appropriate.

4.2.8 FTIR

1µm thick slices were taken from the surface of dentine discs from each group (n=3) by a diamond knife mounted on a microtome. The slices were sandwiched between two potassium bromide (KBr) discs to ensure the slices were flat and supported during data acquisition using a Fourier-transform infrared spectrometer (FTIR; Bruker, Germany). Data was collected from 1600 to 500 cm^{-1} wavenumber, with a spectral resolution of 16cm^{-1} with 8 repeat scans. To avoid any atmospheric influence on the data a spectrum was taken of the background before each scan which was applied to the final data.

The crystallinity index (CI_{FTIR}) was calculated using the "height method" and represents a measure of the average crystallite size. A baseline was applied to the spectra from 750 cm^{-1} to 500cm^{-1}. The intensities of the two symmetrical phosphate peaks (PO_4^{3-} ν_4) at 602 $cm^{-1}$and 553 cm^{-1} as well as the lowest point between the two at 580cm^{-1} were measured and CI_{FTIR} was then calculated by [195]:

$$\mathrm{CI_{FTIR}} = \frac{\mathrm{A_{553}} + \mathrm{A_{602}}}{\mathrm{A_{580}}} \tag{4.2}$$

Where A_{553} and A_{602} are the heights (absorbance) of the two peaks at 553 cm^{-1} and 602cm^{-1} and A_{580} is the absorbance value at the lowest point between these two peaks. A_{553} and A_{602} increase and A_{580} decreases with increasing crystal size, resulting in higher $CI_{FTIR.}$

4.2.9 Raman Spectroscopy

A Raman microscope (Renishaw Plc, Wottonunder- Edge, UK) was used to characterise the surface of dentine discs (n=5) from each group. At the start of the data collection, a silicon sample with a characteristic band at 520 cm^{-1} was used to calibrate the microscope. A laser with a wavelength of 785 nm and power of 50 mW was used to take 3 scans from the surface of each sample with an exposure time of 60 seconds over a 200-1500 cm^{-1} Raman shift range. This spectral range was chosen because the main peaks of both silicate glasses and hydroxyapatite fall within this interval [196]. The resultant 15 scans per treatment group were then imported into Origin analysis software, averaged and plotted as Raman shift vs mean intensity. The area under the phosphate peak (960cm^{-1}) was then calculated by integrating the peak, also using Origin software.

Following the surface measurements, the discs were cross-sectioned using a low speed diamond saw and Raman measurements were repeated at the cross-section of the discs. 3 scans with the same testing conditions as the surface measurements were taken at 5 µm intervals from the surface down to 30 µm to detect any mineral changes and possible remineralisation of the underlying tissues. The resultant spectra were again integrated to calculate the area under the 960cm^{-1} peak at each given distance from the surface.

4.2.10 Statistics

The means of the 6 groups presented in this chapter were initially analysed using a one-way analysis of variance (ANOVA) to determine whether they were significant. This was followed by a t-test (assuming equal variance) to identify any significant differences between the means of the groups with post hoc Bonferroni correction. This correction involved dividing the significant value for the t-test (0.05) by the number of groups. $P \leq 0.0083$ was considered to be significant for all the experiments within this chapter.

4.3 Results

4.3.1 BSE

Figure 4.2 shows the backscattered SEM micrographs of the control and treated dentine samples. The grayscale values (Table 4.1) calculated from the backscattered image show that the layer which was formed by CS had a significantly higher greyscale value compared to the other groups ($p \leq 0.0083$) while the greyscale value for the control group (AS) was significantly lower ($P \leq 0.0083$). The layer with the second highest greyscale value was formed by AG followed by CSPS, FCPS, and CCPS. There was no significant difference between AG and CSPS ($P \geq 0.0083$) however they were significantly higher than FCPS and CCPS ($P \leq 0.0083$).

Table 4. 1: Greyscales from backscattered images

Group	Greyscale value	SD/ ±
AS	94.95	94.95
AG	155.03	16.01
CCPS	117.79	12.89
CS	166.56	15.59
CSPS	151.58	15.46
FCPS	124.38	16.93

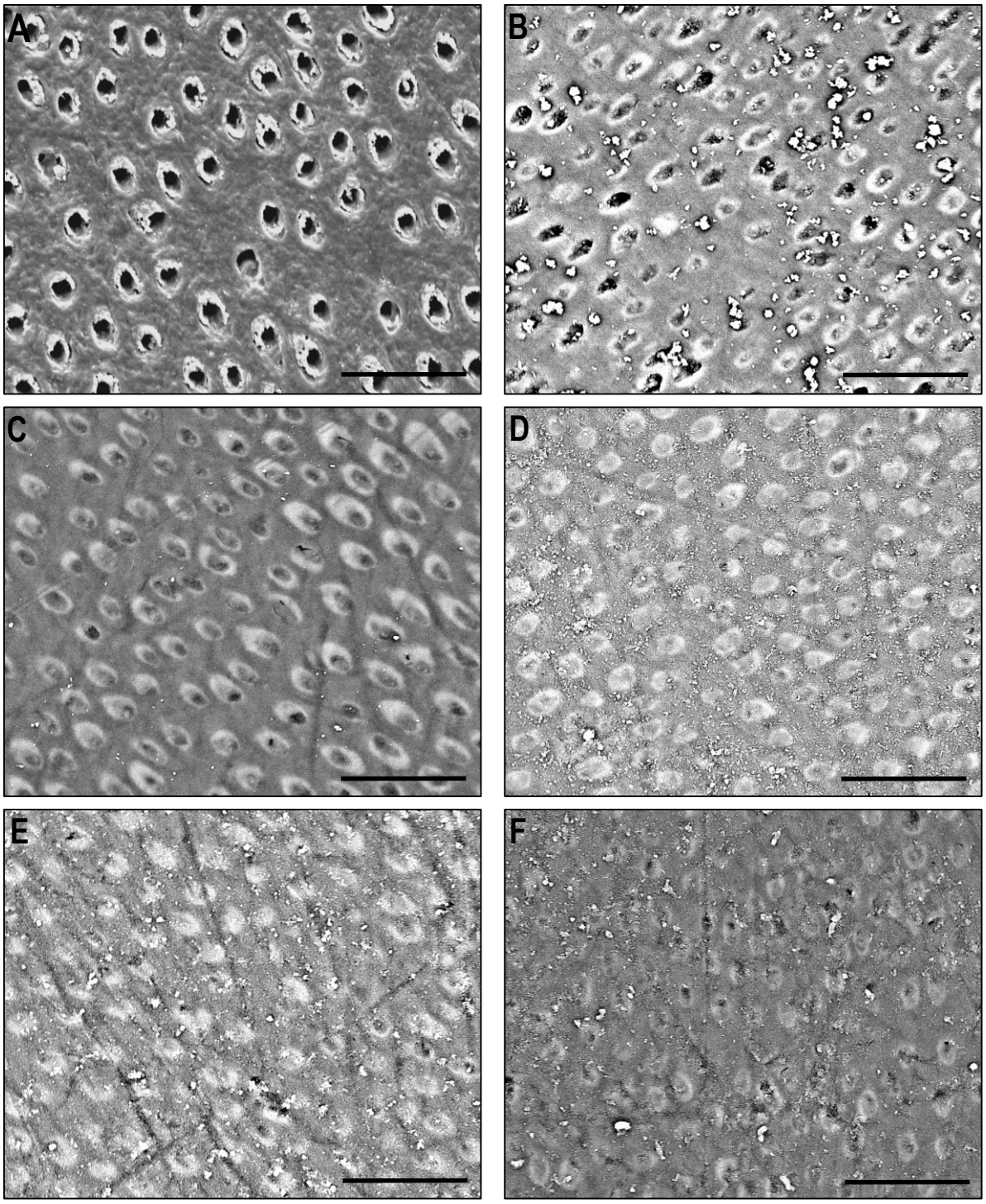

Figure 4. 2: BSE SEM images of the treated and control dentine; artificial saliva (a), AG (b), CCPS (c), CS (d), CSPS (e), FCPS (f), 3000X magnification, scale bar represent 20µm

4.3.2 EDX analysis

EDX analysis was taken from the surface of the control dentine and the layers which had formed over the tubules after treatment with one of the toothpastes (figure 4.3). The control dentine was mainly made up calcium (Ca), phosphorus (P), and oxygen (O) with a small percentage of sodium (Na), magnesium (Mg) and silica (Si) which was expected due to the hydroxyapatite content of the dentine and the impurities within the structure. The spectra taken from the treatment groups also showed similar peaks indicating that the layers were made up of hydroxyapatite like material. A small concentration of Na and Si ions were also detected from the layers which would have sourced from the toothpaste (table 4.2). The intensities of the peak were also higher for the treated samples compared to the control.

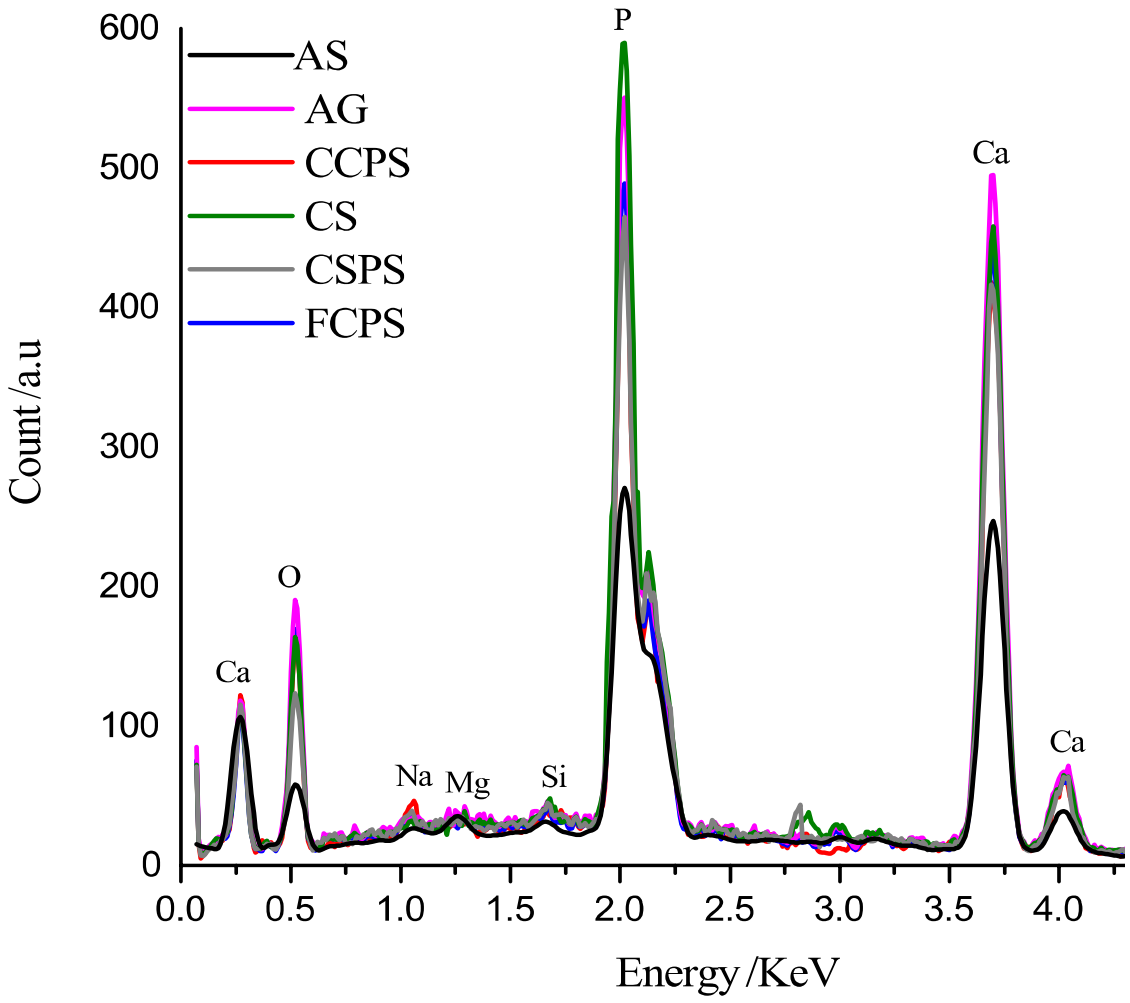

Figure 4. 3: EDX Comparison of control and treated samples

Table 4. 2: Elemental content in weight percentage (wt.%) for each group obtained from EDX

	Ca	P	O	Na	Mg	Si	Total
AS	36.88 (±0.66)	20.96 (±0.63)	37.44 (±0.51)	0.96 (±0.08)	2.87 (±0.09)	0.89 (±0.08)	100
AG	40.10 (±0.90)	19.45 (±0.33)	40.07 (±0.88)	-	-	0.38 (±0.08)	100
CCPS	37.48 (±1.07)	19.52 (±0.24)	39.75 (±0.88)	1.38 (±0.22)	-	1.87 (±0.18)	100
CS	39.12 (±1.07)	22.36 (±0.24)	35.98 (±0.88)	-	-	2.54 (±0.22)	100
CSPS	38.88 (±1.07)	19.48 (±0.24)	39.30 (±0.88)	1.22 (±0.22)	-	1.12 (±0.18)	100
FCPS	38.22 (±1.07)	19.90 (±0.24)	38.40 (±0.88)	1.88 (±0.22)	-	1.60 (±0.18)	100

Following the EDX measurements, the ratio between calcium and phosphate were calculated (Table 4.3). The results showed that the mean Ca:P ratios were significantly higher ($P \leq 0.0083$) for the layers compared to the control, except for the ratio for CS. No significant differences were observed between the 3 BAG group and AG ($P \geq 0.0083$).

Table 4. 3: Ca: P ratios

Treatment group	C:P ratio	SD
AS	1.76	0.04
AG	2.04	0.06
CCPS	1.92	0.05
CS	1.75	0.04
CSPS	2.00	0.08
FCPS	1.93	0.09

4.3.3XRD

Figure 4.4 shows the XRD pattern of the different layers formed by all 5 active ingredients and the surface of the control dentine. The diffraction pattern revealed peaks at 26°, 32°, 39°, 46° and 49° for all 6 groups which were characteristic of hydroxyapatite and confirmed that the layers were structurally similar to HA. The patterns for treated samples had higher peak intensities compared to the control specimen. Amongst the treated samples AG produced the peaks with the highest intensities followed by CSPS, FCPS, CCPS, and CS.

FWHM of the (002) peaks and the average crystal size of the layers are given in table 4.4. Data showed that crystal size for the AG group was significantly ($p \leq 0.0083$) higher with the mean crystal size of 26.59 nm compared to the other 5 groups. This was reflected in the FWHM value for the (002) peak for the AG group which was the lowest. As the crystal size increases the XRD peaks become sharper and more intense reducing the FWHM of the diffraction peak. There was no significant difference ($p \geq 0.0083$) between CCPS, CSPS, and FCPS, however, CSPS had a higher mean crystal size.

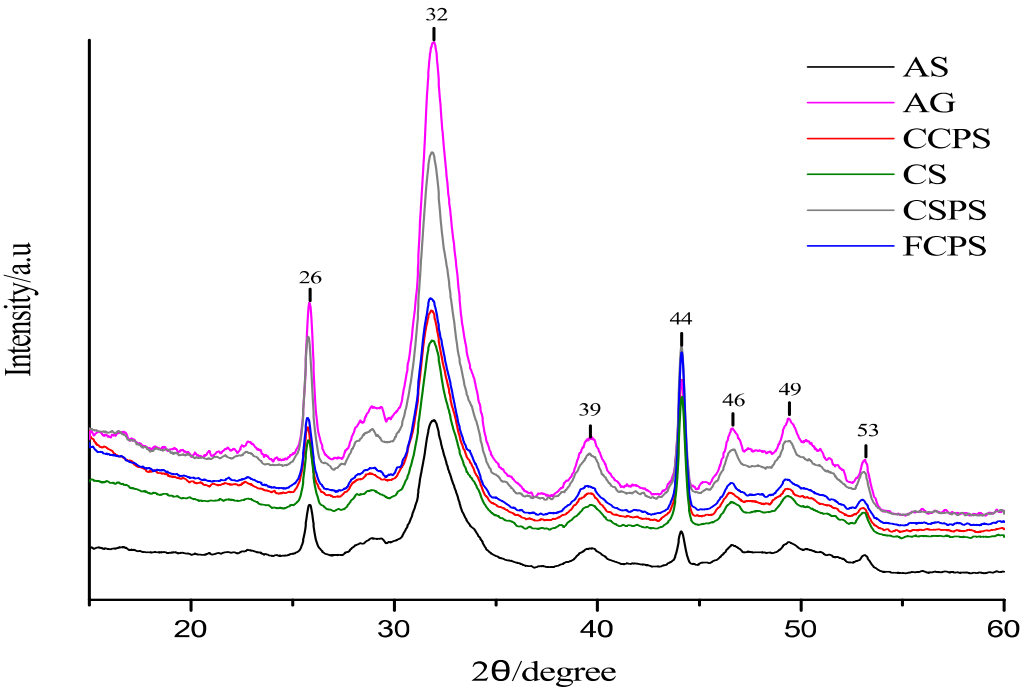

Figure 4. 4: XRD measurements of control and treated samples

Table 4. 4: Average crystallite sizes and crystallinities of the different HA layers

Treatment group	Line width (002) FWHM/º	The average crystallite size (002), D/nm
AS	0.53±0.02	16.79±0.55
AG	0.33±0.01	26.94±0.54
CCPS	0.45±0.02	19.48±0.91
CS	0.53±0.02	16.60±0.76
CSPS	0.42±0.01	21.01±0.49
FCPS	0.45±0.02	19.76±0.68

4.3.4 Raman spectroscopy

Figure 4.5 represents the Raman measurements taken from the surface of the dentine discs within all 6 groups. All spectra have peaks at the same Raman shift, however, the spectra of the treated samples were significantly higher in intensity compared to the AS group. The measurements taken from the dentine disc treated with CS containing toothpaste produced the highest peak intensities compared to other treatment groups. This was followed by AG and the 3 bioactive glasses. Peak intensities are proportional to the number of molecules within the volume of the scanned area and the position of the peaks are characteristic for the vibration, bending and stretching of phosphate (PO_4^{3-}) groups. The spectra demonstrated four different vibration modes of PO_4^{3-} ion at the following shifts; 434cm^{-1} (symmetric bending vibrational mode – PO_4^{-3} v_2), 590cm^{-1} (asymmetric bending vibrational mode – PO_4^{-3} v_4), 960 cm^{-1} (symmetric bending vibrational mode – PO_4^{-3} v_1) and 1070 cm^{-1} (C-O). A collagen band was observed around 1250cm^{-1} (amide III).

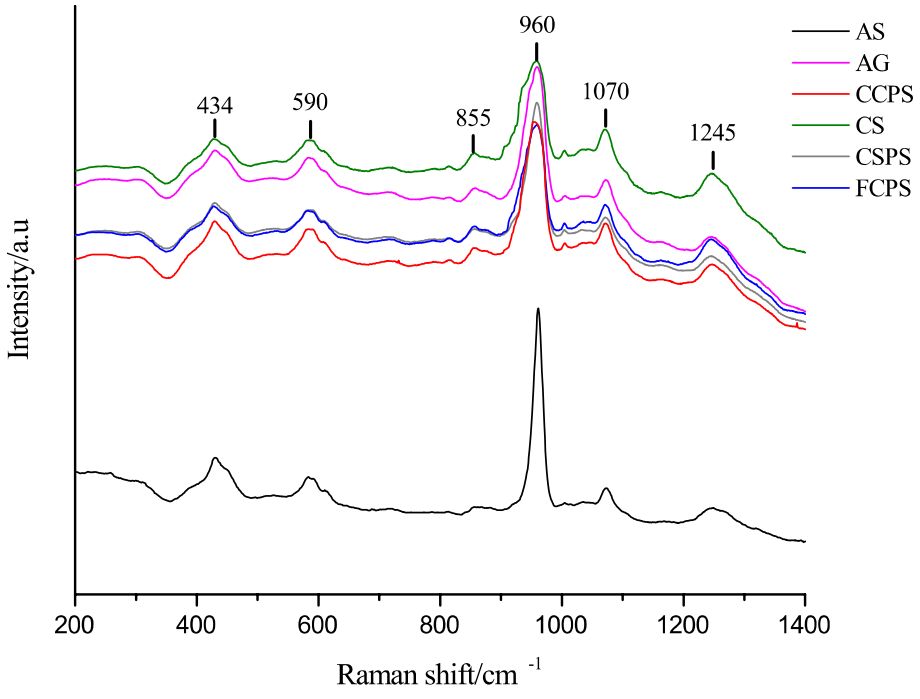

Figure 4. 5: Raman measurements from the surface of dentine discs, treated and control group

The area under the PO_4^{3-} peak at 960 cm^{-1} (from 896 to 997 cm^{-1}) was calculated for surface and cross-section measurements by applying a baseline to the peaks and subsequently integrating them using the Origin software. The area under the PO_4^{3-} (960 cm^{-1}) peak for treated samples at the surface (table 4.5) was significantly higher compared to the control group ($P \leq 0.0083$). CS had a significantly higher area ($P \leq 0.0083$) followed by AG, CSPS, FCPS, CCPS, and AS. There was no significant difference between the 3 bioactive glasses.

Table 4. 5: Area under 960 cm^{-1} peak at the surface at variance distances from the surface

Treatment group	0 µm	5 µm	10 µm	15 µm	20 µm	25µm	30 µm
AS	329.45 (±20.52)	314.88 (±20.17)	297.83 (±19.08)	296.02 (±19.20)	283.24 (±18.14)	276.28 (±17.7)	264.70 (±16.95)
AG	872.64 (±53.88)	834.03 (±52.67)	780.81 (±49.30)	763.21 (±48.20)	723.24 (±45.67)	691.61 (±43.67)	534.32 (±33.74)
CCPS	693.21 (±43.18)	662.55 (±42.45)	631.62 (±40.47)	562.61 (±36.04)	519.58 (±33.29)	453.91 (±29.08)	422.57 (±27.07)
CS	1013.22 (±612.56)	968.37 (±61.15)	426.08 (±26.91)	306.52 (±19.35)	300.47 (±18.97)	272.54 (±17.21)	253.41 (±16.00)
CSPS	765.59 (±54.32)	735.62 (±47.13)	727.09 (±46.59)	608.30 (±39.00)	570.31 (±36.54)	557.98 (±35.75)	498.72 (±31.95)
FCPS	731.14 (±51.50)	702.51 (±44.36)	549.32 (±34.69)	523.07 (±33.03)	474.65 (±29.97)	471.31 (±29.76)	486.97 (±30.75)

Figure 4.6 shows the area under the 960 cm^{-1} at a given distance from the surface for all 6 groups. The data shows that the area decreases as the measurements move from the surface to 30 µm. There was no significant decrease in the area from the surface to 5µm beneath the surface for any of the 6 groups ($P \geq 0.0083$), however at 10 µm away from the surface the peak area for CS was significantly reduced to the lowest between the treatment groups ($P \leq 0.0083$), although still significantly higher than control ($P \leq 0.0083$). At this position AG had a significantly higher area ($P \leq 0.0083$) compared to CCPS, FCPS, CS and AS while CSPS was significantly higher than the other two bioactive glasses ($P \leq 0.0083$). At 15-25 µm AG was significantly higher than all groups ($P \leq 0.0083$) and CS was no longer significantly higher than the control ($P \geq 0.0083$). At 30 µm depth, the area of the peak for the 3 BAG and AG were significantly higher ($P \leq 0.0083$) than the control. AG, CSPS, and FCPS weren't significantly different ($P \geq 0.0083$), however, they were significantly higher than CCPS ($P \leq 0.0083$).

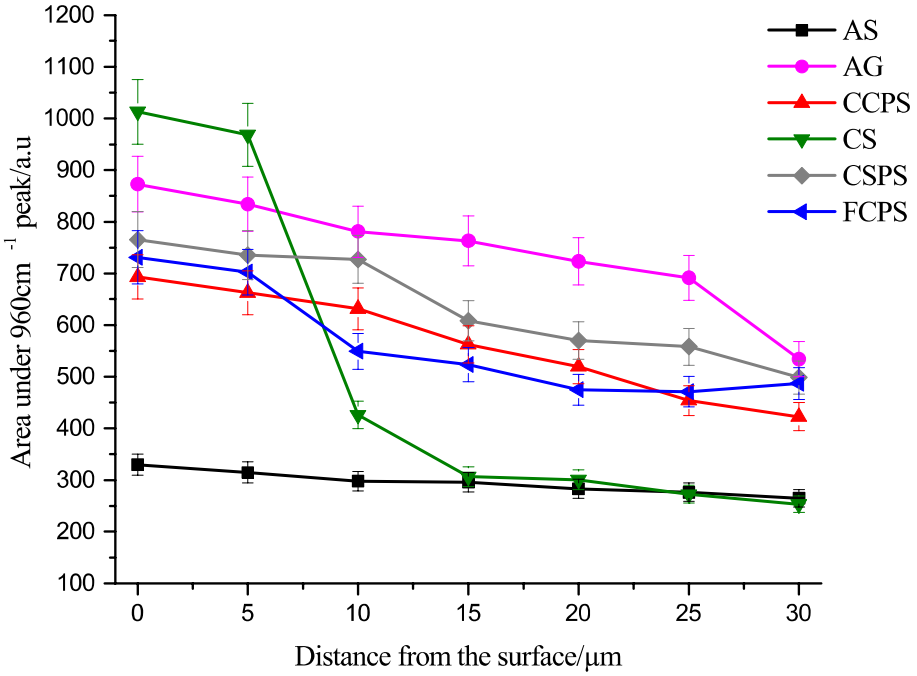

Figure 4. 6: Area under 960cm^{-1} peak at a different distance from the surface

4.3.5 NMR

The ^{31}P MAS spectra (figure 4.7) produced a strong peak at a position around 3.3±0.08 ppm which is assigned to phosphorus in an orthophosphate (PO_4^{3-}) state. Davies et al [158] reported that this peak should consist of two peaks of 3.2 and 3.6ppm. However, a single peak was observed from our data (due to the PO_4^{3-} having undergone a transformation to HA [197]). The peak intensities were also higher for the treated samples compared to the control. The intensities from the NMR were in agreement with the Raman measurements. CS had the highest intensity followed by AG, CSPS, FCPS and CCPS and AS.

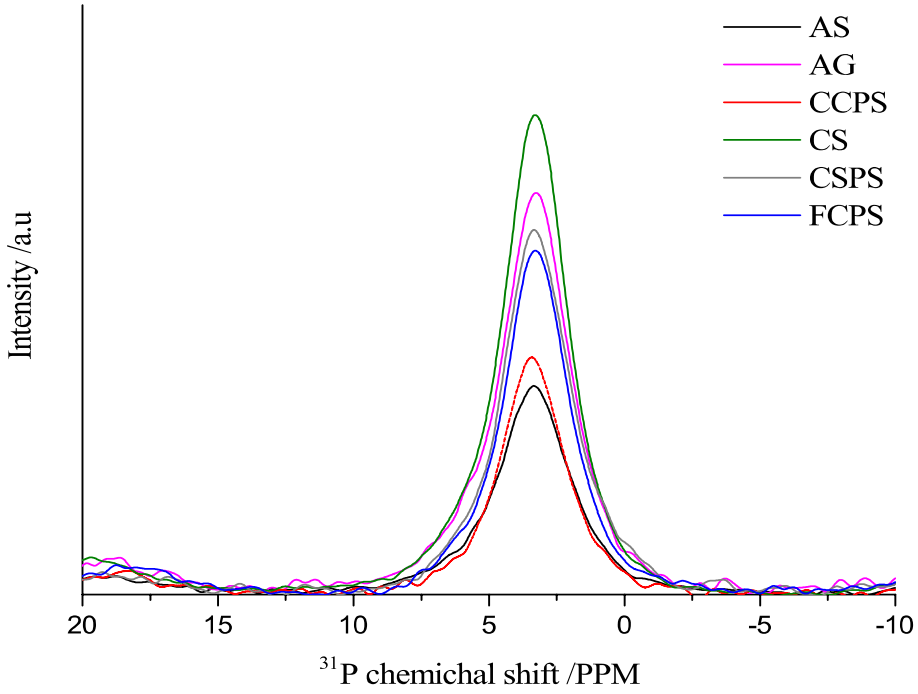

Figure 4. 7: ^{31}P MAS spectra of treated and control dentine discs

4.3.6 FTIR

FTIR spectra of samples from all 6 treatment groups are shown in Figure 4.8. It shows clearly the characteristic bands of apatite. The PO_4^{3-} peaks at 1240, 1027, 602, 553cm^{-1} and carbonate bands at 1450 and 870 cm^{-1} are similar to the peaks for synthetic HA [198]. The intensities of the peaks were higher for the treated groups compared to AS. AG produced a spectrum with the highest intensity followed by CSPS, FCPS, CCPS, and CS. This trend was in agreement with the XRD data.

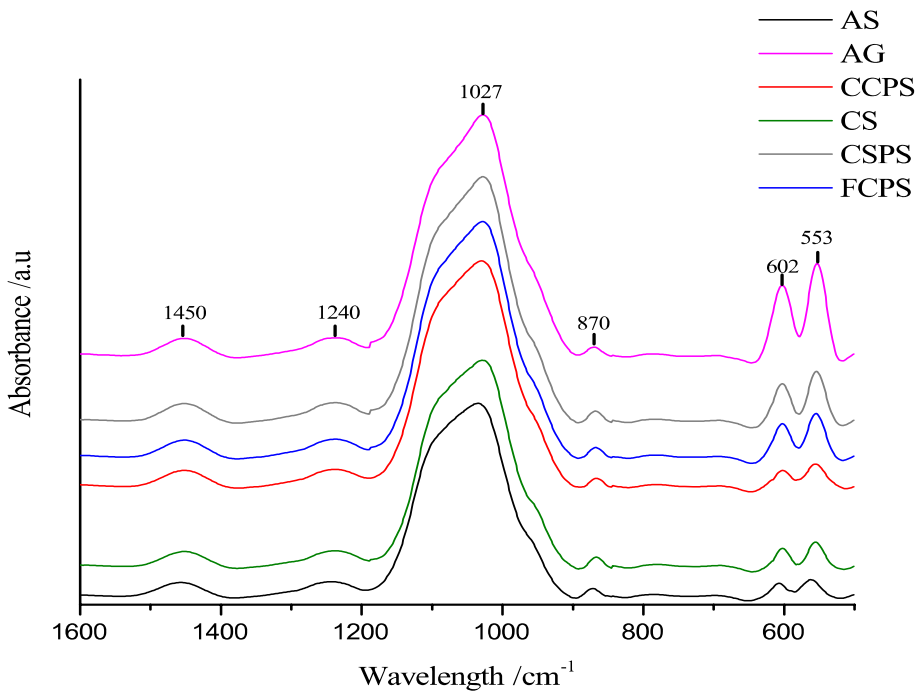

Figure 4. 8: FTIR measurements taken from the surface of control and treated dentine

CI_{FTIR} values provide information about the average crystal size and ordering of the HA layer. The height, splitting of two phosphate peaks at 550cm^{-1} and 600 cm^{-1} was used to determine the transition from amorphous HA to crystallized HA[124]. Figure 4.9 shows the CI_{FTIR} values calculated from figure 4.8 using the "height method". AG had a significantly higher CI_{FTIR} compared to the other five groups ($P \leq 0.0083$). There was no significant difference observed amongst the 3 BAG ($P \geq 0.0083$). The CI_{FTIR} for the CS group was significantly lower than for the AG and CSPS groups ($P \leq 0.0083$) but were not significantly different from AS, CCPS and FCPS ($P \geq 0.0083$).

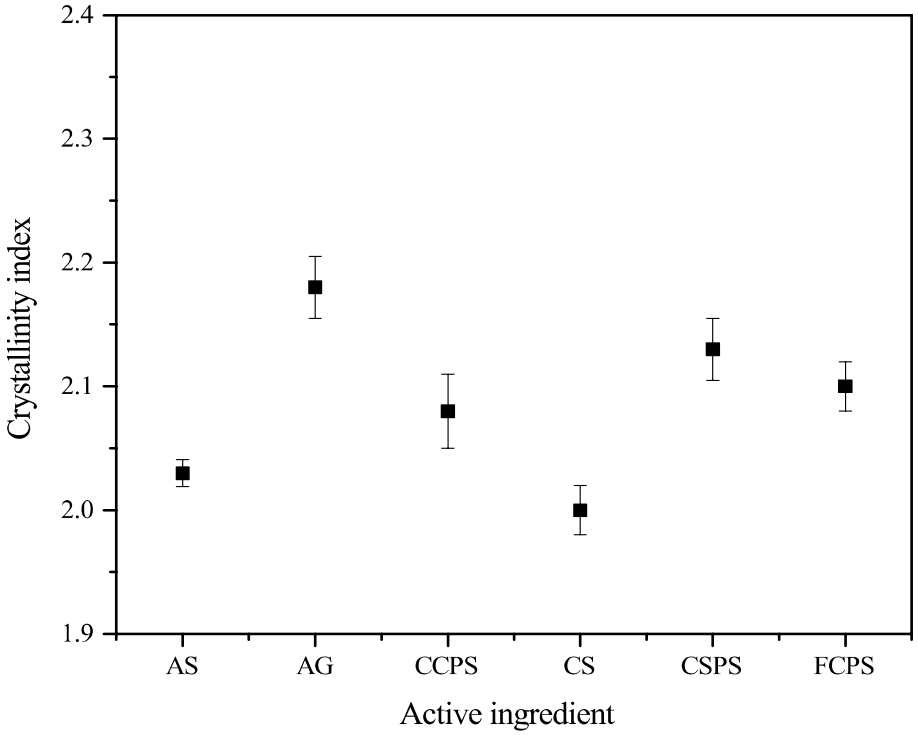

Figure 4. 9: Crystallinity index calculated from the FTIR data

4.4 Discussion

To be able to explain the differences in the mechanics of the layers, a range of different characterisation techniques were used. Backscattered electron (BSE) images were used to compare the mineral density of the layers. The greyscale values from BSE imaging showed substantially higher greyscale values for the treated samples compared to the control. The layer formed by CS had the highest greyscale values followed by AG, CSPS, FCPS, and CCPS respectively. Higher greyscale values indicate an increase in the mineral concentration present on the surface [190].

EDX measurements taken from the surface of the dentine discs showed that these layers were mainly made up of Ca, P and O ions and therefore chemically similar to the control dentine, suggesting the presence of HA like material. The ratios between Ca and P for the treated groups were also higher than the control dentine. The XRD pattern of the layers produced peaks characteristic of the HA, confirming that these layers were also structurally similar to HA.

The crystal size calculation from the XRD data showed that the HA like layer formed by AG had the highest crystal size and CS had the smallest crystal size. The smaller crystal size and smaller crystallinity index of CS mean it is more amorphous and therefore more prone to dissolution under acidic environment [199]. This explains why the AG layer had a superior acid resistivity and CS performed poorly when challenged by citric acid.

Raman spectroscopy was used to identify the chemical structure of the layers. The spectra for all groups produced a sharp peak related to the inorganic components at ~960 cm^{-1} (phosphate apatite). The intensities and area under the peaks were significantly higher for treated samples compared to the control which is indicative of HA with higher mineral density.

This, however, only tells us what is happening at the surface of the dentin. To confirm remineralisation of the dental tissues the Raman measurements were taken at the cross-section of the discs at 5µm intervals up to 30µm away from the surface. The area under the 960 cm^{-1} decreased as the measurements moved from the surface to 30 µm. the area for CS was higher than the other 5 groups at the surface and at 5 µm, however, the area was significantly reduced at 10 µm. Once the measurements moved to 15 µm, the area for CS was similar to that of the control while for other treatment groups the area was still higher. This suggests that the measurements taken at 5 µm were still within the layer and that the layer thickness lies between 5-10 µm with no mineralisation to the underlying dentine. The data for the other groups also indicates that the layer thickness was within the same range as the CS. A significant drop in the area for CSPS occurred at 15 µm and therefore layer thickness would be in the range of 10-15 µm. At 15-25 µm AG had a significantly higher peak area than all groups while still significantly higher than the control at 30 µm. This shows an increase in the phosphate below the surface and sign of mineralisation of the dentine.

The NMR measurements, like the Raman data taken from the surface of the discs, also demonstrated that the spectra for CS had the highest intensities amongst treatment groups. The chemical shift produced by these two techniques gives an inventory of the elements present. These peaks were associated with PO_4^{3-} ions with the higher intensities resulting from a higher concentration of phosphate ions present within the layers.

FTIR spectra were higher for the treated groups compared to AS. AG produced a spectrum with the highest intensity followed by CSPS, FCPS, CCPS, and CS. The HA crystallinity will have an influence on the mechanical and tribological properties as well as acid resistivity. Crystallinity was expressed in the form of an index (CI) and was measured using FTIR (CI_{FTIR}). It provides information about the average crystal size and ordering of a sample. The height, splitting and area of two phosphate peaks at 550 cm^{-1} and at 600 cm^{-1} was used to determine the transition from amorphous HA to crystallized HA [124]. AG had the highest CI_{FTIR} and therefore more crystalline while CS was the least crystalline. This trend was in agreement with the average crystal size calculated form the XRD measurements.

The NMR and Raman microscopy results indicate that CS has formed a layer with higher phosphate concentration. These findings coupled with a lower Ca/P ratio from the EDX suggest the formation of Biphasic tricalcium phosphate (BCP) composite [200], a mixture of β-tricalcium phosphate (TCP) and HA. β- TCP contains 42 PO_4^{3-} tetrahedra in its unit cell compared to only 6 PO_4^{3-} for HA. [201].

Viswanath et al. [202] showed that β- TCP crystals have both a higher hardness and modulus than HA crystals by using nanoindentation. This explains the higher mechanical properties of the layer for CS groups. The poor acid resistivity of the CS also supports the formation of BCP as a number of studies shown that BCP has a higher dissolution rate in the acidic environment compared to HA due to smaller crystal size [200,203].

Nucleation agents play a crucial role in deposition and precipitation of Ca^{2+} and PO_4^{3-} ions and further crystallisation into an HA layer. Silica act as the crystallisation nuclei in CCPS, CSPS, FCPS, and CS. The splitting of the silica network occurs by hydrolysis of Si-O-Si bonds via OH^- ions forming a negatively charged silica-rich gel on to the dentine surface which binds to the collagen of the dentine attracting the Ca^{2+} and PO_4^{3-} ions. Further contribution Ca^{2+} and PO_4^{3-} from the surrounding solution facilitate the growth of this layer which crystallises into an HA like layer. The combination of amino and carboxyl groups on AG creates a better nucleation site which leads to a higher concentration of ions attracted to the dentine surface. Due to the high stability constant of the $HArgCa^{2+}$ and guanidinium/phosphate complex the attracted ions are retained, this generates a favourable environment for the formation of HA, with higher crystal size [199]. This leads to a layer with better mechanics and higher acid resistivity.

4.5 Conclusion

The mechanical testing results in chapter 3 showed the layers formed by the active ingredients were harder and stiffer than the dentine, therefore they can be a protective barrier to the dentine tissue against further mechanical and chemical challenges as well as treating mild sensitivity. EDX measurements confirmed that these layers were chemically similar to the control dentine. Further characterisation with XRD revealed that these layers were also structurally similar to the control sample thus they are HA like. EDX and Raman spectroscopy both demonstrated an increase in the mineral content on the tooth surface. The Ca:P ratio and crystallinity index revealed a correlation between apatite density, higher crystallinity, mechanical properties and acid resistivity of the layers. Arginine with calcium carbonate formed the most crystalline layer with the highest crystallinity index and average crystal size which explains its superior acid resistivity. Arginine provides a better nucleation site for calcium and phosphate ions due to the presence of amino, hydroxyl and carboxyl groups that facilitated the retention and precipitations of these two ions that develop into crystalline HA with bigger crystal size.

Chapter 5 Serial Block Face Scanning Electron Microscopy

The work presented in this chapter focuses on developing a new imaging method for the determination of tubule occlusion. The suitability of a serial block face scanning electron microscopy (SBF SEM) to section and image dentine was assessed. This technique was then used to draw a comparison between Calcium sodium phosphosilicate (CSPS) and stannous fluoride (SnF_2) in terms of their tubule occlusion and mineralisation capabilities. This technique combines an ultra-microtome with the high resolution imaging capability of an SEM to generate 3D images of samples. The imaging setup enabled the study of the level of tubule occlusion, both by determining the number of occluded tubules per unit volume but also the depth of penetration of the active ingredients down the tubules.

SBF SEM uses backscattered electron imaging. The greyscale values from these images enabled comparison of the mineral density of the dentine tissues between the control and the treated samples and the detection of any possible mineralisation of the dentine tissue. Successful sectioning of dentine by SBF SEM allowed a relatively large volume analysis at high resolution, this will be highly beneficial in the development and research of new dental materials.

The study presented in this chapter was funded by GlaxoSmithKline who were interested in the comparison between SnF_2 and CSPS. Therefore two toothpastes containing these two active ingredienst were used rather than the 5 used in chaper 3 and 4 of this thesis.

5.1 Introduction

Teeth can become sensitive for several reasons such as cracks, dental decay, and deep fillings. However, two of the main causes of dentine hypersensitivity (DH) are gum recession and thinning of the enamel due to over brushing or acid erosion, exposing dentine tubules [1].

In the early stages, it is possible to manage and reduce sensitivity symptoms by using dentifrices designed to occlude these tubules by either depositing a layer over the exposed surface or by plugging materials down the tubules [86]. Stannous fluoride (SnF_2) [204–206] and Calcium sodium phosphosilicate (CSPS) [90,207,208] are two of the active ingredients used in toothpastes to occlude tubules and treat sensitivity symptoms.

CSPS releases calcium and phosphate ions when it comes in contact with saliva, these ions get deposited onto the dentine surface and form a layer that is chemically and structurally similar to hydroxyapatite [163]. SnF_2 rapidly hydrolyses in the presence of saliva, fluoride ions are released and get incorporated into the hydroxyapatite structure forming a fluroapatite [209]. The stannous ions are then oxidised from Sn (II) to Sn (IV) and form insoluble oxides which plug the tubules [206].

He et al. [205] demonstrated that SnF_2 dentifrice provided an immediate and significant sensitivity relief in a clinical study compared to the sodium monofluorophosphate control. An in vitro study by Takamizawa et al. [206] showed significant tubule occlusion after treatment with SnF_2. Earl et al. [16] used a focused ion beam (FIB) and scanning electron microscopy (SEM) to investigate the depth of tubules occlusion after treatment with CSPS. The results showed that dentine tubules were occluded to approximately 1μm (the depth of FIB cut). It is extremely time-consuming to mill a large volume of material to high depths by FIB-SEM. Earls et al. [210] used FIB-SEM to study the structure of the dentine where only 15 tubules were managed over 20 hours. SEM, on the other hand, does not provide information about the depth of occlusion.

Serial block face SEM (SBF-SEM) is a 3D imaging technique that uses a diamond knife in a microtome sitting within the chamber of an SEM to cut nanometre sized slices from the surface of a sample (block face). An image is initially taken from the block face, the sample is then cut at a given depth by the microtome, exposing a new block face. This process continues automatically and resulting images are compiled to provide a 3D reconstruction of the sample [211].

The present study aimed to determine the level of tubule occlusion by CSPS and SnF_2, both by determining the number of occluded tubules per unit volume but also the depth of penetration of the active ingredients using SBF SEM. It also aimed to use the backscattered images from the SBF SEM to investigate the mineralisation potential of the two ingredients by using the greyscale values of the images which are proportional to the mineral density [188].

Milling material with FIB-SEM [16] is more time consuming than cutting with a diamond knife. While some areas of the sample surface can be left uncut by the ion beam. The milling process can also be extremely time consuming and expensive with limited depth measurments.These limitations can be avoided by the use fo SBF-SEM. The null hypotheis tested in this in vitro study was that both CSPS and SnF_2 would produce same percentage of blockage with similar depth, while both minerlise the dentine tissue.

5.2 Materials and Method

5.2.1 Dentin Discs and Toothpaste Treatment

Bovine dentine discs (n=6) with a thickness of 1.00 ± 0.3 mm were supplied by Modus Laboratories Ltd (Reading, UK). Each disc was polished using 3µm and 1µm diamond suspensions to get a smooth surface finish, etched with 1% citric acid for 30 seconds to remove the smear layer and washed with deionised water for 1 minute. The discs were then randomly divided into two equal treatment groups (n=3). Discs were halved with one half treated with either Sensodyne® Repair and Protect (CSPS) or Rapid Relief (SnF_2) toothpastes (table 5.1) and one half as control. 2.0 ± 0.1mg of respective toothpaste was weighed onto a medium manual toothbrush (Colgate) and brushed on to the dentine discs for two minutes, twice per day for 7 days. 0.50 ml of artificial saliva (AS) was pipetted on to the toothbrush with toothpaste to stimulate the reaction of active ingredients in conditions that were more representative of the oral environment. The control discs were only brushed with AS. All dentine discs were stored in AS between brushing. The composition of the AS is described in section 3.2.2.

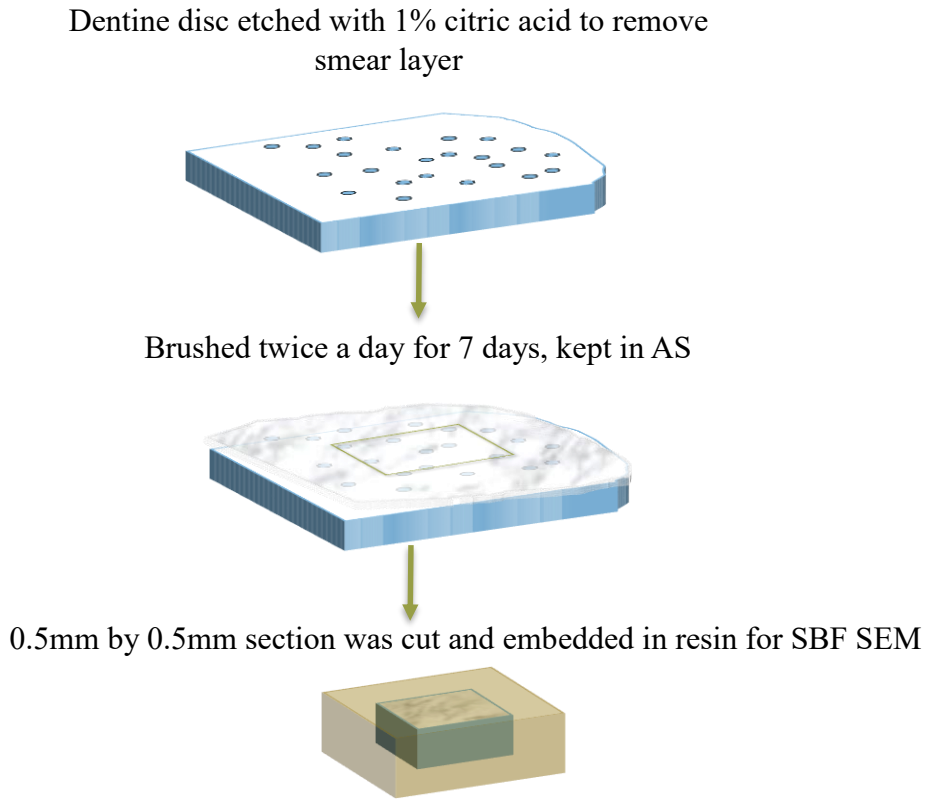

Figure 5. 1: Sample preparation protocol

Table 5. 1: Toothpastes and their active ingredient

Toothpaste	Active ingredient	Other ingredients	Company
Sensodyne Repair and Protect ®	Calcium Sodium Phosphosilicate (CSPS), 5% w/w	glycerin, PEG-8, hydrated silica, cocamidopropyl betaine, sodium methyl cocoyl taurate, aroma, titanium dioxide, carbomer, sodium saccharin, sodium fluoride (1450ppm)	GlaxoSmithKline
Sensodyne Rapid Relief ®	Stannous fluoride (SnF_2), 0.454% w/w	glycerin, PEG-8, hydrated silica, pentasodium triphosphate, aroma, sodium lauryl sulfate, titanium dioxide, carbomer, stannous fluoride, cocamidopropyl betaine, sodium saccharin, sodium fluoride, limonene., sodium fluoride 0.072% w/w (1450ppm fluoride).	GlaxoSmithKline

5.2.2 SBF SEM Imaging

0.5 by 0.5 mm blocks were cut out from the dentine discs, the blocks were infiltrated with resin and polymerised at 60 °C overnight (Agar low viscosity (ALV) resin, Agar Scientific, Stansted, UK) (figure 5.1). The excess resin was trimmed away and the block glued on to aluminium pin using conductive glue before sputter coating with gold/palladium to increase the conductivity of the block. Blocks were imaged using a Gatan 3View (Gatan, Abingdon, UK) inside an FEI Quanta 250 FEGSEM (Thermo Fisher, Eindhoven, the Netherlands) at 2.5 kV accelerating voltage, and with a vacuum level of 30 Pa (table 5.2). Stacks of 6000 x 6000 pixel images were collected at a pixel size of 19 nm resulting in a 114 x 114 µm field of view. 600 slices were cut by an ultrasonic diamond knife with a thickness of 60nm during data acquisition resulting in an imaging depth of approximately 36µm. After each slice, the dentine surface was imaged with a backscatter electron (BSE) detector.

Table 5. 2: Experimental setup

Instrument	Gatan 3View2XP
Microscope	FEI Quanta 250
Number of samples /data sets	3
Voltage	2.5 kv
Vacuum	Low- 30 Pa
Slice thickness	60 nm
Number of slices	600
Approximate depth	36 µm

5.2.3 Image Processing

Once the images were collected they were analysed by Image J software. All tubules were identified using the segmentation function (trainable weka segmentation). 3 random slices were chosen from the stack to train the classifier used for segmentation (figure 5.2) to separate tubules (open or occluded) from the surface.

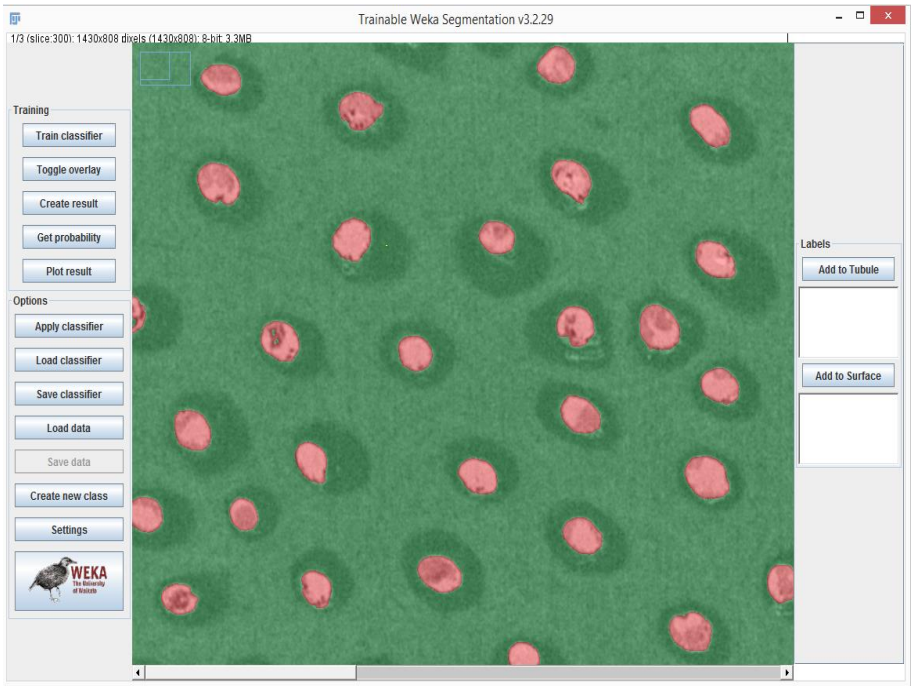

Figure 5. 2: Tubule classification training example

The segmentation results were thresholded (figure 5.3) and particle analyser was run on the entire stack to identify only the tubules with the following parameters: size=2.5-30 μm^2, circularity=0.10-1.00, and including holes. This created a new image containing only the identified particles (tubules). Figure 5.4 shows the 'overlay masks' option being used followed by the 'masks'.

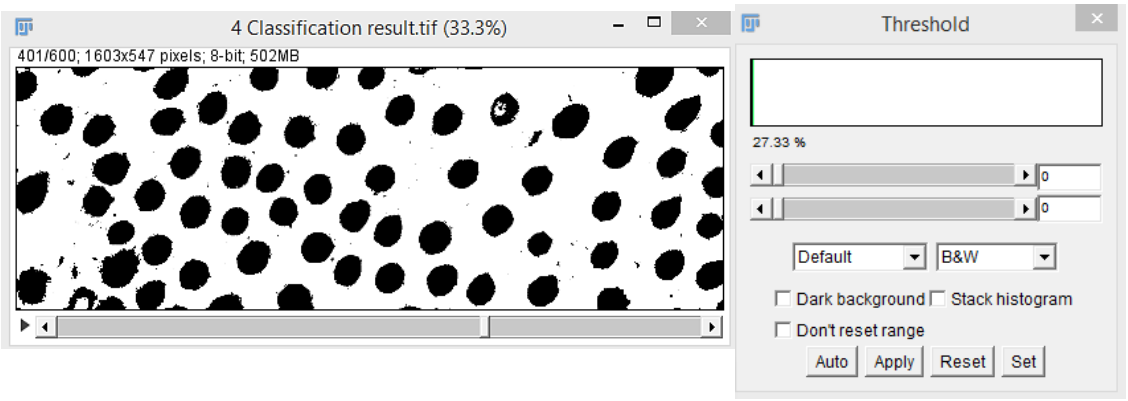

Figure 5. 3: Thresholded segmentation stack

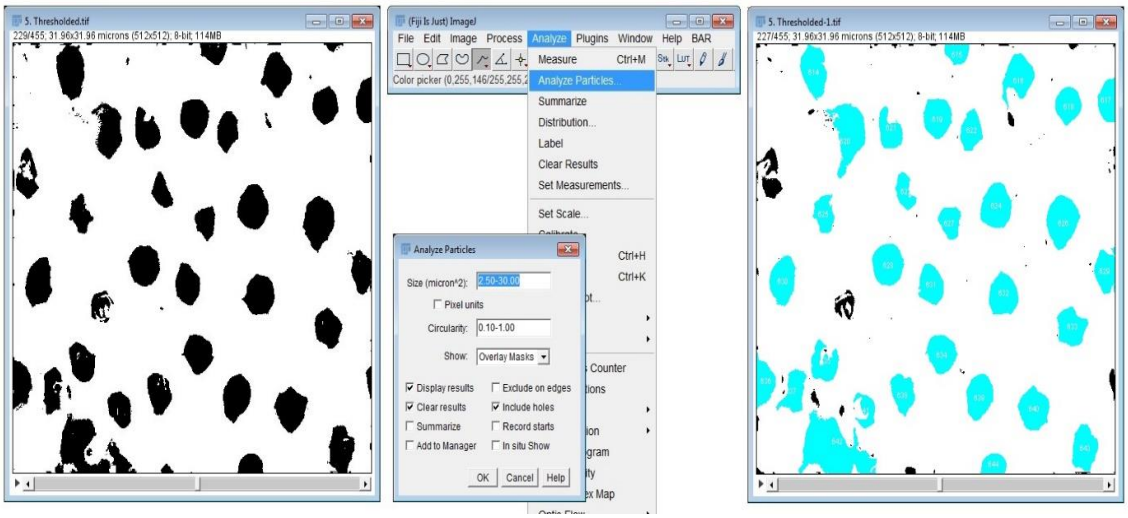

Figure 5. 4: Particle analyser example

After the particle analysis smaller objects were flittered out using the size opening 2D/3D function. (Use Plugins > MorpholibJ > binary images > size opening 2D/3D. Choose size 100000 voxels.)

The resulting stack now consisted of only tubules, this was used to measure the drift and align the stack so that the tubules can be straightened for occlusion measurements. The raw stack could not be used to measure the drift due to the fast 'movement' of the tooth surface across the image. The calibration data such as pixel size and thickness were inserted into digital micrograph (Gatan Microscopy Suite® (GMS)) software and the tubule mask stack was imported into the software. The drift was then measured by running the image alignment on the software. The stack of raw data was then imported to the GMS software and the drift measurement was applied to the raw data set (figure 5.5).

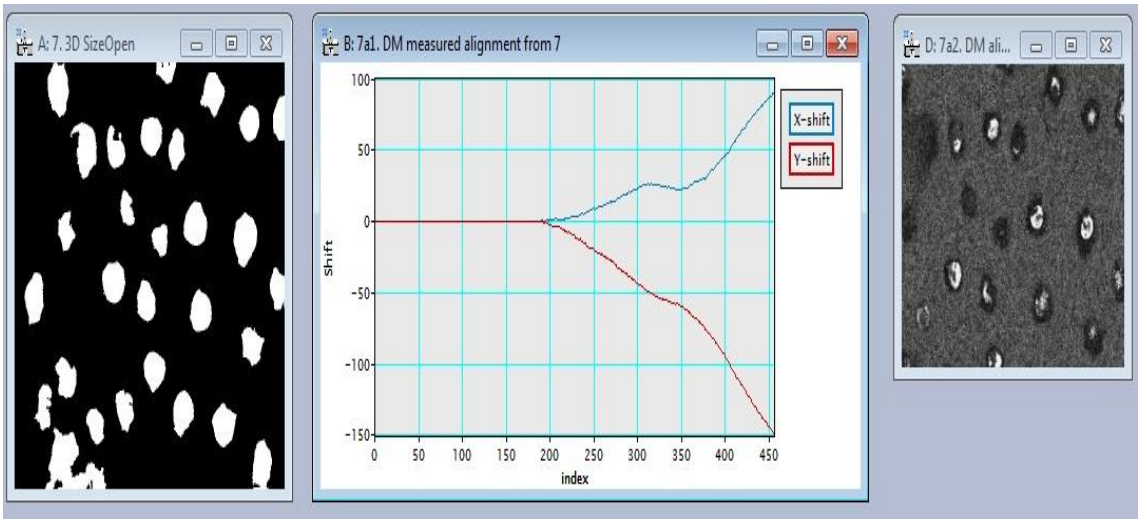

Figure 5. 5: Measured drift in DM software from a sub stack

The next step was the identification of the tooth surface. The aligned stack was resliced from the bottom to give the side view and the classification step above was repeated. Once the classification was completed the stack was resliced from the top to return it to the original orientation. Due to the similarity in contrast between the surfaces and the unoccluded sections of the tubules the classifier failed to only identify the surface and some tubules were also identified. To overcome this, the tubules mask from the earlier step was multiplied with the classified surface stack (figure 5.6).

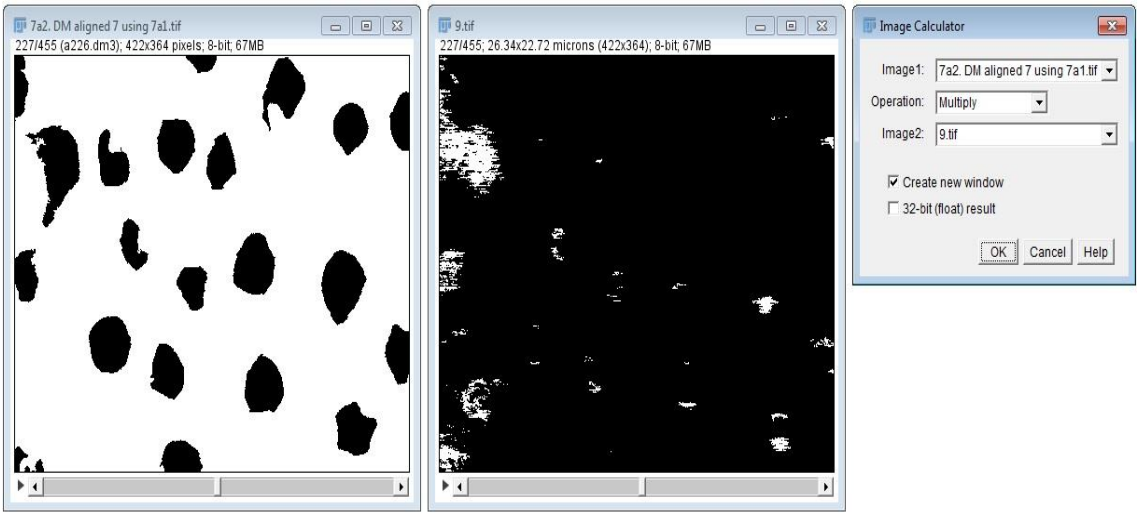

Figure 5. 6: Multiplying the tubule mask with the surface classification result to eliminate tubule

Any small disconnected sections were eliminated by using the following function on image J: Morpholib > Binary images > keep largest region.

The resulting stack was then used to create an image that represents the height of the inner surface (tubule-side / upper surface in Z direction) at each XY location. The TopoJ tool was used to create a height-map from a stack (figure 5.7). Starting with the maximum slice, for each XY pixel, TopoJ looks down through decreasing Z and stores the z depth. This would identify the outer surface (away from tubules). However, the inner surface (where the tubules meet the surface) is required. Therefore the surface stack was reversed and TopoJ was run again. Now the stored value would represent the actual slice number of the inner extent of the surface.

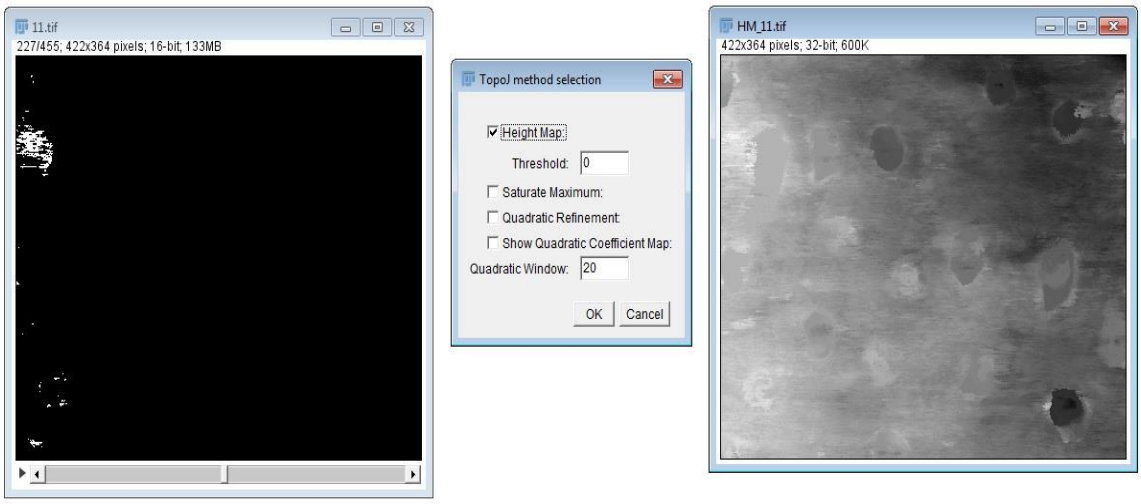

Figure 5. 7: Creating a heightmap from the reversed surface stack

The tubules were now separated from the surface and the distance to the inner surface was measured. Few tubules were still connected to the surface by small protrusions, therefore Gblur3D, size = 1 pixel was used and then threshold so that they are well separated. 3D size opening again (size 100000) was also run to remove a few small stragglers (figure 5.8).

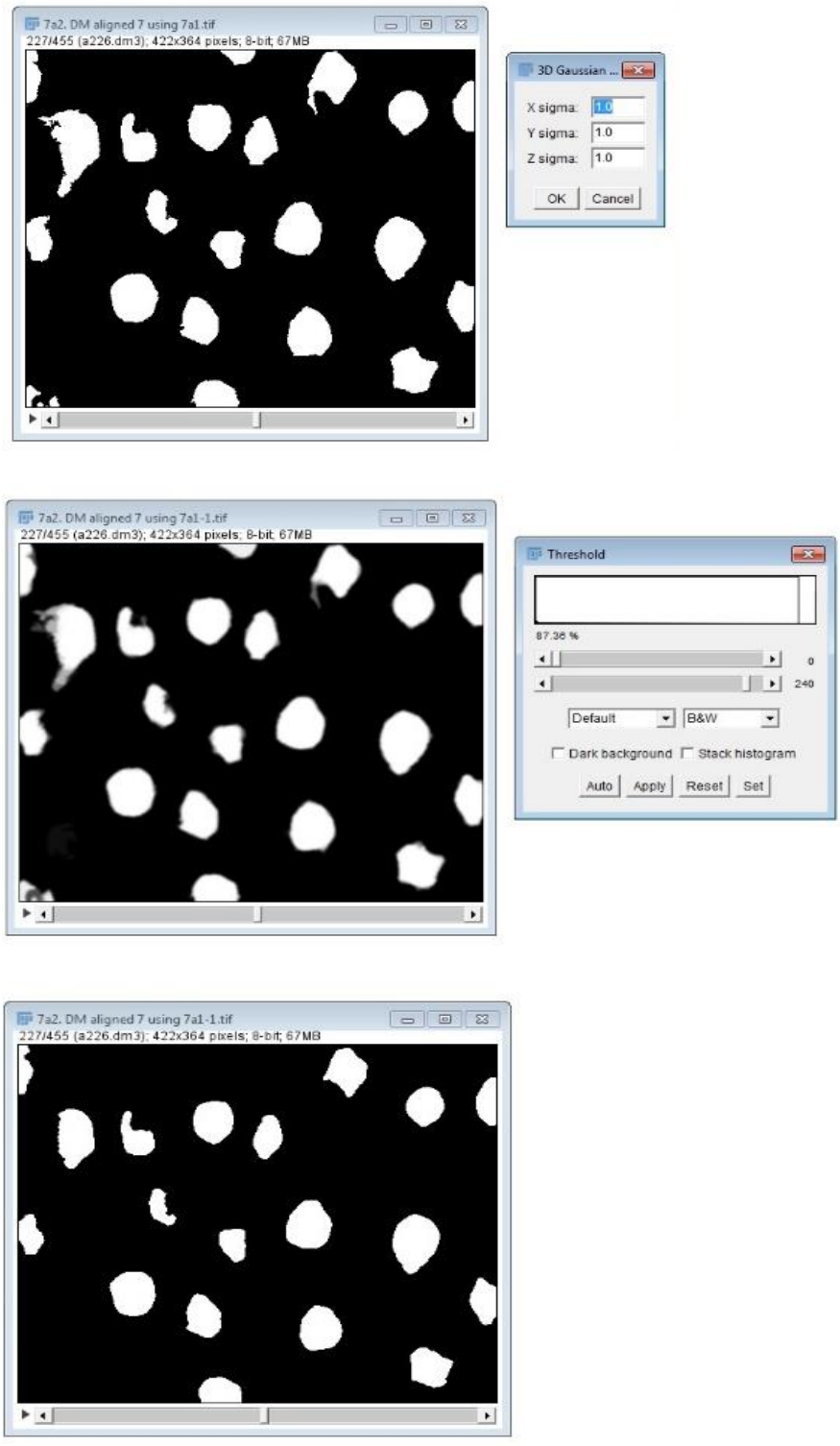

Figure 5. 8: Gblur3D and threshold of tubule mask so that they are well separated

Individual tubules were identified by using connected component labelling. This gave each individual tubule a unique grey level by running Plugins > MorpholibJ > Binary Image > Connected component labelling (figure 5.9).

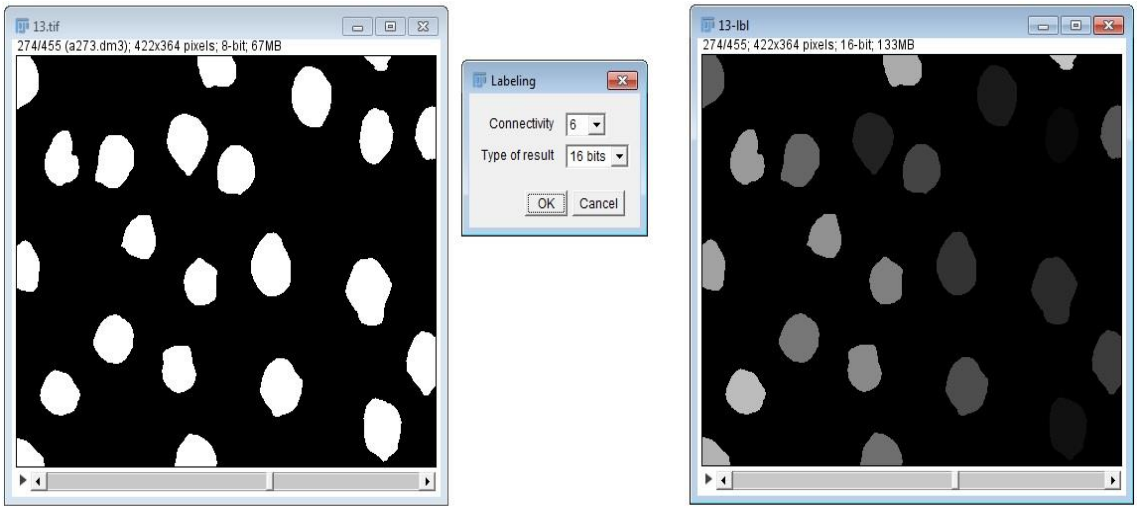

Figure 5. 9: Connected component ladling giving each tubule a greyscale value

Each identified tubule was given a number throughout the stack, isolated and straighten individually. Tubules that went more than 1µm off the edge of the stack were disregarded. Once the tubules were identified, their length was measured from the surface down. The level of the blockage was evaluated by scanning through the core of each one and recording the greyscale values (Figure 5.10). As demonstrated in the example given in figure 5.10 there is a big drop in greyscale value to below 40 at around 7µm when the line moves past the occluded portion of the tubule. Therefore this value was chosen as the benchmark to separate filled vs unfilled tubules. Tubule occlusion was measured every 3µm to a depth of 30 µm from the surface.

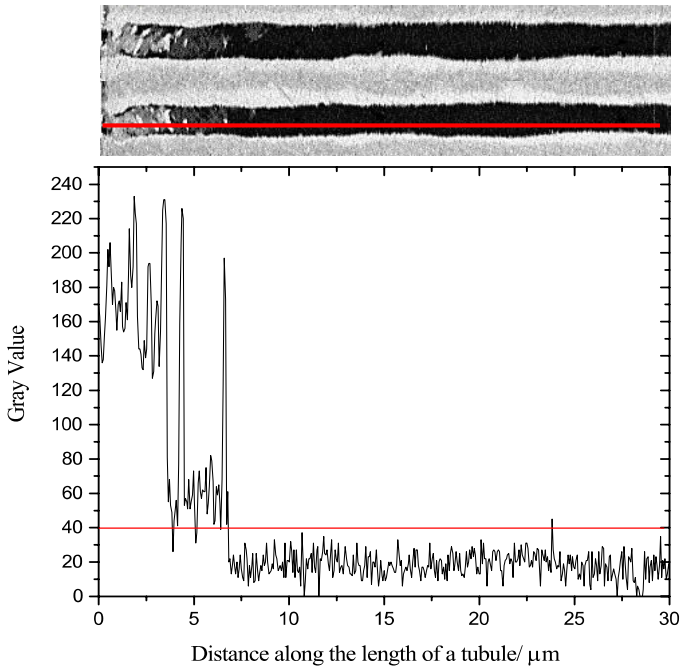

Figure 5. 10: Example of tubule taken from Novamin treatment group, joined pair shows XZ and YZ planes

5.2.4 Remineralisation Potential and Diameter of Tubule Opening

To compare the mineral density of the dentine samples the greyscale values of the BSE images were taken from the block face images by ImageJ software. The greyscale values from 100 random areas around the tubules and the surface were recorded at every 3µm from the surface to the depth of 30µm. After each tubule was identified, a stack of all images for that tubule was made and a thickness graphic mask was applied to generate a heat map. The diameter of these heat objects was then measured throughout the stack which represented the open section of the tubule. Areas that had a grayscale value of more than 40 (occluded) were thresholded to appear black and excluded from the measurement. The outputted values included the highest, lowest, mean and standard deviation diameter throughout the entire stack.

5.3 Statistics

The data sets within this chapter were initially analysed using a one-way analysis of variance (ANOVA) to determine whether there were significant differences. This was followed by t-tests (assuming equal variance) to identify any significant differences between the means of the groups. $P \leq 0.05$ was considered to be significant.

5.4 Result

5.4.1 Tubule Occlusion

The SEM images (Figure 5.11) taken before slicing showed that both toothpastes were successful in occluding tubules compared to the control samples. CSPS formed a layer over the tubules (figure 5.11b) whereas there was no layer formed by SnF_2 (figure 5.11c)

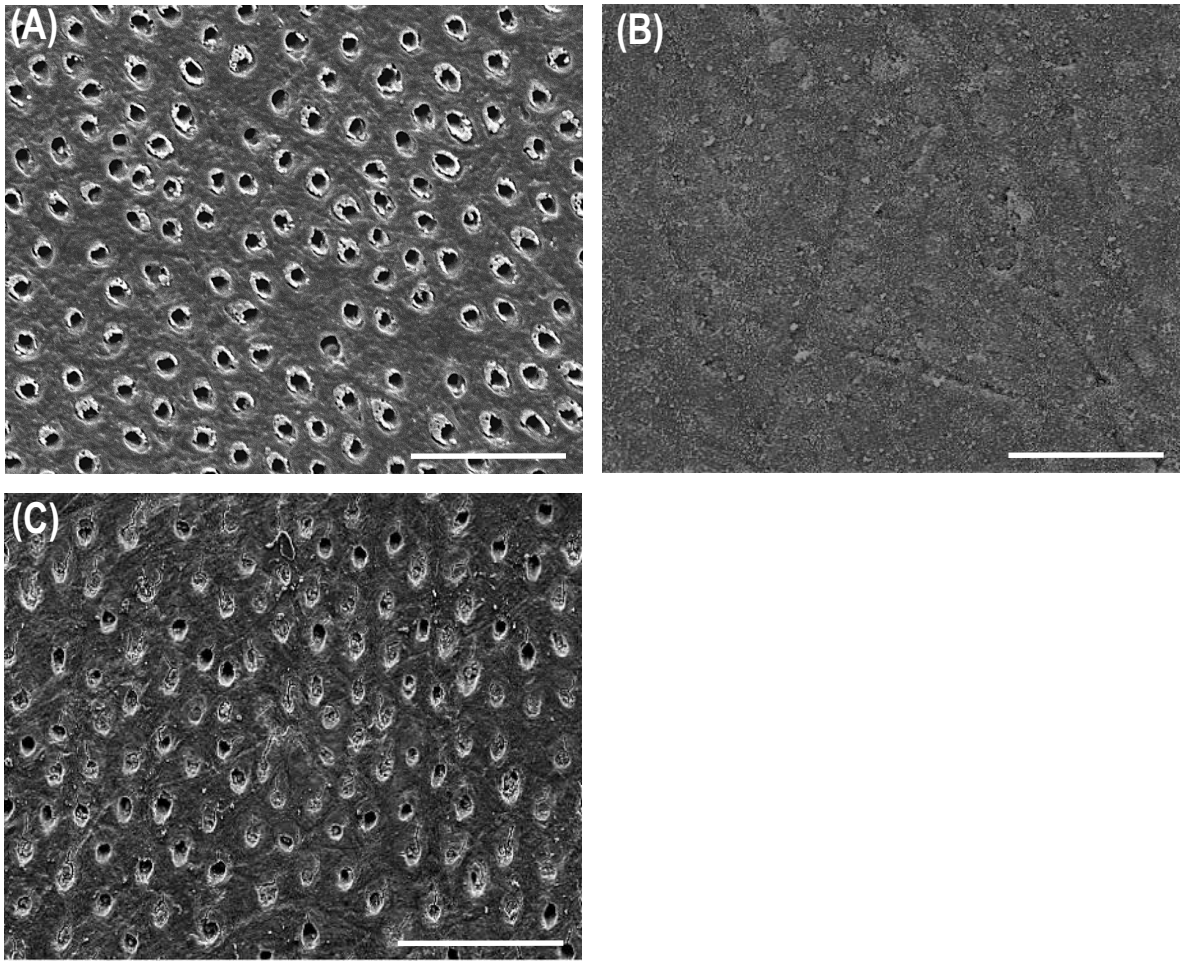

Figure 5. 11: SEM pictures of Control (a), CSPS (b), and SnF_2 (c) treated dentine surface

Cross-sections of the tubules showed that the tubules within the control group were empty (figure 5.12). The bottom raw images are flood-filled from the bottom (thresholded to appear black and white) to make it easier to spot occlusion of the tubules. Occluding particles would appear white and if the tubules were blocked, the black tubule would not have reached the surface. This does not happen for any of these tubules presented in figure 5.12 which shows that there was no occlusion has occurred and there is a clear path to the surface for each tubule.

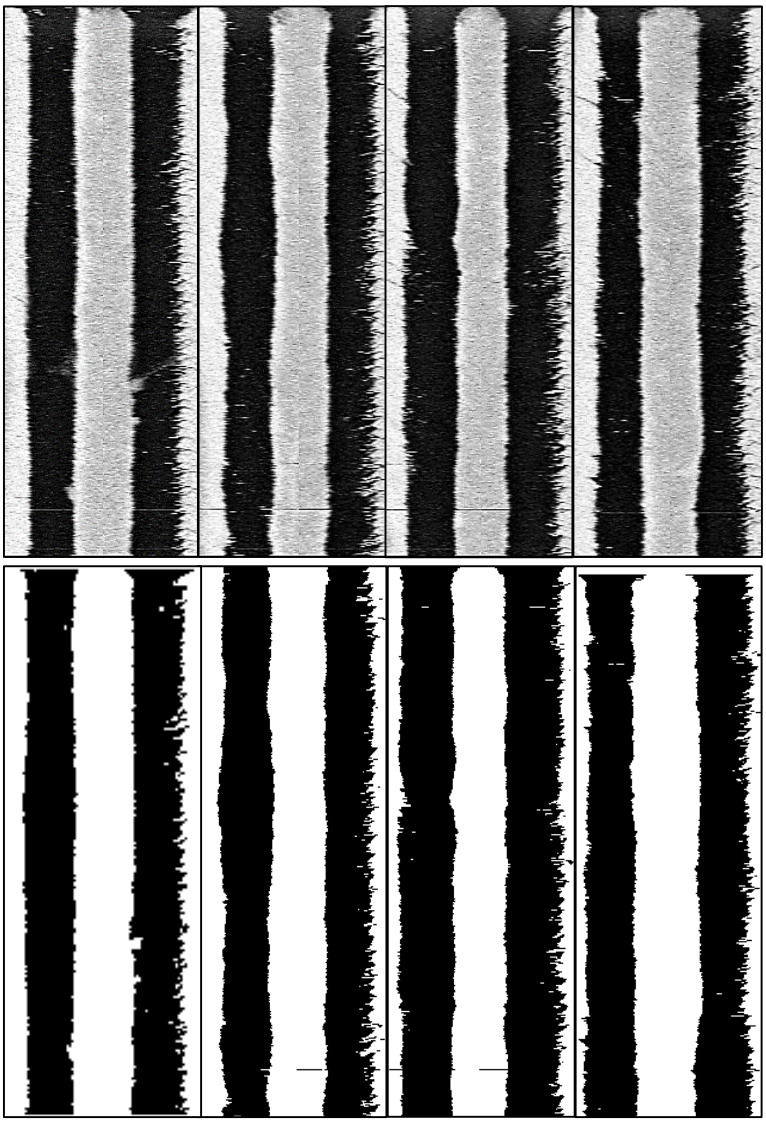

Figure 5. 12: Random tubules taken from control discs Top row: Each joined pair shows XZ (left) and YZ (right) planes for a tubule. Bottom row: Each tubule was 3D-flood-filled from the bottom.

Figure 5.13 shows the tubules extracted from 4 dentine discs brushed with CSPS. For a tubule which is connected to the outer material, even by a small path, the black flood fill will extend to the top of the image. This does not happen for any of these indicating blockages at the surface. 100 percent of tubules were occluded at the surface when treated with CSPS.

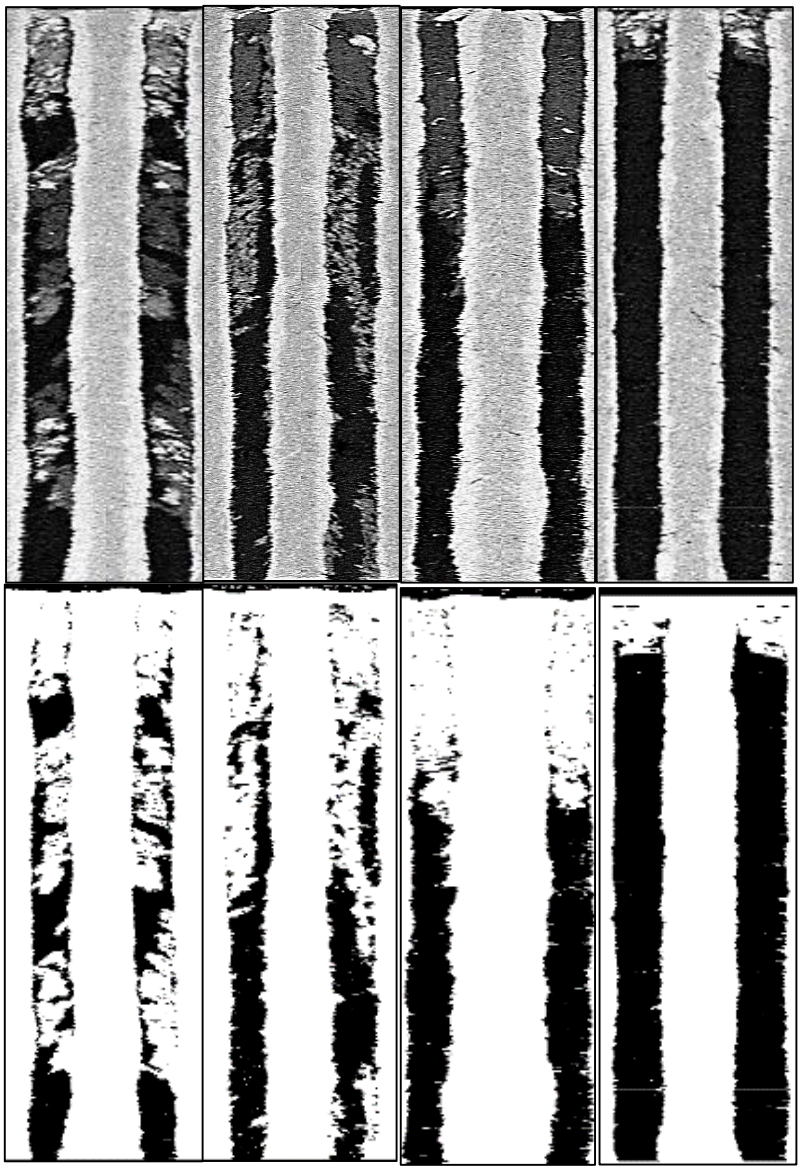

Figure 5. 13: Random tubules from dentine discs treated with CSPS

Although SnF_2 was also capable of occluding dentine tubules, it was not as effective as CSPS and occluded 83 percent of the tubules at the surface (table 5.3). Figure 5.14 represents 4 random tubules from the SnF_2 group.

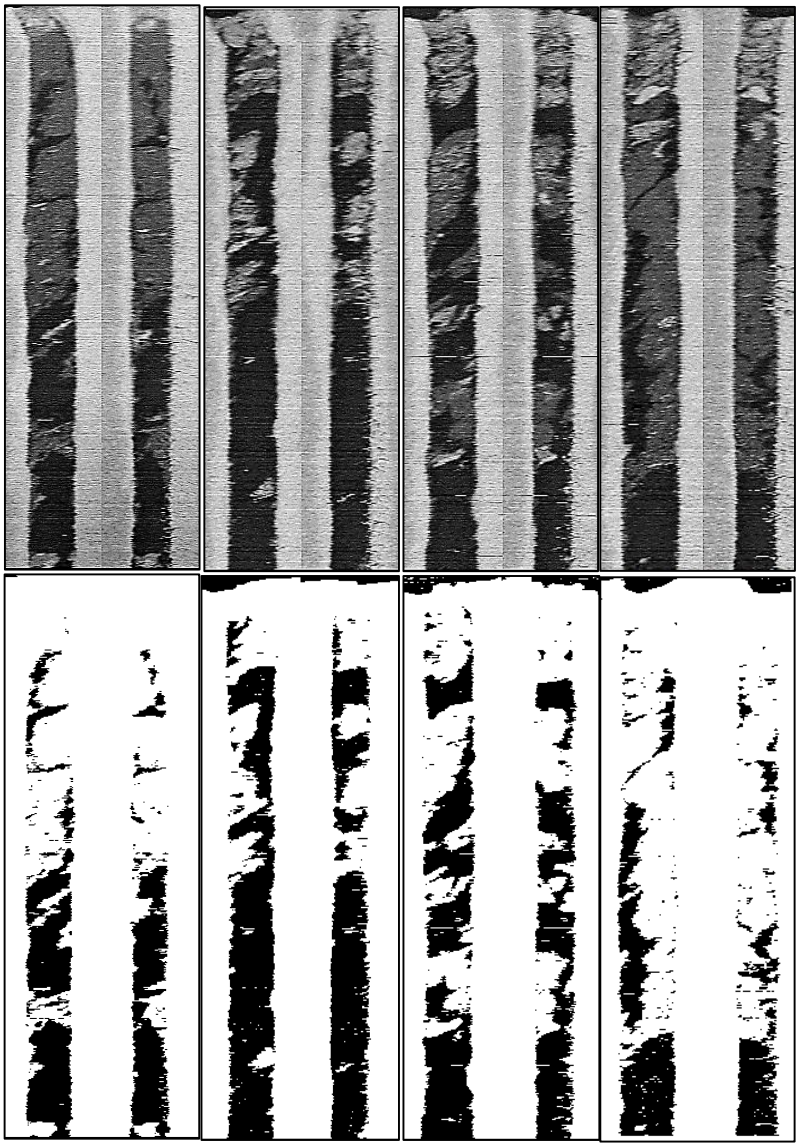

Figure 5. 14: Random tubules from dentine discs treated with SnF_2

Tubules treated with CSPS and SnF_2 contain occluding material throughout the length of the tubules at various depths. The level of tubule occlusion reduced as the distance from the surface increased and at 3 µm, the percentage of tubules with occlusion was significantly ($P \leq 0.05$) reduced for both treatment groups. Although CSPS had better occlusion at the surface, SnF_2 occluded more tubules between 3 and 24µm from the surface. However, between 24-30µm CSPS had a superior occlusion rate although the difference was non-significant ($P \geq 0.05$) (table 5.3).

Table 5. 3: Percentage of blocked tubules from the surface (0µm) to 30µm

Depth /µm	CSPS	SnF_2
0	100	83
3	63	72
6	41	50
9	33	37
12	27.56	33
15	24.41	28
18	21.65	26
21	19.69	26
24	23.62	17
27	23.23	14
30	20.87	14

5.4.2 Tubule Diameter

The average diameter of the tubule opening over the length of the tubule significantly ($p \leq 0.05$) reduced from 0.79±0.05µm to 0.66±0.21 µm after treatment with CSPS no significant ($p \geq 0.05$) change was seen after SnF_2 treatment (figure 5.15). CSPS particles that had entered the tubules have reacted and have formed a layer along the wall of the tubule. Figure 5.16 is a high magnification SEM image of a CSPS treated sample after it had been through a cutting and imaging process. (30 µm was removed from the surface). The growth of material around the tubule is evident (red arrow). This explains the reduction in the diameter of the opening section of the tubules in this group.

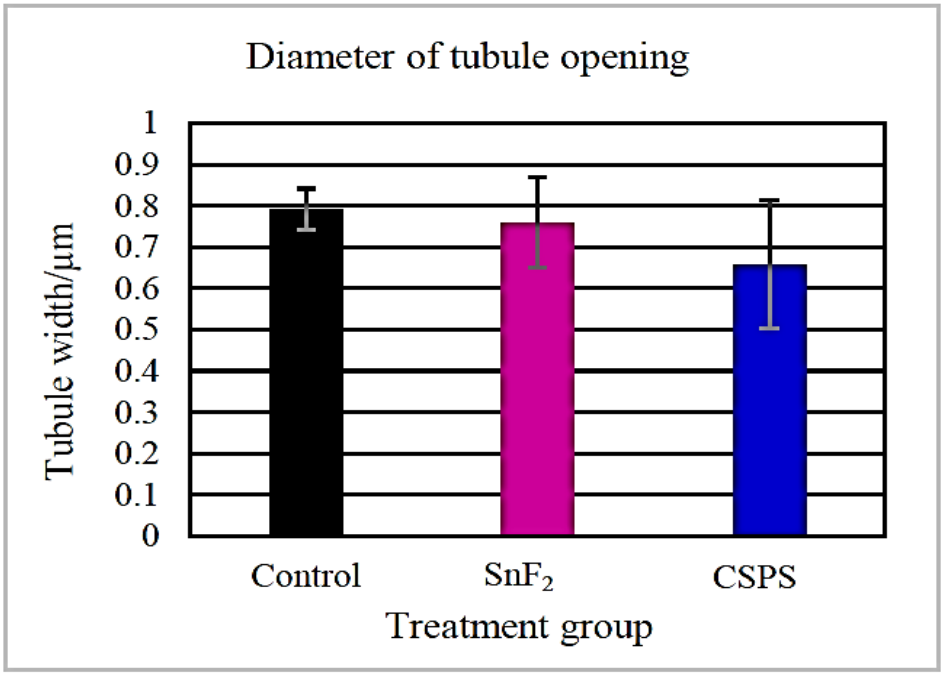

Figure 5. 15: Diameter of the tubule opening over the length of the tubule (30 µm)

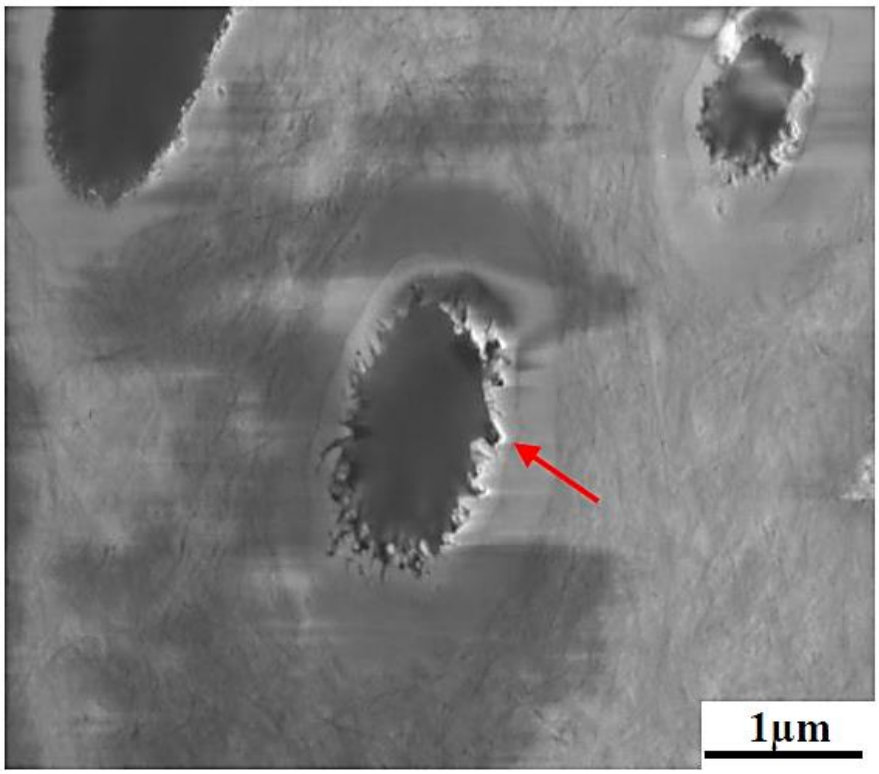

Figure 5. 16: SEM image taken from a CSPS treated dentine disc after 30µm was removed from the surface

5.4.3 Grey Scales

Greyscale values around the tubules and the surface of dentine (figure 5.17) were significantly higher ($p \leq 0.05$) for CSPS treated samples at the surface and 30µm below the surface (230.42 and 213.55 respectively) compared to SnF_2 (222.06 and 192.76) and the control (196.37, 192.35). The higher greyscale value is due to higher mineral content which is linked to mineralisation of the dentine.

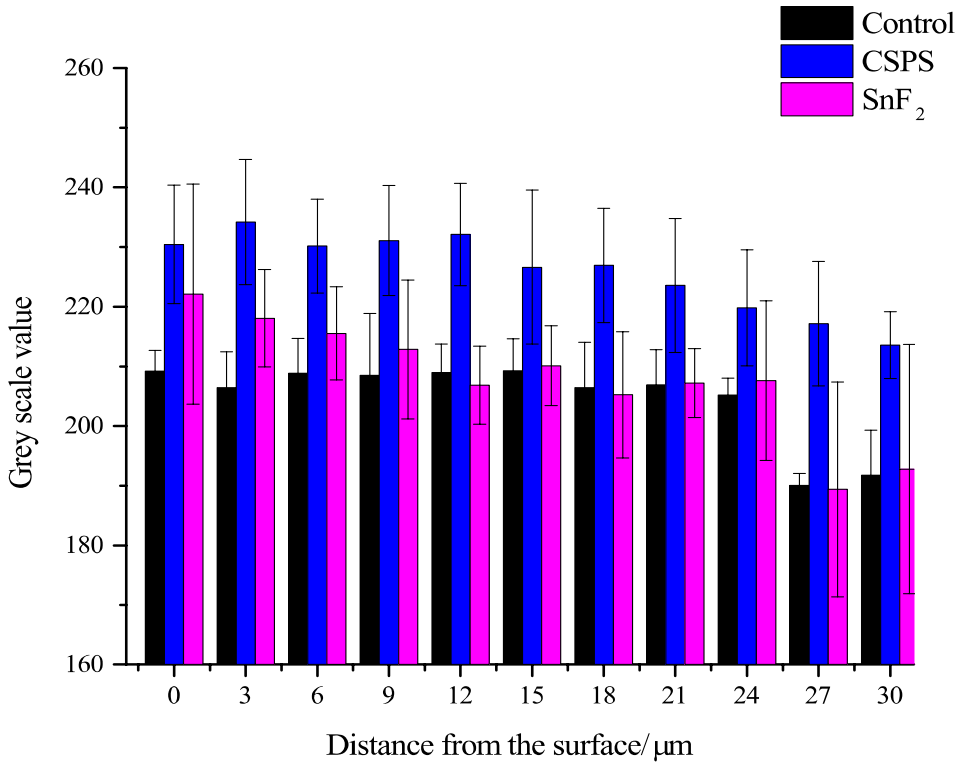

Figure 5. 17: Greyscale values of control, CSPS and SnF_2 treated dentine taken from around the tubules and the surface of dentine

5.5 Discussion

For prevention and treatment of dentine hypersensitivity (DH) the permeability of the tissue needs to be reduced to inhibit stimuli from altering the fluid follow and stimulating the nerve endings inside of the tooth. This can be achieved by occlusion of the exposed dentine tubules.

In the present in vitro study, serial block face scanning electron microscopy (SBF SEM) was used to compare dentine tubule occlusion by Sensodyne® Repair and Protect and Rapid Relief toothpaste containing CSPS and SnF_2 respectively as active ingredients to treat DH. The backscattered electron (BSE) imaging also made it possible to compare the mineral density of the dentine tissues between the control and the treated samples. SBF SEM imaged approximately 100 tubules per sample with a 19 x 19 x 60 nm voxels size over ~12 hours. This resulted in an imaging volume of approximately 4.4355 x 105μm^3. A higher volume of dentine could have been imaged by using a lower magnification, however, as the area around the tubules was of an interest higher magnification was used. Although this limited the number of tubules assessed, the 100 tubules were sufficient for statistical analysis.

X-ray microtomography and focused ion bean SEM (FIB SEM) has previously been used as a 3D characterization technique to study dentine [210,212]. However, the spatial resolution X-ray microtomography is restricted to a few hundred nanometres, while milling materials for FIB SEM require a significant amount of time. Several 2D imaging techniques such as scanning electron microscopy (SEM) and transmission electron microscopy (TEM) have also been used to study the dentine structure [213–215]. While TEM provides high-resolution imaging in the nanometre range and the sample is limited to a few hundred nanometres in thickness. The SEM offers imaging in both nano and micrometre. Although it can not provide any information regarding the depth to which the tubules are occluded.

The SEM images presented in this chapter showed that both materials were capable of occluding a significant number of tubules, while in the control group they were still open. However, the occlusion percentage decreased with increasing depth away from the surface.

CSPS produced a better level of occlusion both at the surface and at 30µm. It also resulted in a reduction in tubule opening by forming a layer down the walls of the tubules. Based on the characterisation results in chapter 4 it can be assumed that this is hydroxyapatite like material. However, it needs to be confirmed and it is part of the future work (chapter 6).

The greyscale values around the tubules were higher for CSPS treated samples at each given depth compared to the control and SnF_2. These results are similar to studies in literature, Parkinson et al.[21] used SEM to investigate the occlusion and mineralization of CSPS and SnF_2. They reported that CSPS containing toothpaste had a significantly higher level of dentin tubule occlusion and mineralisation to compare to SnF_2 after being brushed for two minutes twice per day over four days. Thus the initial hull hypothesis on tubule occlusion and mineralisation of both active ingredients was rejected. As it was previously mentioned CSPS forms a layer over the exposed tubules and therefore resulted in better occlusion as the surface. Its superior mineralisation compared to SnF_2 is attributed to the composition. it is made up of the naturally occurring ions found in the hydroxyapatite. The extra supply of calcium and phosphate ions create a favorable environment for the diffusion of these ions into the apatite structure. Although not statistically significant CSPS had a lower level of occlusion further away from the surface. this would be due to the much larger particle size (15µm to 20µm) compared to the diameter of the tubules which are around 2 µm. These particles are broken down into smaller sizes by brushing which allows some to enter the tubules however the percentage can be improved by using smaller particle sizes in the formulation.

An in vitro SEM study by Kulal et al. [216] reported 98.1% dentine tubule occlusion following a 7 day (two minutes per day) treatment with a CSPS containing toothpaste. whereas another in vitro SEM study reported 92.73% occlusion after brushing with CSPS containing toothpaste for 6 min twice a day for 7 days [217]. A recent in vitro SEM study by Hines et al. [218] reported that SnF_2 containing toothpaste occluded 82% of tubules. A clinical study comparing CSPS and SnF_2 for treating DH also reported that CSPS

reduced DH significantly more than SnF_2 after 12 weeks [139]. The findings in this study encourage the use of CSPS containing toothpaste over a toothpaste with SnF_2 as an active ingredient due to a better occlusion and mineralisation potential of CSPS. Also, SBF-SEM enabled the study of a much larger volume of dentine over a short period with high resolution. To analyse a similar number of tubules at this resolution with other techniques such as focused ion beam (FIB) SEM would have required significantly more sample preparation which would be time-consuming, costly and the depth would be limited to the FIB slice.

5.6 Limitations

Although the use of SBF-SEM has a number of advantages over some of the most common techniques such as ordinary SEM, FIB and hydraulic conductance, the resulting image stack requires extensive image processing to obtain relevant information. The data files are relatively large and therefore require more advanced computing equipment. Finally, due to the size of the sample holder, the samples are required to be 1mm or less (ideally between 0.5-0.7mm). This makes the handling of the sample difficult.

5.7 Conclusion

CSPS and SnF_2 containing dentifrice have the ability to occlude dentine tubules, with CSPS able to occlude 100% of the tubules due to penetration of material into the tubules and the formation of the surface layer. The CSPS and SnF_2 both increased the dentine mineralization level as quantified by greyscale values from the backscattered images. The increased level of tubule occlusion and dentine mineralisation by the CSPS containing dentifrice may provide better relief and protection from dental hypersensitivity.

SBF SEM is a high resolution imaging technique which can provide a new quantitative method of assessing dentine tubule occlusion depth and percentage of occluded tubules, while also allowing for the assessment of mineralisation changes within the treated tissues.

Chapter 6 Conclusion and Future Work

6.1 Conclusion

Dentine once exposed is vulnerable to further damage in the oral cavity due to its soft nature and therefore the tissue needs to be protected. Active ingredients such as bioactive glasses, arginine, and calcium silicate have demonstrated clinical efficacy in reducing dentine hypersensitivity. They also have the potential to provide the required protection to the dentine as they are capable of forming a layer onto the dentine surface. However voids exist in this area of research, there have been limited studies exploring the protective nature of these layers and therefore a more in-depth understanding of the mechanical and structural properties of these layers was required.

The present work is the first comprehensive study comparing the mechanical properties of the hydroxyapatite like layers formed by 5 different commercially available toothpastes. The approach of testing these layers on a nanoscale level avoided the effect of dentine substrate on the results due to a small interaction volume. The use of the unique liquid cell also enabled the dentine discs to be indented while fully immersed in deionised water to keep them fully hydrated and make the testing condition more representative of the oral environment. In the oral cavity, these layers would face acid challenges through the consumption of acid food, drinks, and the production of acid by the bacteria. Therefore the acid resistivity of the layers was also assessed by challenging the layers to citric acid and measuring the hardness change.

Furthermore, this study developed a new technique to assess the occlusion of dentine tubules on a much higher volume, inclusive of the depth of occlusion. This technique not only required significantly less sample preparation compared to the existing technique, but it also provided a mean of measuring the mineral density of the dentine at various depths which can be related to the mineralisation of the tissue.

The main findings of the present study were:

- AG, CCPS, CS, CSPS, and FCPS occluded dentine tubules by forming a layer over the surface of the dentine. these layers were structurally and chemically similar to the dentine.

- The layers were harder and stiffer than the control dentine. CS formed a layer with the highest H and E values followed by AG, CSPS, FCPS, and CCPS. There was a significant difference between CS, AG and the 3 BAG, however, no significant differences were seen between CCPS, CSPS, and FCPS.

- AG layer had a significantly higher H/E compared to AS and CS followed by CSPS, CCPS, and FCPS. All 5 layers had a significantly higher ERP value compared to the control dentine. AG layer had the highest ERP. The ERP for the 3 BAG and CS were not statistically significant.

- Citric acid removed the protective HA like layer in CCPS, CS, and FCPS while it was still partly intact for AG and CSPS. However, there was still evidence of tubules occlusion in all but the CS group. AG had a significantly smaller reduction in mean hardness while CS had the highest reduction compared to other treatment groups.

- Scratch data showed no critical failure or delamination of the layers. For all of the layers, the tip cut and displaced the layer material to the sides of the scratches. The AG layer had a significantly lower penetration depth compared to the other treatment groups (AG<CSPS<CS<FCPS<CCPS).

- AG had a significantly higher elastic recovery to plastic deformation ratio compared to other treatment groups. It also had a significantly higher CI_{FTIR} and mean crystal size.

- Over 100 tubules were successfully imaged using the SBF SEM. CSPS and SnF_2 occluded a significant number of tubules with occluding materials throughout the length of the tubules at various depth group. The occlusion percentage decreased with an increase in depth away from the surface.

- CSPS had better occlusion at the surface compared to SnF_2, however, it had occluded fewer tubules further down the surface. However, between 24-30µm it had a superior occlusion rate compared to SnF_2.

- The tubule diameter was significantly reduced after treatment with CSPS. No significant change was seen after SnF_2 treatment.

- The Greyscale values around the tubules were significantly higher for CSPS at the surface and 30µm depth Compared to SnF_2 and the control.

6.2 Summary

Arginine with calcium carbonate formed the most crystalline layer with a bigger mean crystal size. This layer was also the most acid resistant with a higher H/E ratio and ERP compared to other treatment groups. The scratch penetration depth and elastic-plastic ratio data also suggest that this layer behaves more elastically under abrasion which would result in a more wear resistant HA. Therefore it may provide better protection against the mechanical, chemical and abrasive challenges within the oral cavity.

The key parameter that would influence the mechanical properties, as well as the acid resistivity of the layers, was the level of crystallinity including the crystal size of the hydroxyapatite like material that was formed on the surface of the dentine. The nucleation agent plays a crucial role in attracting Ca^{2+} and PO_4^{3-} ions to the dentine surface and retaining them to allow the formation and crystallisation of hydroxyapatite like layer.

The SBF SEM data showed that Repair and Protect toothpaste containing CSPS produced a better level of occlusion both at the surface and 30 µm below the surface. It also resulted in increased dentine mineralization quantified by greyscale values from the backscattered images. Therefore it may provide better relief against dental hypersensitivity and help with mineralisation of the dentine.

6.3 Future Work

6.3.1 EDX Mapping Coupled With SBF SEM

Serial block face SEM was successfully used in the previous chapter to quantify the percentage of tubule occluded by two desensitising toothpastes and determined the depth to which occluding materials had penetrated to. The future work in this area will involve investigating the mineralisation of CSPS further using a combination of SBF SEM and EDX to provide higher resolution EDX elemental mapping of the dentine at various depths from the surface. The EDX mapping at set points during the sectioning will provide evidence of changes in the elemental makeup of the tissues due to the remineralisation effects of the toothpaste ingredients. This also provides a means of studying the contents of the dentine tubules and the components of the toothpaste formulation which provide the tubule occlusion.

6.3.2 Particle Size Variation

The effect of CSPS particle size on the integrity and mechanics of the layer formed will also be studied. CSPS has a median particle size of 20 microns and the purpose of this study will be to evaluate whether smaller/bigger particles would form the layer quicker and if this has any effect on the mechanics and tubule penetration which will be governed by the rate at which the particles are broken down and ions such as Ca^{2+} and PO_4^{-3} are released from the structure. The SBF SEM will then be used to investigate the tubule occlusion and depth of penetration of different CSPS sizes while the level of protection they offer will be investigated through nanomechanical testing such as nanoindentation and nano scratch test. Their acid resistivity will also be evaluated by subjecting the materials to acid challenge. The tubule diameter ranges between 0.9-2µm and we hypothesise that smaller particle sizes would penetrate deeper into the tubules, react faster due to increased surface area to volume ratio and overall provide a better and longer-lasting relief against sensitivity. Reducing the particle size will also reduce the abrasivity of the CSPS within the toothpaste which will also be beneficial as it will minimise damage to the tooth enamel.

6.3.3 Variation in CSPS Concentration

The existing formulation of Sensodyne repair and protect toothpastes contains 5% CSPS. The future work will involve changing the CSPS concentrations within the formulation and investigate its effect on the properties of the layer formed and the level of tubule occlusion. As the results within chapter 4 showed the more crystallised a layer is the better the mechanical and wear properties. It would also be more stable under acidic environment. By increasing the concentration of CSPS within the formulation more calcium and phosphate ions will be present which could result in faster apatite formation with bigger crystal size.

6.3.4 Nanoindentation at Cross Section

Measuring the hardness is a useful tool for detecting mineralisation of the dentine. Indenting the dentine samples at the cross-section can be useful in detecting the change in mechanics of the dental tissue underneath the layers following the treatment with the 5 different toothpastes. In order to indent the cross-section with accuracy at a given distance from the surface, the indentation needs to be set up under a microscope. This function was not previously available with the liquid cell set up, however with the new improved set up here at the University of Southampton this is possible and can be used in conjunction with the cross-section data from Raman microscopy for the mineralisation study.

6.3.5 Micro-Abrasion

To investigate the wear resistivity of the layer further micro-abrasion test will be carried out using the TE66 abrasion rig. It is a highly repeatable and consistent technique that will provide a measure of the wear rates of the different layers, enabling a direct comparison of their protective abilities.

Appendix A Supplementary Data from Chapter 3

Mean ±standard deviation (SD) of H and E values for the control group

Sample number	Hardness/GPa	±SD	Modulus /GPa	±SD
1	0.56	0.04	13.91	1.31
2	0.53	0.03	14.14	1.13
3	0.54	0.06	14.30	1.26
4	0.56	0.06	13.97	1.14
5	0.59	0.07	14.70	1.17
6	0.54	0.05	14.55	1.32
7	0.56	0.06	14.71	1.99
8	0.52	0.05	14.49	1.81
9	0.55	0.04	14.73	1.36
10	0.52	0.05	14.47	1.53
Average	**0.55**	**0.05**	**14.43**	**1.40**

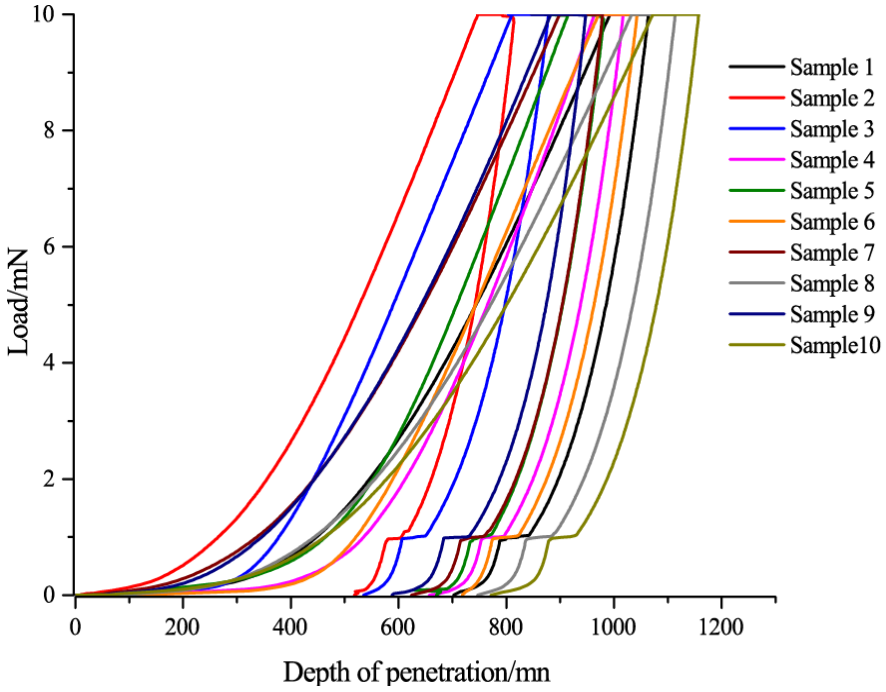

Load vs depth measurements of control dentine discs

Mean ±standard deviation (SD) of H and E values for the AG layer

Sample number	Hardness/GPa	±SD	Modulus /GPa	±SD
1	0.81	0.09	18.09	1.44
2	0.81	0.10	18.40	1.63
3	0.78	0.12	18.70	1.65
4	0.84	0.13	21.28	2.47
5	0.82	0.11	20.13	1.88
6	0.83	0.11	19.45	1.74
7	0.78	0.08	17.24	1.45
8	0.78	0.06	19.52	2.01
9	0.79	0.08	18.95	1.60
10	0.80	0.07	18.71	1.66
Average	**0.81**	**0.095**	**19.05**	**1.75**

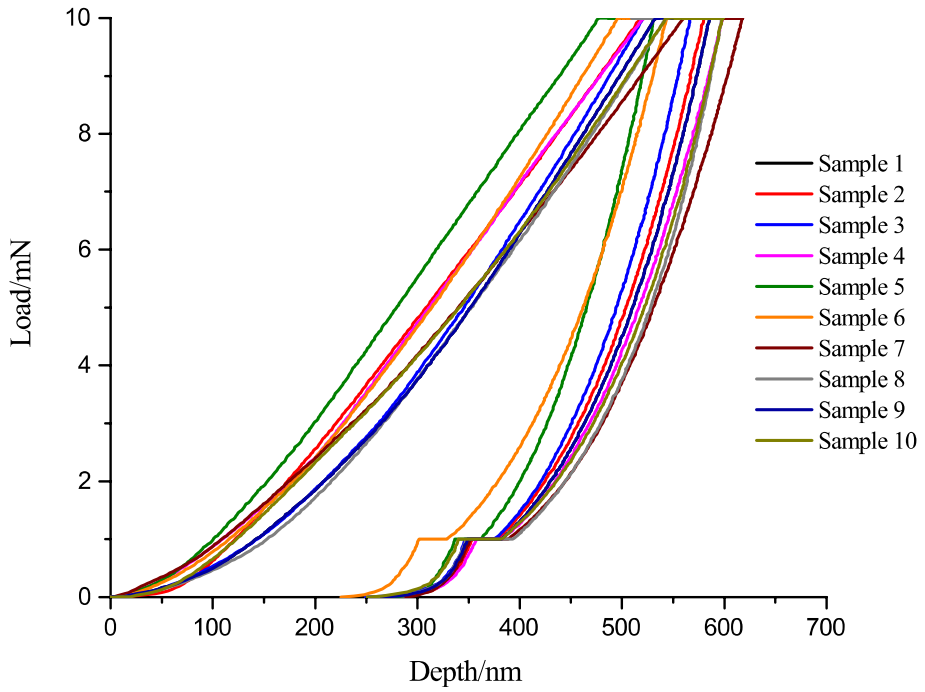

Load vs Depth from AG treatment group

Mean ±standard deviation (SD) of H and E values for the CS layer

Sample number	Hardness/GPa	±SD	Modulus /GPa	±SD
1	0.83	0.06	21.66	1.37
2	0.81	0.05	20.83	1.21
3	0.83	0.07	22.16	1.94
4	0.93	0.12	25.94	2.19
5	0.91	0.12	25.00	2.07
6	0.94	0.15	24.90	2.22
7	0.90	0.16	24.37	2.23
8	0.87	0.11	23.61	3.47
9	0.86	0.13	24.15	3.31
10	0.88	0.12	23.52	3.10
Average	**0.88**	**0.11**	**23.61**	**2.31**

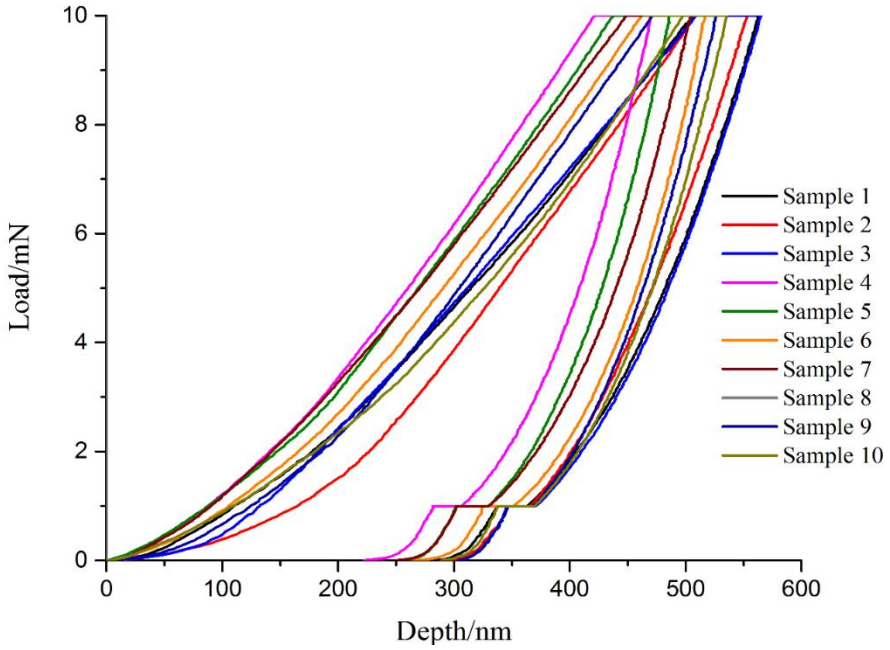

Load vs depth measurements, CS group

Mean ±standard deviation (SD) of H and E values for CCPS layer

Sample number	Hardness/GPa	±SD	Modulus /GPa	±SD
1	0.76	0.06	19.37	2.15
2	0.75	0.09	19.19	2.10
3	0.73	0.11	18.65	1.90
4	0.72	0.08	18.25	2.10
5	0.73	0.08	17.25	1.90
6	0.68	0.04	14.89	1.78
7	0.70	0.09	17.66	2.30
8	0.74	0.08	17.35	2.60
9	0.71	0.07	18.37	1.95
10	0.70	0.09	18.33	1.92
Average	**0.72**	**0.08**	**17.92**	**2.10**

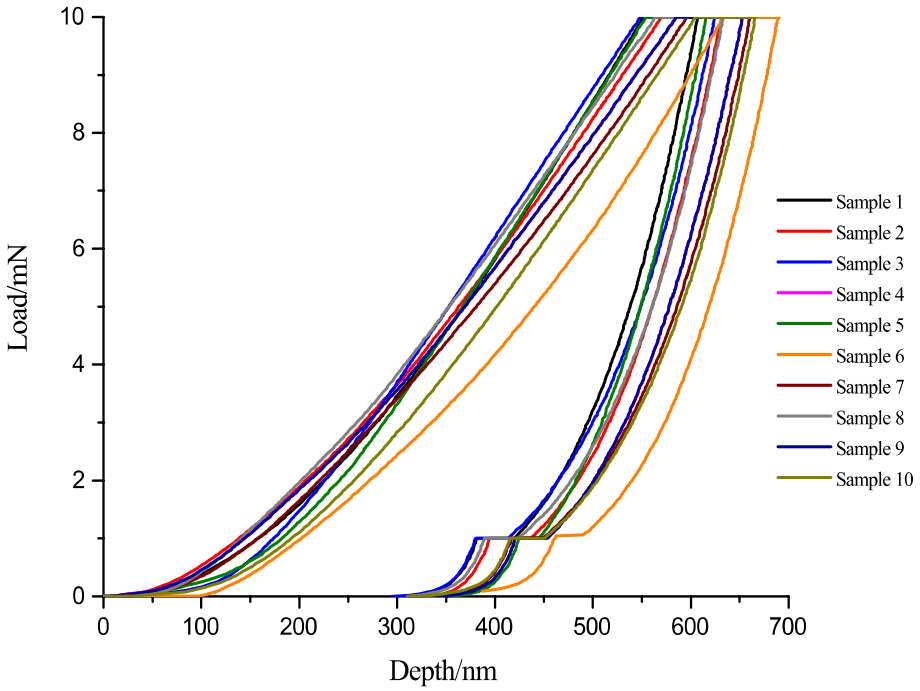

Load vs depth measurements, CCPS group

Mean ±standard deviation (SD) of H and E values for CSPS layer

Sample number	Hardness/GPa	±SD	Modulus /GPa	±SD
1	0.71	0.08	17.51	1.38
2	0.70	0.08	17.34	1.57
3	0.76	0.10	18.03	1.90
4	0.73	0.08	17.40	1.85
5	0.79	0.05	18.57	1.11
6	0.77	0.09	17.49	2.00
7	0.82	0.07	19.81	1.36
8	0.75	0.09	18.57	1.54
9	0.77	0.09	18.35	1.78
10	0.72	0.07	17.36	1.57
Average	**0.75**	**0.08**	**18.04**	**1.61**

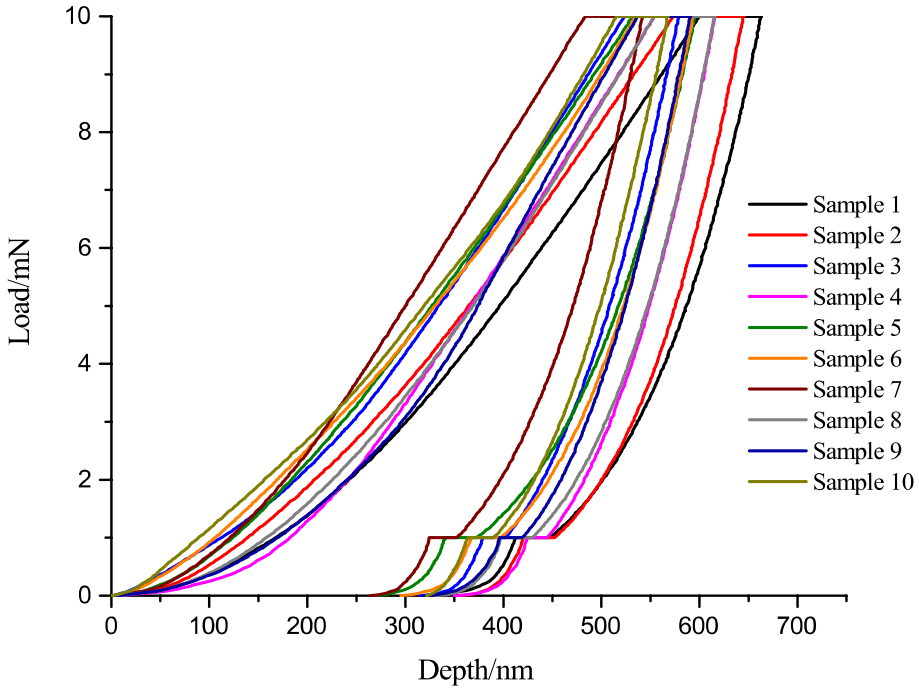

Load vs depth measurements, CSPS group

Mean ±standard deviation (SD) of H and E values for FCPS layer

Sample number	Hardness/GPa	±SD	Modulus /GPa	±SD
1	0.76	0.10	16.85	1.63
2	0.76	0.06	17.18	1.02
3	0.79	0.05	19.40	1.29
4	0.74	0.07	19.58	1.57
5	0.70	0.07	17.05	1.53
6	0.69	0.06	19.34	1.20
7	0.73	0.07	19.83	1.4
8	0.73	0.05	19.14	0.96
9	0.73	0.07	18.95	1.36
10	0.72	0.05	18.65	1.49
Average	**0.74**	**0.07**	**18.60**	**1.35**

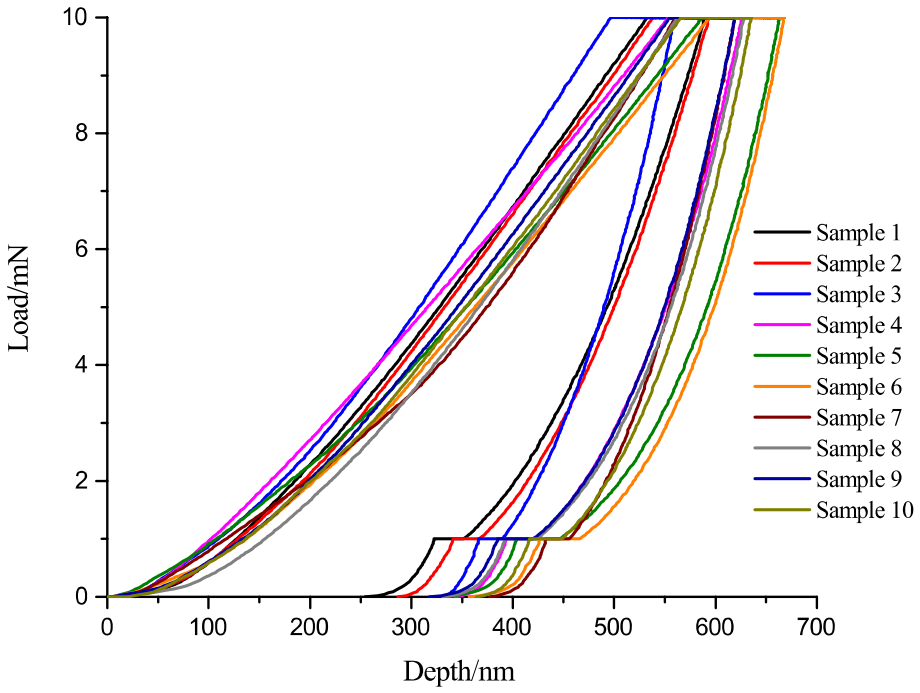

Load vs depth measurements, FCPS group

Appendix B Publications and Conference Proceedings

- Publications

Nanomechanical Properties of Hydroxyapatite like Coatings Formed by Bioactive Glasses, Arginine and Calcium Silicate for Dentine Protection

B.Mahmoodi, R. wood, R.B. Cook

Journal of the Mechanical Behavior of Biomedical Materials, published May 2020, doi:10.1016/j.jmbbm.2020.103702.

Tubule Occlusion and Mineralisation by NovaMin® and Stannous Fluoride

B.Mahmoodi, P. Goggin, C. Fowler, R.B. Cook
Have been submitted to the Journal of Biomedical Materials Research Part B:Applied Biomaterials

- Conference proceedings

Protection Effects of Bioglass® and Pro-Argin® Layers Formed On Dentine

B. Mahmoodi, R.J.K. Wood, R. B. Cook

British Society for Oral and Dental Research, 6-8 Sep 2017, Plymouth

Protection and Acid Resistivity of Bioactive-Glasses, Arginine and Calcium Silicate

B. Mahmoodi, R.J.K. Wood, R. B. Cook

International Association for Dental Research, 25-28 Jul 2018, London

Assessment of Dentine Tubule Occlusion and Remineralisation Using Serial-Block-Face SEM

B.Mahmoodi, C. Fowler, P. Goggin, R.B. Cook

International Association for Dental Research, 19-22 June 2019, Vancouver

Crystallinity Comparison between Hydroxyapatite-Like Layers Formed By Five Hypersensitivity Toothpastes

B. Mahmoodi, R.J.K. Wood, R. B. Cook

British Society for Oral and Dental Research, 3-5 Sep 2019, Leeds

Quantification of Dentine Tubule Occlusion and Remineralisation by Serial Block Face SEM

B.Mahmoodi, C. Fowler, P. Goggin, R.B. Cook

British Society for Oral and Dental Research, 3-5 Sep 2019, Leeds

References

[1] Porto ICCM, Andrade AKM, Montes MAJR. Diagnosis and treatment of dentinal hypersensitivity. J Oral Sci 2009;51:323–32. https://doi.org/10.2334/josnusd.51.323.

[2] Addy M. Etiology and clinical implications of dentine hypersensitivity. Dent Clin North Am 1990;34:503–14.

[3] Litkowski LJ, Hack GD, Sheaffer HB GD 1. Occlusion of Dentin Tubules By 45S5 Bioglass®. Proc. 10th Int. Symp. Ceram. Med., 1997, p. 32615.

[4] Mehta AB, Kumari V, Jose R, Izadikhah V. Remineralization potential of bioactive glass and casein phosphopeptide-amorphous calcium phosphate on initial carious lesion: An in-vitro pH-cycling study. J Conserv Dent 2014;17:3–7. https://doi.org/10.4103/0972-0707.124085.

[5] Xie K, Zhang L, Yang X, Wang X, Yang G, Zhang L, et al. Preparation and Characterization of Low Temperature Heat-Treated 45S5 Bioactive Glass-Ceramic Analogues. Biomed Glas 2015;1:80–92. https://doi.org/10.1515/bglass-2015-0008.

[6] Chen X, Karpukhina N, Brauer DS, Hill RG. High chloride content calcium silicate glasses. Phys Chem Chem Phys 2017;19:7078--7085. https://doi.org/10.1039/c6cp07905a.

[7] Hench LL. Chronology of Bioactive Glass Development and Clinical Applications. New J Glas Ceram 2013;03:67–73. https://doi.org/10.4236/njgc.2013.32011.

[8] T.Lakshmi vidya K. Bioglass: A novel biocompatible innovation. J Adv Pharm Technol Res 2015;4:25–30. https://doi.org/10.4103/2231.

[9] Mneimne M, Hill RG, Bushby AJ, Brauer DS. High phosphate content significantly increases apatite formation of fluoride-containing bioactive glasses.

Acta Biomater 2011;7:1827–34. https://doi.org/10.1016/j.actbio.2010.11.037.

[10] Cummins D. Dentin hypersensitivity: From diagnosis to a breakthrough therapy for everyday sensitivity relief. J Clin Dent 2009;20:1–9.

[11] Lavender SA, Petrou I, Heu R, Stranick MA, Cummins D, Kilpatrick-Liverman L, et al. Mode of action studies on a new desensitizing dentifrice containing 8.0% arginine, a high cleaning calcium carbonate system and 1450 ppm fluoride. Am J Dent 2010;23:14–9.

[12] Nathoo S, Delgado E, Zhang YP, DeVizio W, Cummins D, Mateo LR. Comparing the efficacy in providing instant relief of dentin hypersensitivity of a new toothpaste containing 8.0% Arginine, Calcium carbonate, and 1450 ppm fluoride relative to a benchmark desensitizing toothpaste containing 2% Potassium ion and 1450 ppm . J Clin Dent 2009;20:123–30.

[13] Gandolfi MG, Iacono F, Pirani C, Prati C. The use of calcium-silicate cements to reduce dentine permeability. Arch Oral Biol 2012;57:1054–61. https://doi.org/10.1016/j.archoralbio.2012.02.024.

[14] Gandolfi MG, Silvia F, Pashley DH, Gasparotto G, Carlo P. Calcium silicate coating derived from Portland cement as treatment for hypersensitive dentine. J Dent 2008;36:565–78. https://doi.org/10.1016/j.jdent.2008.03.012.

[15] Dong Z, Chang J, Joiner A, Sun Y. Tricalcium silicate induces enamel remineralization in human saliva. J Dent Sci 2013;8:440–3. https://doi.org/10.1016/j.jds.2013.04.005.

[16] Earl JS, Leary RK, Muller KH, Langford RM, Greenspan DC. Physical and chemical characterization of dentin surface following treatment with NovaMin technology. J Clin Dent 2011;22:62–7.

[17] Deng M, Wen HL, Dong XL, Li F, Xu X, Li H, et al. Effects of 45S5 bioglass on surface properties of dental enamel subjected to 35% hydrogen peroxide. Int J Oral Sci 2013;5:103–10. https://doi.org/10.1038/ijos.2013.31.

[18] Sauro S, Thompson I, Watson T. Effects of Common Dental Materials Used in

Preventive or Operative Dentistry on Dentin Permeability and Remineralization. Oper Dent 2011;36:222–30. https://doi.org/10.2341/10-225-L.

[19] Aguiar JD, Medeiros IS, e Souza Junior MHS, Loretto SC. Influence of the extended use of desensitizing toothpastes on dentin bonding, microhardness and roughness. Braz Dent J 2017;28:346–53. https://doi.org/10.1590/0103-6440201601292.

[20] Huang Y, Duan Y, Qian Y, Huang R, Yang Z, Li Y, et al. Remineralization efficacy of a toothpaste containing 8% arginine and calcium carbonate on enamel surface. Am J Dent 2013;26:291–7.

[21] Parkinson CR WR. A comparative in vitro study investigating the occlusion and mineralization properties of commercial toothpastes in a four-day dentin disc model. J Clin Dent 2011;22:74–81.

[22] Zhang Y-R, Du W, Zhou X-D, Yu H-Y. Review of research on the mechanical properties of the human tooth. Int J Oral Sci 2014;6:61–9. https://doi.org/10.1038/ijos.2014.21.

[23] Metivier A, Bland K. Dental Anatomy: A Review. Contin Dent Educ 2013:11–9.

[24] Nakamichi I, Iwaku M, Fusayama T. Bovine teeth as possible substitutes in the adhesion test. J Dent Res 1983;62:1076–81. https://doi.org/10.1177/00220345830620101501.

[25] Mendis BRRM, Darling AI. Distribution with age and attrition of peritubular dentine in the crowns of human teeth. Arch Oral Biol 1979;24:131–9. https://doi.org/10.1016/0003-9969(79)90061-X.

[26] Anatomical and histological features of the teeth' structure. Age-related changes in them. The concept of periodontium, its functions. Saliva, oral fluid: composition, properties, functions n.d. http://intranet.tdmu.edu.ua/data/kafedra/internal/stomat_ter/classes_stud/en/stomat/ptn/Propaedeutics of Therapeutic dentistry/2 year/02. Anatomical and histological features of tooth structure.htm (accessed March 8, 2016).

[27] Baker SP. Between nanoindentation and scanning force microscopy: measuring mechanical properties in the nanometer regime. Thin Solid Films 1997;308–309:289–96. https://doi.org/10.1016/S0040-6090(97)00556-7.

[28] Kerebel B, Daculsi G, Kerebel LM. Ultrastructural studies of enamel crystallites. J Dent Res 1979;58:844-51. https://doi.org/10.1177/00220345790580023701.

[29] Poole DF BA. The arrangement of crystallites in enamel prisms. Arch Oral Biol 1961;5:12–26.

[30] Jeng YR, Lin TT, Hsu HM, Chang HJ, Shieh D Bin. Human enamel rod presents anisotropic nanotribological properties. J Mech Behav Biomed Mater 2011;4:515–22. https://doi.org/10.1016/j.jmbbm.2010.12.002.

[31] Shellis RP, Featherstone JDB, Lussi A. Understanding the chemistry of dental erosion. Monogr Oral Sci 2014;20:66–76. https://doi.org/10.1159/000359943.

[32] Goldberg M, Kulkarni AB, Young M, Boskey A. Dentin: Structure, composition and mineralization. Front Biosci - Elit 2011;1:711–35.

[33] Abusallamah DA. No Title n.d. http://image.slidesharecdn.com/histologyofdentin-100531154923-phpapp01/95/histology-of-dentin-18-728.jpg?cb=1275321612 (accessed August 2, 2016).

[34] Garberoglio R, Brännström M. Scanning electron microscopic investigation of human dentinal tubules. Arch Oral Biol 1976;21:355–62. https://doi.org/10.1016/S0003-9969(76)80003-9.

[35] Kinney JH, Marshall SJ, Marshall GW. The mechanical properties of human dentin: A critical review and re-evaluation of the dental literature. Crit Rev Oral Biol Med 2003. https://doi.org/10.1177/154411130301400103.

[36] Marshall GW, Habelitz S, Gallagher R, Balooch M, Balooch G, Marshall SJ. Nanomechanical properties of hydrated carious human dentin. J Dent Res 2001;80:1768–71. https://doi.org/10.1177/00220345010800081701.

[37] Oyen ML. Nanoindentation hardness of mineralized tissues. J Biomech

2006;39:2699–702. https://doi.org/10.1016/j.jbiomech.2005.09.011.

[38] Ziskind D, Hasday M, Cohen SR, Wagner HD. Young's modulus of peritubular and intertubular human dentin by nano-indentation tests. J Struct Biol 2011;174:23–30. https://doi.org/10.1016/j.jsb.2010.09.010.

[39] Guidoni G, Denkmayr J, Schöberl T, Jäger I. Nanoindentation in teeth: influence of experimental conditions on local mechanical properties. Philos Mag 2006;86:5705–14. https://doi.org/10.1080/14786430600599757.

[40] Kinney JH, Gladden JR, Marshall GW, Marshall SJ, So JH, Maynard JD. Resonant ultrasound spectroscopy measurements of the elastic constants of human dentin. J Biomech 2004;37:437–41. https://doi.org/10.1016/j.jbiomech.2003.09.028.

[41] Wang RZ, Weiner S. Strain-structure relations in human teeth using Moiré fringes. J Biomech 1998;31:135–41. https://doi.org/10.1016/S0021-9290(97)00131-0.

[42] Angker L, Nockolds C, Swain M V., Kilpatrick N. Correlating the mechanical properties to the mineral content of carious dentine - A comparative study using an ultra-micro indentation system (UMIS) and SEM-BSE signals. Arch Oral Biol 2004. https://doi.org/10.1016/j.archoralbio.2003.12.005.

[43] Kinney JH, Balooch M, Marshall SJ, Marshall GW, Weihs TP. Hardness and Young's modulus of human peritubular and intertubular dentine. Arch Oral Biol 1996;41:9–13. https://doi.org/10.1016/0003-9969(95)00109-3.

[44] Chen Y, Wang J, Sun J, Mao C, Wang W, Pan H, et al. Hierarchical structure and mechanical properties of remineralized dentin. J Mech Behav Biomed Mater 2014;40:297–306. https://doi.org/10.1016/j.jmbbm.2014.08.024.

[45] Li X, An B, Zhang D. Determination of elastic and plastic mechanical properties of dentin based on experimental and numerical studies. Appl Math Mech (English Ed 2015;36:1347–58. https://doi.org/10.1007/s10483-015-1987-9.

[46] Cohen SR, Apter N, Jesse S, Kalinin S, Barlam D, Peretz AI, et al. AFM

Investigation of Mechanical Properties of Dentin. Isr J Chem 2008;48:65–72. https://doi.org/10.1560/ijc.48.2.65.

[47] Chan YL, Ngan AHW, King NM. Nano-scale structure and mechanical properties of the human dentine-enamel junction. J Mech Behav Biomed Mater 2011. https://doi.org/10.1016/j.jmbbm.2010.09.003.

[48] Marshall GW, Balooch M, Gallagher RR, Gansky SA, Marshall SJ. Mechanical properties of the dentinoenamel junction: AFM studies of nanohardness, elastic modulus, and fracture. J Biomed Mater Res 2001;54:87–95. https://doi.org/10.1002/1097-4636(200101)54:1<87::AID-JBM10>3.0.CO;2-Z.

[49] Murray C, Ca I, F P. Hardness Evaluation of Biological Tissue Using Nanoindentation Prepared by 2013.

[50] Joves GJ, Inoue G, Sadr A, Nikaido T, Tagami J. Nanoindentation hardness of intertubular dentin in sound, demineralized and natural caries-affected dentin. J Mech Behav Biomed Mater 2014;32:39–45. https://doi.org/10.1016/j.jmbbm.2013.12.017.

[51] Rivera-Muñoz EM. Hydroxyapatite-Based Materials: Synthesis and Characterization. Biomed Eng - Front Challenges 2000:75–98. https://doi.org/10.5772/19123.

[52] R.Jones J, Clare AG. Bio-glass: an introduction. 2012.

[53] Monchois V, Arguello-Morales M, Russell RR. Isolation of an active catalytic core of Streptococcus downei MFe28 GTF-I glucosyltransferase. J Bacteriol 1999;181:2290–2.

[54] Featherstone J. Dental caries: a dynamic disease process. Aust Dent J 2008;53:286–91. https://doi.org/10.1111/j.1834-7819.2008.00064.x.

[55] Anderson P, Hector MP, Rampersad MA. Critical pH in resting and stimulated whole saliva in groups of children and adults. Int J Paediatr Dent 2001;11:266–73. https://doi.org/10.1046/j.1365-263X.2001.00293.x.

[56] Larsen MJ. Degrees of saturation with respect to apatites in parotid saliva at

various ph values. Scand J Dent Res 1975;83:7–12.

[57] Sakiyama-Elbert SE HJ. FUNCTIONAL BIOMATERIALS : Design of Novel 2001:183–201.

[58] Hairul Nizam BR, Lim CT, Chng HK, Yap AUJ. Nanoindentation study of human premolars subjected to bleaching agent. J Biomech 2005;38:2204–11. https://doi.org/10.1016/j.jbiomech.2004.09.023.

[59] Chng HK, Ramli HN, Yap AUJ, Lim CT. Effect of hydrogen peroxide on intertubular dentine. J Dent 2005;33:363–9. https://doi.org/10.1016/j.jdent.2004.10.012.

[60] Angker L, Swain M V., Kilpatrick N. Characterising the micro-mechanical behaviour of the carious dentine of primary teeth using nano-indentation. J Biomech 2005;38:1535–42. https://doi.org/10.1016/j.jbiomech.2004.07.012.

[61] Ten Cate JM. Remineralization of deep enamel dentine caries lesions. Aust. Dent. J., 2008, p. 281–5. https://doi.org/10.1111/j.1834-7819.2008.00063.x.

[62] Sauro S, Osorio R, Osorio E, Watson TF, Toledano M. Novel light-curable materials containing experimental bioactive micro-fillers remineralise mineral-depleted bonded-dentine interfaces. J Biomater Sci Polym Ed 2013. https://doi.org/10.1080/09205063.2012.727377.

[63] Fernando D, Attik N, Pradelle-Plasse N, Jackson P, Grosgogeat B, Colon P. Bioactive glass for dentin remineralization: A systematic review. Mater Sci Eng C 2017:1369–77. https://doi.org/10.1016/j.msec.2017.03.083.

[64] Vollenweider M, Brunner TJ, Knecht S, Grass RN, Zehnder M, Imfeld T, et al. Remineralization of human dentin using ultrafine bioactive glass particles. Acta Biomater 2007;3:936–43. https://doi.org/10.1016/j.actbio.2007.04.003.

[65] Wang Z, Jiang T, Sauro S, Wang Y, Thompson I, Watson TF, et al. Dentine remineralization induced by two bioactive glasses developed for air abrasion purposes. J Dent 2011. https://doi.org/10.1016/j.jdent.2011.08.006.

[66] Brännström M. The hydrodynamic theory of dentinal pain: Sensation in preparations, caries, and the dentinal crack syndrome. J Endod 1986. https://doi.org/10.1016/S0099-2399(86)80198-4.

[67] Rees JS, Addy M. A cross-sectional study of dentine hypersensitivity. J Clin Periodontol 2002;29:997–1003.

[68] Koenigs PM, Faller R V. Oral Health Benefits in a Tube 2013.

[69] ABSI EG, ADDY M, ADAMS D. Dentine hypersensitivity – the effect of toothbrushing and dietary compounds on dentine in vitro: an SEM study. J Oral Rehabil 1992. https://doi.org/10.1111/j.1365-2842.1992.tb01086.x.

[70] Partner G health. Effect of Enamel & Tooth Surface Wear on Patients' Quality of Life n.d. https://www.gskhealthpartner.com/en-us/oral-health/conditions/enamel-wear/impact-on-quality-of-life/ (accessed November 20, 2019).

[71] continuing dental education for life long Learning. Dentin Hypersensitivity: An Update on Diagnosis and Etiology n.d. https://cdeworld.com/courses/21205-dentin-hypersensitivity-an-update-on-diagnosis-and-etiology (accessed November 20, 2019).

[72] Imfeld T. Dental erosion. Definition, classification and links. Eur J Oral Sci 1996;104:151–5. https://doi.org/10.1111/j.1600-0722.1996.tb00070.x.

[73] Voronets J, Jaeggi T, Buergin W, Lussi A. Controlled toothbrush abrasion of softened human enamel. Caries Res 2008;42:286–90. https://doi.org/10.1159/000148160.

[74] Ferreira MC, Ramos-Jorge ML, Delbem ACB, Vieirac RDS. Effect of Toothpastes with Different Abrasives on Eroded Human Enamel: An in situ/ex vivo Study. Open Dent J 2013;7:132–9. https://doi.org/10.2174/1874210601307010132.

[75] Kodaka T1, Kuroiwa M, Kuroiwa M, Okumura J, Mori R, Hirasawa S KM. Effects of brushing with a dentifrice for sensitive teeth on tubule occlusion and abrasion of dentin. Electron Microscompy 2001;50:57–64.

[76] Ruschel HC1 CO. A comparative study of dentin thickness of primary human molars. J Clin Pediatr Dent 2003;27:277–81.

[77] Philpotts CJ, Weader E, Joiner A. The measurement in vitro of enamel and dentine wear by toothpastes of different abrasivity. Int Dent J 2005;2005:183–7. https://doi.org/10.1111/j.1875-595x.2005.tb00057.x.

[78] Hunter ML, Addy M, Pickles MJ, Joiner a. The role of toothpastes and toothbrushes in the aetiology of tooth wear. Int Dent J 2002;52:399–405. https://doi.org/10.1111/j.1875-595X.2002.tb00729.x.

[79] Schemehorn BR, Moore MH PM. Abrasion, polishing, and stain removal characteristics of various commercial dentifrices in vitro. J Clin Dent 2011;22:11–8.

[80] D??rfe CE, Hefferren J, Gonz??lez-Cabezas C, Imfeld T, Addy M. Methods to determine dentifrice abrasiveness. J Clin Dent 2010;21.

[81] Addy M. Determination of Relative Dentifrice Abrasivity to Enamel and Dentine by a Surface Profile Method. J Clin Dent 2010.

[82] Mair LH, Stolarski TA, Vowles RW, Lloyd CH. Wear: Mechanisms, manifestations and measurement. Report of a workshop. J. Dent., 1996, p. 141–8. https://doi.org/10.1016/0300-5712(95)00043-7.

[83] Grippo JO. Abfractions: a new classification of hard tissue lesions of teeth. J Esthet Dent 1991;3:14–9. https://doi.org/10.1111/j.1708-8240.1991.tb00799.x.

[84] Lambrechts P, Braem M, Vuylsteke-Wauters M, Vanherle G. Quantitative in vivo wear of human enamel. J Dent Res 1989;68:1752–4. https://doi.org/10.1177/00220345890680120601.

[85] Pradeep K, Rajababu P, Satyanarayana D, Sagar V. Gingival Recession: Review and Strategies in Treatment of Recession. Case Rep Dent 2012. https://doi.org/10.1155/2012/563421.

[86] Arnold WH, Prange M, Naumova EA. Effectiveness of various toothpastes on

dentine tubule occlusion. J Dent 2015;43:440–9. https://doi.org/10.1016/j.jdent.2015.01.014.

[87] Walters PA. Dentinal hypersensitivity: A review. J Contemp Dent Pract 2005;6:107–17. https://doi.org/1526-3711-229 [pii].

[88] Addy M, Smith SR. Dentin hypersensitivity: An overview on which to base tubule occlusion as a management concept. J Clin Dent 2010:20–30.

[89] Gillam DG, Tang JY, Mordan NJ, Newman HN. The effects of a novel Bioglass® dentifrice on dentine sensitivity: A scanning electron microscopy investigation. J Oral Rehabil 2002;29:305–13. https://doi.org/10.1046/j.1365-2842.2002.00824.x.

[90] Mahale S, Badade P, Panjwani A. Dentinal tubule occlusion by desensitizing dentifrices : SEM study. J Dent Med Sci 2015;14:21–4. https://doi.org/10.9790/0853-141012124.

[91] Wang Z, Sa Y, Sauro S, Chen H, Xing W, Ma X, et al. Effect of desensitising toothpastes on dentinal tubule occlusion : A dentine permeability measurement and SEM in vitro study. J Dent 2010;38:400–10. https://doi.org/10.1016/j.jdent.2010.01.007.

[92] Litkowski L, Greenspan DC. A clinical study of the effect of calcium sodium phosphosilicate on dentin hypersensitivity-Proof of principle. J Clin Dent 2010;21:77–81.

[93] Nuss KMR, Rechenberg B von. Biocompatibility Issues with Modern Implants in Bone - A Review for Clinical Orthopedics. Open Orthop J 2008:66–78. https://doi.org/10.2174/1874325000802010066.

[94] Zachariasen WH. The atomic arrangement in glass. J Am Chem Soc 1932;54:3841–51. https://doi.org/doi:10.1021/ja01349a006.

[95] Edén M. The split network analysis for exploring composition-structure correlations in multi-component glasses: I. Rationalizing bioactivity-composition trends of bioglasses. J Non Cryst Solids 2011:1595–602.

https://doi.org/10.1016/j.jnoncrysol.2010.11.098.

[96] Tilocca a. Structural models of bioactive glasses from molecular dynamics simulations. Proc R Soc A Math Phys Eng Sci 2009;465:1003–27. https://doi.org/10.1098/rspa.2008.0462.

[97] Li R, Clark AE, Hench LL. An investigation of bioactive glass powders by sol-gel processing. J Appl Biomater 1991;2:231–9. https://doi.org/10.1002/jab.770020403.

[98] O'Donnell MD, Watts SJ, Hill RG, Law R V. The effect of phosphate content on the bioactivity of soda-lime-phosphosilicate glasses. J Mater Sci Mater Med 2009;20:1611–8. https://doi.org/10.1007/s10856-009-3732-2.

[99] Hill R. An alternative view of the degradation of bioglass. J Mater Sci Lett 1996;15:1122–5. https://doi.org/10.1007/BF00539955.

[100] Fujibayashi S, Neo M, Kim H-M, Kokubo T, Nakamura T. A comparative study between in vivo bone ingrowth and in vitro apatite formation on Na2O-CaO-SiO2 glasses. Biomaterials 2003;24:1349–56. https://doi.org/10.1016/S0142-9612(02)00511-2.

[101] R.Jones JAGC. Bio-Glasses: An Introduction. John Wiley & Sons; 2012.

[102] Hench LL. Bioceramics. J Am Ceram Soc 1998;81:1705–28.

[103] Lin FENGIHUEI. A study on bioglass ceramics in the NazO-CaO-SiO2-P2Os system 1988;23:4295–9.

[104] Hench LL. The story of Bioglass?? J. Mater. Sci. Mater. Med., vol. 17, 2006, p. 967–78. https://doi.org/10.1007/s10856-006-0432-z.

[105] Greenspan DC. Bioactive glass : mechanisms of bone bonding. Tandläkartidningen Árk 1999;91:1–32.

[106] Kokubo T, Ito S, Huang ZT, Hayashi T, Sakka S, Kitsugi T, et al. Ca,P-rich layer formed on high-strength bioactive glass-ceramic A-W. J Biomed Mater Res

1990;24:331–43. https://doi.org/10.1002/jbm.820240306.

[107] Forsback AP, Areva S, Salonen JI. Mineralization of dentin induced by treatment with bioactive glass S53P4 in vitro. Acta Odontol Scand 2004. https://doi.org/10.1080/00016350310008012.

[108] Xie D, Zhao J, Weng Y, Park JG, Jiang H, Platt JA. Bioactive glass-ionomer cement with potential therapeutic function to dentin capping mineralization. Eur J Oral Sci 2008. https://doi.org/10.1111/j.1600-0722.2008.00562.x.

[109] Curtis AR, West NX, Su B. Synthesis of nanobioglass and formation of apatite rods to occlude exposed dentine tubules and eliminate hypersensitivity. Acta Biomater 2010. https://doi.org/10.1016/j.actbio.2010.02.045.

[110] Osorio R, Yamauti M, Sauro S, Watson TF, Toledano M. Experimental resin cements containing bioactive fillers reduce matrix metalloproteinase-mediated dentin collagen degradation. J Endod 2012. https://doi.org/10.1016/j.joen.2012.05.011.

[111] Patel JP, Parsania PH. Characterization, testing, and reinforcing materials of biodegradable composites. Biodegrad. Biocompatible Polym. Compos., 2018, p. 55–79. https://doi.org/10.1016/b978-0-08-100970-3.00003-1.

[112] Maçon ALB, Valliant EM, Earl JS, Jones JR. Bioactivity of toothpaste containing bioactive glass in remineralizing media: Effect of fluoride release from the enzymatic cleavage of monofluorophosphate. Biomed Glas 2015;1:41–50. https://doi.org/10.1515/bglass-2015-0005.

[113] Ramakrishnaiah R, Rehman GU, Basavarajappa S, Al Khuraif AA, Durgesh BH, Khan AS, et al. Applications of Raman Spectroscopy in Dentistry: Analysis of Tooth Structure. Appl Spectrosc Rev 2014;50:332–50. https://doi.org/10.1080/05704928.2014.986734.

[114] Bertoluzza A, Fagnano C, Monti P, Simoni R, Tinti A, Tosi MR, et al. Raman spectroscopy in the study of biocompatibility. Clin Mater 1992;9:49–68. https://doi.org/10.1016/0267-6605(92)90010-Q.

[115] Combes C, Rey C. Amorphous calcium phosphates: Synthesis, properties and uses in biomaterials. Acta Biomater 2010;6:3362–78. https://doi.org/10.1016/j.actbio.2010.02.017.

[116] Ko AC-T, Choo-Smith L-P, Hewko M, Leonardi L, Sowa MG, Dong CCS, et al. Ex vivo detection and characterization of early dental caries by optical coherence tomography and Raman spectroscopy. J Biomed Opt 2005;10. https://doi.org/10.1117/1.1915488.

[117] Rothwell WP, Waugh JS, Yesinowski JP. High-Resolution Variable-Temperature 31P NMR of Solid Calcium Phosphates. J Am Chem Soc 1980. https://doi.org/10.1021/ja00528a020.

[118] Gunawidjaja PN, Lo AYH, Izquierdo-Barba I, García A, Arcos D, Stevensson B, et al. Biomimetic apatite mineralization mechanisms of mesoporous bioactive glasses as probed by multinuclear^{31}P,^{29}Si,^{23}Na and^{13}C solid-state NMR. J Phys Chem C 2010. https://doi.org/10.1021/jp105408c.

[119] Mathew R, Gunawidjaja PN, Izquierdo-Barba I, Jansson K, García A, Arcos D, et al. Solid-state 31P and 1H NMR investigations of amorphous and crystalline calcium phosphates grown biomimetically from a mesoporous bioactive glass. J Phys Chem C 2011. https://doi.org/10.1021/jp206237n.

[120] AIFA S, HAMMAMI K, El FEKI H, DROUET C, ELLOUMI J. Synthesis and Characterization of Hydroxyapatite Ceramics Organofunctionalized with ATP (Adenosine Triphosphate). J Adv Chem 2018. https://doi.org/10.24297/jac.v9i1.2304.

[121] Kanwal N, Brauer DS, Earl J, Wilson RM, Karpukhina N, Hill RG. In-vitro apatite formation capacity of a bioactive glass - containing toothpaste. J Dent 2018;68:51–8. https://doi.org/10.1016/j.jdent.2017.10.015.

[122] Takagi S, Liao H, Chow LC. Effect of Tooth-Bound Fluoride on Enamel Demineralization/Remineralization in vitro. Caries Res 2000;34:281–8. https://doi.org/10.1159/000016603.

[123] Derrick MR, Stulik D, Landry JM, The. Infrared Spectroscopy in Conservation Science. 1999. https://doi.org/10.1007/s13398-014-0173-7.2.

[124] Termine JD, Posner AS. Infra-red determination of the percentage of crystallinity in apatitic calcium phosphates. Nature 1966;211:268–70. https://doi.org/10.1038/211268a0.

[125] Liu Y, Yao X, Liu YW, Wang Y. A fourier transform infrared spectroscopy analysis of carious dentin from transparent zone to normal zone. Caries Res 2014. https://doi.org/10.1159/000356868.

[126] Efflandt SE, Magne P, Douglas WH, Francis LF. Interaction between bioactive glasses and human dentin. J Mater Sci Mater Med 2002;13:557–65. https://doi.org/10.1023/A:1015174726415.

[127] Bakry AS, Marghalani HY, Amin OA, Tagami J. The effect of a bioglass paste on enamel exposed to erosive challenge. J Dent 2014;42:1458–63. https://doi.org/10.1016/j.jdent.2014.05.014.

[128] Balamurugan A, Balossier G, Laurent-Maquin D, Pina S, Rebelo AHS, Faure J, et al. An in vitro biological and anti-bacterial study on a sol-gel derived silver-incorporated bioglass system. Dent Mater 2008;24:1343–51. https://doi.org/10.1016/j.dental.2008.02.015.

[129] Layer TJC. Development of a fluoridated, daily-use toothpaste containing NovaMin® technology for the treatment of dentin hypersensitivity. Dentistry 2011;22.

[130] Litkowski L, Greenspan DC. A clinical study of the effect of calcium sodium phosphosilicate on dentin hypersensitivity-Proof of principle. J Clin Dent 2010;21:77–81. https://doi.org/10.4317/jced.50955.

[131] White DJ. The application of in vitro models to research on demineralization and remineralization of the teeth. Adv Dent Res 1995;9:175–93; discussion 194-7.

[132] Alauddin SS (University of F. In Vitro Remineralization of Human Enamel with Bioactive Glass conatining Dentrifice using confocal microscopy and

nanoindentation analysis for early caries defense 2004.

[133] Burwell AK, Litkowski LJ, Greenspan DC. Calcium Sodium Phosphosilicate (NovaMin(R)): Remineralization Potential. Adv Dent Res 2009;21:35–9. https://doi.org/10.1177/0895937409335621.

[134] Neto FCR, Maeda FA, Turssi CP, Serra MC. Potential agents to control enamel caries-like lesions. J Dent 2009;37:786–90. https://doi.org/10.1016/j.jdent.2009.06.008.

[135] Earl JS, Topping N, Elle J, Langford RM GDJC. Physical and chemical characterization of surface layers formed on dentin following treatment with a fl uoridated toothpaste containing NovaMin®. Dent 2011;22:68–73.

[136] Schmidlin PR, Zehnder M, Imfeld T, Swain M V. Comparative assessment of hardening of demineralized dentin under lining materials using an ultramicroindentation system. J Biomed Mater Res - Part B Appl Biomater 2007;83B:199–205. https://doi.org/10.1002/jbm.b.30784.

[137] Lynch E, Brauer DS, Karpukhina N, Gillam DG, Hill RG. Multi-component bioactive glasses of varying fluoride content for treating dentin hypersensitivity. Dent Mater 2012;28:168–78. https://doi.org/10.1016/j.dental.2011.11.021.

[138] Salian S, Thakur S, Kulkarni S, Latorre G. A randomized controlled clinical study evaluating the efficacy of two desensitizing dentifrices. J Clin Dent 2010.

[139] Sharma N, Roy S, Kakar A, Greenspan DC, Scott R. A clinical study comparing oral formulations containing 7.5% calcium sodium phosphosilicate (novamin®), 5% potassium nitrate, and 0.4% stannous fluoride for the management of dentin hypersensitivity. J Clin Dent 2010.

[140] Larry L. HenchDerek B. SpilmanJune W. Hench. Fluoride-containing Bioglass^{TM} compositions 1998.

[141] Lusvardi G, Malavasi G, Cortada M, Menabue L, Menziani MC, Pedone A, et al. Elucidation of the structural role of fluorine in potentially bioactive glasses by experimental and computational investigation. J Phys Chem B 2008.

https://doi.org/10.1021/jp803031z.

[142] Stebbins JF, Zeng Q. Cation ordering at fluoride sites in silicate glasses: A high-resolution19F NMR study. J Non Cryst Solids 2000. https://doi.org/10.1016/S0022-3093(99)00695-X.

[143] Lusvardi G, Malavasi G, Menabue L, Aina V, Morterra C. Fluoride-containing bioactive glasses: Surface reactivity in simulated body fluids solutions. Acta Biomater 2009. https://doi.org/10.1016/j.actbio.2009.06.009.

[144] Larry L. HenchDerek B. SpilmanJune W. Hench. Fluoride-containing Bioglass.TM. compositions., 1986.

[145] Brauer DS, Karpukhina N, Donnell MDO, Law R V, Hill RG. Fluoride-containing bioactive glasses : Effect of glass design and structure on degradation , pH and apatite formation in simulated body fluid. Acta Biomater 2010;6:3275–82. https://doi.org/10.1016/j.actbio.2010.01.043.

[146] Pereira R, Dg G, Shaikh K, Phad S. Comparative Evaluation of Desensitizing Dentifrices containing BioMin ® , Novamin ® and Fluoride on Dentinal Tubule Occlusion before and after a Citric Acid Challenge – A scanning Electron Microscope in-vitro Study. J Odontol 2018;2:1–6.

[147] Alhussain AM, Alhaddad AA, Ghazwi MM, Farooq I. Remineralization of artificial carious lesions using a novel fluoride incorporated bioactive glass dentifrice. Dent Med Probl 2018. https://doi.org/10.17219/dmp/97311.

[148] Ashwini S, Swatika K, Kamala DN. Comparative evaluation of desensitizing efficacy of dentifrice containing 5% fluoro calcium phosphosilicate versus 5% calcium sodium phosphosilicate: A randomized controlled clinical trial. Contemp Clin Dent 2018. https://doi.org/10.4103/ccd.ccd_735_17.

[149] Patel VR, Shettar L, Thakur S, Gillam D, Kamala DN. A randomised clinical trial on the efficacy of 5% fluorocalcium phosphosilicate-containing novel bioactive glass toothpaste. J Oral Rehabil 2019. https://doi.org/10.1111/joor.12847.

[150] Da Cruz LPD, Hill RG, Chen X, Gillam DG. Dentine Tubule Occlusion by Novel Bioactive Glass-Based Toothpastes. Int J Dent 2018;2018. https://doi.org/10.1155/2018/5701638.

[151] Kleinberg I. SensiStat. A new saliva-based composition for simple and effective treatment of dentinal sensitivity pain. Dent Today 2002.

[152] Schiff T, Delgado E, Zhang YP, Cummins D, Devizi W, Mateo R. Clinical evaluation of the efficacy of an in-office desensitizing paste containing 8% arginine and calcium carbonate in providing instant and lasting relief of dentin hypersensitivity. Am J Dent 2009.

[153] Hamlin D, Kathleen PW, Delgado E, Zhang YP, Devizi W, Mateo R. Clinical evaluation of the efficacy of a desensitizing paste containing 8% arginine and calcium carbonate for the in-office relief of dentin hypersensitivity associated with dental prophylaxis. Am J Dent 2009. https://doi.org/10.3389/fpls.2018.00916.

[154] Clarke ER, Martell AE. Metal chelates of arginine and related ligands. J Inorg Nucl Chem 1970;32:911–26. https://doi.org/10.1016/0022-1902(70)80070-7.

[155] Tavafoghi Jahromi M, Yao G, Cerruti M. The importance of amino acid interactions in the crystallization of hydroxyapatite. J R Soc Interface 2013;10:20120906. https://doi.org/10.1098/rsif.2012.0906.

[156] Hirano A, Shiraki K, Kameda T. Effects of Arginine on Multimodal Chromatography: Experiments and Simulations. Curr Protein Pept Sci 2019;20:40–8. https://doi.org/10.2174/1389203718666171024115407.

[157] P Yuan, W Lu, H Xu, J Yang, C Liu, P Xu. In vitro dentin tubule occlusion by an arginine-containing dentifrice. Am J Dent 2019;32:133–7.

[158] Davies M, Paice EM, Jones SB, Leary S, Curtis AR, West NX. Efficacy of desensitizing dentifrices to occlude dentinal tubules. Eur J Oral Sci 2011;119:497–503. https://doi.org/10.1111/j.1600-0722.2011.00872.x.

[159] Dong Z, Chang J, Deng Y, Joiner A. Tricalcium silicate induced mineralization

for occlusion of dentinal tubules. Aust Dent J 2011;56:175–80. https://doi.org/10.1111/j.1834-7819.2011.01321.x.

[160] Sun Y, Li X, Deng Y, Sun JN, Tao D, Chen H, et al. Mode of action studies on the formation of enamel minerals from a novel toothpaste containing calcium silicate and sodium phosphate salts. J Dent 2014. https://doi.org/10.1016/S0300-5712(14)50005-X.

[161] Outhwaite WC, Mckenzie DM, Pashley DH. A Versatile Split-chamber Device for Studying Dentin Permeability. J Dent Res 1974. https://doi.org/10.1177/00220345740530064101.

[162] Ghazali FBC. Permeability of dentine. Malaysian J Med Soc 2003;10:27–36.

[163] Prabhati Gupta SMJ and RB. IN VITRO EVALUATION OF DENTINAL TUBULE OCCLUSION BY NOVAMIN (BIOACTIVE GLASS) 2019;09:26934–8.

[164] Bakri MM, Hossain MZ, Razak FA, Saqina ZH, Misroni AA, Ab-Murat N, et al. Dentinal tubules occluded by bioactive glass-containing toothpaste exhibit high resistance toward acidic soft drink challenge. Aust Dent J 2017;62:186–91. https://doi.org/10.1111/adj.12484.

[165] He Q, Hsueh M, Zhang G, Joy DC, Leapman RD. Biological serial block face scanning electron microscopy at improved z-resolution based on Monte Carlo model. Sci Rep 2018. https://doi.org/10.1038/s41598-018-31231-w.

[166] Zankel A, Kraus B, Poelt P, Schaffer M, Ingolic E. Ultramicrotomy in the ESEM, a versatile method for materials and life sciences. J Microsc 2009;233:140–8. https://doi.org/10.1111/j.1365-2818.2008.03104.x.

[167] Müllner T, Zankel A, Mayrhofer C, Reingruber H, Höltzel A, Lv Y, et al. Reconstruction and characterization of a polymer-based monolithic stationary phase using serial block-face scanning electron microscopy. Langmuir 2012;28:16733–7. https://doi.org/10.1021/la3038395.

[168] Cummins D. Recent advances in dentin hypersensitivity: Clinically proven

treatments for instant and lasting sensitivity relief. Am J Dent 2010;23:3–13.

[169] Gambhir R, Galhotra V, Yadav K, Sofat A. Dentin hypersensitivity following tooth preparation: A clinical study in the spectrum of gender. J Nat Sci Biol Med 2014;5:21–4. https://doi.org/10.4103/0976-9668.127277.

[170] Fonseca RB, Haiter-Neto F, Carlo HL, Soares CJ, Sinhoreti MAC, Puppin-Rontani RM, et al. Radiodensity and hardness of enamel and dentin of human and bovine teeth, varying bovine teeth age. Arch Oral Biol 2008;53:1023–9. https://doi.org/10.1016/j.archoralbio.2008.06.012.

[171] Nogueira BCL, Fernandes PM, Paiva ACJ, Fagundes NCF, Teixeira FB, Lima RR. Surface microhardness evaluation of enamel and dentin in bovine and human teeth (permanent and deciduous). Pesqui Vet Bras 2014;22:311–6. https://doi.org/10.1590/S0100-736X2014000500017.

[172] Camargo CHR, Siviero M, Camargo SEA, de Oliveira SHG, Carvalho CAT, Valera MC. Topographical, Diametral, and Quantitative Analysis of Dentin Tubules in the Root Canals of Human and Bovine Teeth. J Endod 2007;33:422–6. https://doi.org/10.1016/j.joen.2006.12.011.

[173] Humphrey SP, Williamson RT. A review of saliva: Normal composition, flow, and function. J Prosthet Dent 2001;85:162–9. https://doi.org/10.1067/mpr.2001.113778.

[174] Lin J, Han S, Zhu J, Wang X, Chen Y, Vollrath O, et al. Influence of fluoride-containing acidic artificial saliva on the mechanical properties of Nickel-Titanium orthodontics wires. Indian J Dent Res 2012;23:591–5. https://doi.org/10.4103/0970-9290.107332.

[175] Bingel L, Groh D, Karpukhina N, Brauer DS. Influence of dissolution medium pH on ion release and apatite formation of Bioglass® 45S5. Mater Lett 2015. https://doi.org/10.1016/j.matlet.2014.12.124.

[176] Leyland A, Matthews A. On the significance of the H/E ratio in wear control: A nanocomposite coating approach to optimised tribological behaviour. Wear

2000;246:1–11. https://doi.org/10.1016/S0043-1648(00)00488-9.

[177] Joshi S, Gowda AS, Joshi C. Comparative evaluation of NovaMin desensitizer and Gluma desensitizer on dentinal tubule occlusion: A scanning electron microscopic study. J Periodontal Implant Sci 2013;43:269–78. https://doi.org/10.5051/jpis.2013.43.6.269.

[178] Soares P, Laurindo CAH, Torres RD, Kuromoto NK, Peitl O, Zanotto ED. Effect of a bioactive glass-ceramic on the apatite nucleation on titanium surface modified by micro-arc oxidation. Surf Coatings Technol 2012;206:4601–5. https://doi.org/10.1016/j.surfcoat.2012.05.019.

[179] Bertassoni LE, Swain MV. Influence of hydration on nanoindentation induced energy expenditure of dentin. J Biomech 2012;45:1679–83. https://doi.org/10.1016/j.jbiomech.2012.03.021.

[180] Poolthong S, Mori T, Swain M V. Determination of elastic modulus of dentin by small spherical diamond indenters. Dent Mater J 2001;20:227–36.

[181] Habelitz S, Marshall GW, Balooch M, Marshall SJ. Nanoindentation and storage of teeth. J Biomech 2002;35:995–8. https://doi.org/10.1016/S0021-9290(02)00039-8.

[182] Zheng L, Hilton JF, Habelitz S, Marshall SJ, Marshall GW. Dentin caries activity status related to hardness and elasticity. Eur J Oral Sci 2003;111:243–52. https://doi.org/10.1034/j.1600-0722.2003.00038.x.

[183] Guidoni G, Swain M, Jäger I. Nanoindentation of wet and dry compact bone: Influence of environment and indenter tip geometry on the indentation modulus. Philos Mag 2010;90:553–65. https://doi.org/10.1080/14786430903201853.

[184] Oberle TL. Properties influencing wear of metals. J Met 1951;1951:438.

[185] Fox-Rabinovich GS, Veldhuis SC, Weatherly GC, Kovalev AI, Korshunov SN, Scvortsov VN, et al. Improvement of “duplex” PVD coatings for HSS cutting tools by ion mixing. Surf Coatings Technol 2004;187:230–7. https://doi.org/10.1016/j.surfcoat.2004.02.015.

[186] Chen CL, Parolia A, Pau A, Celerino De Moraes Porto IC. Comparative evaluation of the effectiveness of desensitizing agents in dentine tubule occlusion using scanning electron microscopy. Aust Dent J 2015;2015:65–72. https://doi.org/10.1111/adj.12275.

[187] Jena A, Kala S, Shashirekha G. Comparing the effectiveness of four desensitizing toothpastes on dentinal tubule occlusion: A scanning electron microscope analysis. J Conserv Dent 2017;20:269–72. https://doi.org/10.4103/JCD.JCD_34_17.

[188] Bloebaum RD, Skedros JG, Vajda EG, Bachus KN, Constantz BR. Determining mineral content variations in bone using backscattered electron imaging. Bone 1997;20:485–90. https://doi.org/10.1016/S8756-3282(97)00015-X.

[189] Koutsopoulos S. Synthesis and characterization of hydroxyapatite crystals: A review study on the analytical methods. J Biomed Mater Res 2002. https://doi.org/10.1002/jbm.10280.

[190] Kirkpatrick RJ, Brow RK. Nuclear magnetic resonance investigation of the structures of phosphate and phosphate-containing glasses: A review. Solid State Nucl Magn Reson 1995;5:9–21. https://doi.org/10.1016/0926-2040(95)00042-O.

[191] Handschin RG, Stern WB. Crystallographic lattice refinement of human bone. Calcif Tissue Int 1992;51:111–20. https://doi.org/10.1007/BF00298498.

[192] Rusu VM, Ng CH, Wilke M, Tiersch B, Fratzl P, Peter MG. Size-controlled hydroxyapatite nanoparticles as self-organized organic-inorganic composite materials. Biomaterials 2005. https://doi.org/10.1016/j.biomaterials.2005.01.051.

[193] Thamaraiselvi T V., Prabakaran K, Rajeswari S. Synthesis of hydroxyapatite that mimic bone minerology. Trends Biomater Artif Organs 2006;19:81–3.

[194] Ye F, Guo H, Zhang H. Biomimetic synthesis of oriented hydroxyapatite mediated by nonionic surfactants. Nanotechnology 2008;19. https://doi.org/10.1088/0957-4484/19/24/245605.

[195] Weiner S, Bar-Yosef O. States of preservation of bones from prehistoric sites in

the Near East: A survey. J Archaeol Sci 1990;17:187–96. https://doi.org/10.1016/0305-4403(90)90058-D.

[196] Antonakos A, Liarokapis E, Leventouri T. Micro-Raman and FTIR studies of synthetic and natural apatites. Biomaterials 2007;28:3043–54. https://doi.org/10.1016/j.biomaterials.2007.02.028.

[197] Vương BX, Hiệp ĐT. In vitro studies of bioglass material by X-ray diffraction and solid-state MAS-NMR. Glas Phys Chem 2016;42:188–93. https://doi.org/10.1134/S108765961602005X.

[198] Rehman I, Bonfield W. Characterization of hydroxyapatite and carbonated apatite by photo acoustic FTIR spectroscopy. J Mater Sci Mater Med 1997;8:1–4. https://doi.org/10.1023/A:1018570213546.

[199] Cui W, Li X, Xie C, Zhuang H, Zhou S, Weng J. Hydroxyapatite nucleation and growth mechanism on electrospun fibers functionalized with different chemical groups and their combinations. Biomaterials 2010;31:4620–9. https://doi.org/10.1016/j.biomaterials.2010.02.050.

[200] Legeros RZ, Lin S, Rohanizadeh R, Mijares D, Legeros JP. Biphasic calcium phosphate bioceramics: Preparation, properties and applications. J Mater Sci Mater Med 2003;14:201–9. https://doi.org/10.1023/A:1022872421333.

[201] Cuscó R, Guitián F, Aza S d., Artús L. Differentiation between hydroxyapatite and β-tricalcium phosphate by means of μ-Raman spectroscopy. J Eur Ceram Soc 1998;18:1301–5. https://doi.org/10.1016/s0955-2219(98)00057-0.

[202] Viswanath B, Raghavan R, Gurao NP, Ramamurty U, Ravishankar N. Mechanical properties of tricalcium phosphate single crystals grown by molten salt synthesis. Acta Biomater 2008;4:1448–54. https://doi.org/10.1016/j.actbio.2008.02.031.

[203] Daculsi G, Laboux O, Malard O, Weiss P. Current state of the art of biphasic calcium phosphate bioceramics. J Mater Sci Mater Med 2003;14:195–200. https://doi.org/10.1023/A:1022842404495.

[204] Blong MA, Volding B, Thrash WJ, Jones DL. Effects of a gel containing 0.4 percent stannous fluoride on dentinal hypersensitivity. Dent Hyg (Chic) 1985;59:489–92.

[205] He T, Barker ML, Qaqish J, Sharma N. Fast onset sensitivity relief of a 0.454% stannous fluoride dentifrice. J Clin Dent 2011;22:46–50.

[206] Takamizawa T, Tsujimoto A, Ishii R, Ujiie M, Kawazu M, Hidari T, et al. Laboratory evaluation of dentin tubule occlusion after use of dentifrices containing stannous fluoride. J Oral Sci 2019;61:276–83. https://doi.org/10.2334/josnusd.18-0176.

[207] Reynolds EC. Calcium phosphate-based remineralization systems: Scientific evidence? Aust. Dent. J., vol. 53, 2008, p. 268–73. https://doi.org/10.1111/j.1834-7819.2008.00061.x.

[208] NS DVB, Dave DPN, Bhanushali DP V. Comparative Analysis of Remineralizing Potential of Three Commercially Available Agents- An in Vitro Study. IOSR J Dent Med Sci 2017;16:01–5. https://doi.org/10.9790/0853-1602030105.

[209] Miller S, Truong T, Heu R, Stranick M, Bouchard D, Gaffar A. Recent advances in stannous fluoride technology: antibacterial efficacy and mechanism of action towards hypersensitivity. Int Dent J 1994;44:83–98.

[210] Earl JS, Leary RK, Perrin JS, Brydson R, Harrington JP, Markowitz K, et al. Characterization of dentine structure in three dimensions using FIB-SEM. J Microsc 2010;240:1–5. https://doi.org/10.1111/j.1365-2818.2010.03396.x.

[211] Smith D, Starborg T. Serial block face scanning electron microscopy in cell biology: Applications and technology. Tissue Cell 2019;57:111–22. https://doi.org/10.1016/j.tice.2018.08.011.

[212] Kawabata M, Hector MP, Davis GR, Parkinson CR, Rees GD, Anderson P. Diffusive transport within dentinal tubules: An X-ray microtomographic study. Arch Oral Biol 2008;53:736–43.

https://doi.org/10.1016/j.archoralbio.2008.03.012.

[213] Hoshi K, Ejiri S, Probst W, Seybold V, Kamino T, Yaguchi T, et al. Observation of human dentine by focused ion beam and energy-filtering transmission electron microscopy. J Microsc 2001;201:44–9. https://doi.org/10.1046/j.1365-2818.2001.00784.x.

[214] Nalla RK, Porter AE, Daraio C, Minor AM, Radmilovic V, Stach EA, et al. Ultrastructural examination of dentin using focused ion-beam cross-sectioning and transmission electron microscopy. Micron 2005;36:672–80. https://doi.org/10.1016/j.micron.2005.05.011.

[215] Engqvist H, Schultz-Walz JE, Loof J, Botton GA, Mayer D, Phaneuf MW, et al. Chemical and biological integration of a mouldable bioactive ceramic material capable of forming apatite in vivo in teeth. Biomaterials 2004;25:2781–7. https://doi.org/10.1016/j.biomaterials.2003.09.053.

[216] Kulal R, Jayanti I, Sambashivaiah S, Bilchodmath S. An in-vitro comparison of nano hydroxyapatite, novamin and proargin desensitizing toothpastes -A SEM study. J Clin Diagnostic Res 2016;10:51–4. https://doi.org/10.7860/JCDR/2016/18991.8649.

[217] Reddy GV, Akula S, Malgikar S, Babu PR, Reddy GJ, Josephin JJ. Comparative scanning electron microscope analysis of diode laser and desensitizing toothpastes for evaluation of efficacy of dentinal tubular occlusion. J Indian Soc Periodontol 2017;21:102–6. https://doi.org/10.4103/jisp.jisp_153_17.

[218] Hines D, Xu S, Stranick M, Lavender S, Pilch S, Zhang YP, et al. Effect of a stannous fluoride toothpaste on dentinal hypersensitivity: In vitro and clinical evaluation. J Am Dent Assoc 2019;150:47–59. https://doi.org/10.1016/j.adaj.2019.01.006.